

Porcine neonatal pancreatic clusters –
Characterization of cellular and molecular dynamics
during the *in vitro* culture period

von Martin Leopold Kraetzl

Inaugural-Dissertation zur Erlangung der Doktorwürde der
Tierärztlichen Fakultät der Ludwig-Maximilians-Universität
München

Porcine neonatal pancreatic clusters –
Characterization of cellular and molecular dynamics
during the *in vitro* culture period

von Martin Leopold Kraetzel

aus Freising

München 2025

Aus dem Veterinärwissenschaftlichen Department
der Tierärztlichen Fakultät
der Ludwig-Maximilians-Universität München

Lehrstuhl für Molekulare Tierzucht und Biotechnologie

Arbeit angefertigt unter der Leitung von

Prof. Dr. Elisabeth G. Kemter

Mitbetreuung durch Univ.-Prof. Dr. Eckhard Wolf

Gedruckt mit Genehmigung der Tierärztlichen Fakultät
der Ludwig-Maximilians-Universität München

Dekan: Univ.-Prof. Dr. Reinhard K. Straubinger, Ph.D.

Berichterstatter: Prof. Dr. Elisabeth G. Kemter

Korreferenten: Univ.-Prof. Dr. Laurent Frantz
Univ.-Prof. Dr. Markus Meissner
Priv.-Doz. Dr. Sonja Härtle
Univ.-Prof. Dr. Mathias Ritzmann

Tag der Promotion: 26. Juli 2025

Für meine Familie

Parts of this work have been presented at international congresses:

Islet symposium 2024, IDR-L - Helmholtz Center Munich; Munich, Germany

French-German Summer School 2024; Lyon, France

IPITA-IXA-CTMR Joint Congress 2023; San Diego, USA

EPITA Symposium 2023; Innsbruck, Austria

Additionally, the following publications in peer-reviewed journals were published:

Spheroids Composed of Reaggregated Neonatal Porcine Islets and Human Endothelial Cells Accelerate Development of Normoglycemia in Diabetic Mice

Honarpisheh M, Lei Y, Follenzi A, Cucci A, Olgasi C, Berishvili E, Lebreton F, Bellofatto K, Piemonti L, Citro A, Campo F, Pignatelli C, Thauinat O, Kemter E, **Kraetzl M**, Wolf E, Seissler J, Wolf-van Buerck L, Vanguard Consortium

Cells. 2025 Mar. doi: 10.3390/cells14050366

Functional maturation and longitudinal imaging of intraportal neonatal porcine islet grafts in genetically diabetic pigs

Pilz J, Gloddek N, Lindheimer F, Lindner MJ, Pühr-Westerheide D, Ümütlü M, Cyran C, Seidensticker M, Lindner R, **Kraetzl M**, Renner S, Merkus D, Teupser D, Bartenstein P, Ziegler SI, Wolf E, Kemter E

American Journal of Transplantation. 2024 Aug. doi: 10.1016/j.ajt.2024.02.026

Structural and proteomic repercussions of growth hormone receptor deficiency on the pituitary gland: Lessons from a translational pig model

Shashikadze B, Franzmeier S, Hofmann I, **Kraetzl M**, Flenkenthaler F, Blutke A, Fröhlich T, Wolf E, Hinrichs A

Journal of Neuroendocrinology. 2024 Jul. doi: 10.1111/jne.13277

Formation of Re-Aggregated Neonatal Porcine Islet Clusters Improves In Vitro Function and Transplantation Outcome

Honarpisheh M, Lei Y, Zhang Y, Pehl M, Kemter E, **Kraetzl M**, Lange A, Wolf E, Wolf-van Buerck L, Seissler J; VANGUARD Consortium

Transplant International. 2022 Dec. doi: 10.3389/ti.2022.10697

TABLE OF CONTENTS

I.	INTRODUCTION.....	1
II.	REVIEW OF THE LITERATURE	2
1.	The Pancreas and its islets of Langerhans	2
1.1.	Structure and Function of the pancreas	2
1.2.	Development of pancreatic endocrine cells	3
1.3.	β -cell properties and maturation	4
1.4.	Differences and similarities between human, pig, and rodent islets	4
2.	Type 1 diabetes mellitus (T1DM)	6
2.1.	Etiology, pathogenesis, symptoms, and complications	6
2.2.	Burden of T1DM	6
2.3.	Treatment and cure - status quo	7
2.4.	Alternative treatment methods	9
2.4.1.	β -cell regeneration	9
2.4.2.	Usage of alternative β -cell sources for replacement therapy	10
3.	Generation of porcine cell clusters for β-cell replacement therapy.....	11
3.1.	Isolation of adult porcine islets	11
3.2.	Generation of neonatal and juvenile islet-like clusters	12
3.2.1.	General procedure	12
3.2.2.	<i>In vitro</i> maturation	13
3.3.	Neonatal islet-like clusters vs adult porcine islets	14
III.	OBJECTIVES.....	16
IV.	ANIMALS, MATERIALS AND METHODS.....	17
1.	Animals.....	17
2.	Materials	17
2.1.	Devices	17
2.2.	Consumables	18
2.3.	Drugs	19
2.4.	Chemicals and reagents	20

2.5.	Kits.....	21
2.6.	Buffers, Medium and Solutions.....	21
2.6.1.	Pancreas procurement and cluster isolation and culture.....	21
2.6.2.	Solutions for histology, immunostaining and perfusion.....	22
2.7.	Antibodies	25
2.8.	Software	27
3.	Methods	28
3.1.	Organ retrieval and cluster isolation and culture of porcine neonatal pancreatic organoids.....	28
3.2.	Cell cluster size and volume	29
3.3.	Flow cytometry.....	30
3.4.	Immunostaining of sections	31
3.4.1.	Hematoxylin and eosin staining	32
3.4.2.	Immunostaining with PFPE samples	33
3.4.3.	Immunostaining with cryopreserved samples.....	33
3.5.	scRNA-seq.....	34
3.5.1.	Sample preparation.....	34
3.5.2.	Library preparation and sequencing	34
3.5.3.	Improved genome annotation for <i>Sus scrofa</i>	35
3.5.4.	Pre-processing of droplet-based scRNA-seq data.....	35
3.5.4.1.	Data preparation	35
3.5.4.2.	Ambient gene detection.....	36
3.5.4.3.	Empty Droplets.....	36
3.5.4.4.	Quality Control	36
3.5.4.5.	Doublet detection	36
3.5.4.6.	Concatenation and normalization.....	37
3.5.4.7.	Integration.....	37
3.5.4.8.	Single-cell manifolds and visualization	37
3.5.4.9.	Doublet Removal.....	37
3.5.4.10.	Clustering and Cell Type annotation	38
3.5.4.11.	Differential gene expression	38
3.6.	Perfusion Assay for Dynamic Glucose-Stimulated Insulin Secretion	38

3.6.1.	Machine preparation.....	38
3.6.2.	Sample equilibration and perfusion experiment	39
3.7.	Statistics	39
V.	RESULTS.....	41
1.	From pancreatic aggregates to islet-like cell clusters.....	41
1.1.	Significant reduction in cell cluster volume and changes in size distribution during culture period.....	41
1.2.	Gross morphology of pNPCs during the cultivation period: From structural integrity to cellular adaptation	44
1.3.	Early pNPCs consist of all pancreatic cell types	45
1.4.	Enrichment of the endocrine cell fraction and depletion of non-endocrine cell types during <i>in vitro</i> culture of pNPCs.....	48
1.5.	Molecular characterization of pancreatic cell types.....	52
2.	Signs of stress recovery and maturation in endocrine cells.....	56
2.1.	Endocrine cells gain endocrine-lineage transcription factors during culture and exhibit typical expression patterns in β , α , and δ cells.....	56
2.2.	Few multihormonal cells during <i>in vitro</i> culture.....	59
2.3.	Distinct early drop and subsequent recovery in hormone abundance and granularity in endocrine cells during culture period.....	61
2.4.	Insulin secretory profile of β cells	66
3.	Evaluation of proliferation and other dynamic processes.....	68
3.1.	Self-replication of endocrine cells / Changes in cell proliferation with higher proliferation in endocrine cells.....	68
3.2.	Potential for β -cell neogenesis: Presence of endocrine progenitor-like cells.....	73
3.3.	Occurrence of cells with multi-lineage molecular pattern	76
3.4.	Cell-cell interaction & matrix	82
3.5.	Endocrine cells show signs of ER-stress in early but also late culture	83
VI.	DISCUSSION	86
1.	Endocrine enrichment with preserved heterogeneity	87

2.	Switch from initial dominant molecular stress signature towards a maturation signature in endocrine cells.....	89
3.	pNPCs show cellular and molecular heterogeneity and signs of plastic processes.....	92
4.	Challenges to obtain a pNPC product with constant properties for β -cell replacement therapy.....	96
5.	How to further improve <i>in vitro</i> cultivation of pNPCs.....	98
6.	pNPCs as an <i>in vitro</i> model system for islet research.....	101
VII.	SUMMARY	103
VIII.	ZUSAMMENFASSUNG	105
IX.	INDEX OF FIGURES	107
X.	INDEX OF TABLES	112
XI.	REFERENCES.....	113
XII.	ACKNOWLEDGEMENTS.....	143

INDEX OF ABBREVIATIONS

7-AAD	7-Aminoactinomycin D
ABCC8	ATP Binding Cassette Subfamily C Member 8
ADP	Adenosine diphosphate
AEQ	Aggregate equivalent
AMY	Amylase
ARX	Aristaless Related Homeobox
ATP	Adenosine triphosphate
bidest	Bidistilled
BiP	Heat Shock Protein Family A (Hsp70) Member 5
BLOC1S1	Biogenesis of Lysosomal Organelles Complex 1 Subunit 1
BSA	Bovine serum albumin
BW	Body weight
CFTR	Cystic Fibrosis Transmembrane Conductance Regulator
CHGA	Chromogranin A
CHGB	Chromogranin B
CHOP	DNA Damage Inducible Transcript 3
CITRAT	Citrat - 0.5% Tween®20 - buffer
CK7	Cytokeratin 7
CPA1	Carboxypeptidase A1
CPE	Carboxypeptidase E
DAB	3,3'-diaminobenzidine
DAPI	4',6-diamidino-2-phenylindole
DDIT3	DNA Damage Inducible Transcript 3
dGSIS	Dynamic glucose-stimulated insulin secretion
DNAJB9	DnaJ Heat Shock Protein Family (Hsp40) Member B9
ECM	Extracellular Matrix
EDTA	Ethylenediaminetetraacetic acid
EFNA5	Ephrin A5
EIF2AK3	Eukaryotic Translation Initiation Factor 2 Alpha Kinase 3
EIF2S1	Eukaryotic Translation Initiation Factor 2 Subunit Alpha
EMT	Epithelial to mesenchymal transition
EPITA	European Pancreas and Islet Transplant Association
ER	Endoplasmic reticulum
ERN1	Endoplasmic Reticulum to Nucleus Signaling 1
FCS	Fetal Calf Serum
FEV	Fifth Ewing Variant Protein

FOXA2	Forkhead Box A2
G6PC2	Glucose-6-Phosphatase Catalytic Subunit 2
GATA4	GATA Binding Protein 4
GCG	Glucagon
GCK	Glucokinase
GLM	General linear mixed model
GLUT1	Glucose transporter 1
GLUT2	Glucose transporter 2
GLUT3	Glucose transporter 3
H&E	Hematoxylin and Eosin
HIAR	Heat-induced antigen retrieval
hiPSCs	Human induced pluripotent stem cells
HSPA5	Heat Shock Protein Family A (Hsp70) Member 5
IBMX	3-Isobutyl-1-methylxanthin
IEQ	Islet equivalent
IgG	Immunoglobulin G
INS	Insulin
IPITA	International Pancreas and Islet Transplant Association
IRE1	Endoplasmic Reticulum to Nucleus Signaling 1
ISL1	ISL LIM Homeobox 1
ITGA6	Integrin subunits Alpha 6
ITGAV	Integrin subunits Alpha V
ITGB1	Integrin subunits Beta 1
KCNJ11	Potassium Inwardly Rectifying Channel Subfamily J Member 11
KLF4	KLF Transcription Factor 4
KRB	Krebs-Ringer buffer
KRT7	Cytokeratin 7
LAMB1	Laminin subunit Beta 1
LAMC1	Laminin subunit Gamma 1
LDHA	Lactate Dehydrogenase A
MAFA	MAF BZIP Transcription Factor A
MFI	Median fluorescence intensity
MKI67	Marker of Proliferation Ki-67
MPCs	Multipotent progenitor cells
MSC	Mesenchymal stromal cell
MYC	MYC Proto-Oncogene
NCAM1	Neural Cell Adhesion Molecule 1
NEUROD1	Neuronal Differentiation 1

NEUROG3/NGN3	Neurogenin 3
NKX2.2	NK2 Homeobox 2
NKX6-1	NK6 Homeobox 1
PAX6	Paired Box 6
PBS	Phosphate-buffered salt solution
PBS-T	PBS + 0.1% Tween20
PCSK2	Proprotein Convertase Subtilisin/Kexin Type 2
PDX1	Pancreatic and Duodenal Homeobox 1
PERK	Eukaryotic Translation Initiation Factor 2 Alpha Kinase 3
PFA	Paraformaldehyde
PFPE	Paraformaldehyde-fixed paraffin-embedded
pH	Potentia hydrogenii
pNPCs	Porcine neonatal pancreatic clusters
PPY	Pancreatic polypeptide
PRSS2	Serine Protease 2
PTF1A	Pancreas Associated Transcription Factor 1a
RFX3	Regulatory Factor X3
RFX6	Regulatory Factor X6
RT	Room temperature
SCG2	Secretogranin II
SCG5	Secretogranin IV
SD	Standard deviation
SEM	Standard error of means
SIX3	SIX Homeobox 3
SLC16A1	Solute Carrier Family 16 Member 1
SLC2A2	Solute Carrier Family 2 Member 2
SNAP25	Synaptosome Associated Protein 25
SOX17	SRY-Box Transcription Factor 17
SOX2	SRY-Box Transcription Factor 2
SOX9	SRY-Box Transcription Factor 9
SSC-A / SSC-H	side scatter area / height
SST	Somatostatin
SYP	Synaptophysin
T1DM	Type 1 diabetes mellitus
T2DM	Type 2 diabetes mellitus
TBS	Tris-buffer salt solution
TFs	Transcription factors
TRIS	Tris-EDTA - 0.5% Tween20 - buffer

VIM	Vimentin
XBP1	X-Box Binding Protein 1
+	Positive

Units:

cm	Centimeter
g	Gram
h	Hour
kg	Kilogram
L	Liter
M	Molar
mg	Milligram
min	Minute
mL	Milliliter
mm	Millimeter
mm ³	Cubic millimeter
mmol	Millimole
nmol	Nanomole
rpm	Revolutions per minute
sec	Second
μL	Microliter
μm	Micrometer
μmol	Micromole
°C	Degree Celsius

I. INTRODUCTION

Type I diabetes mellitus (T1DM) is one of the fastest-growing noncommunicable chronic health conditions worldwide (GREGORY et al., 2022). It arises from the immune-mediated destruction of β cells in the pancreas, leading to insulin dependency (ZAJEC et al., 2022). Recent advancements in continuous glucose monitoring and insulin pump systems have significantly improved patient management (HOLT et al., 2021). Despite the effectiveness of insulin therapy for most T1DM patients, those with unstable glycemic control may experience life-threatening hypoglycemic events (HIRSCH & GAUDIANI, 2021; CALIMAG et al., 2023). For such cases, the transplantation of a pancreas or islets from deceased donors offers a therapeutic alternative (SHAPIRO et al., 2000; NICLAUSS et al., 2016; MARFIL-GARZA et al., 2023). However, the limited availability of pancreatic donor organs necessitates alternative β -cell sources (MELTON, 2021; JIANG & JIANG, 2023; COOPER et al., 2024).

Porcine tissue for xenotransplantation presents a promising solution (MATSUMOTO & SHIMODA, 2020). In 2022, the clinical application of xenotransplantation began, with genetically modified pig hearts and kidneys in compassionate use cases, such as David Bennett's (GRIFFITH et al., 2022; KAWAI et al., 2025). Pancreas from adult or neonatal pigs can serve as source for β -cell replacement therapy, with neonatal pig pancreas offering advantages like reliable isolation methods and better availability of genetically modified donor piglets compared to retired breeding sows (NAGARAJU et al., 2015).

Neonatal pig pancreas, being immature at isolation, requires an *in vitro* cultivation period prior to transplantation (JIMENEZ-VERA et al., 2015; LAU et al., 2021; HONARPISHEH et al., 2022). Up until now the cellular and molecular dynamics during this culture period have been inadequately understood.

Enhancing islet-like Xeno-products necessitates a comprehensive understanding of these *in vitro* processes. This study provides novel insights into the cellular dynamics within the culture system, elucidates molecular processes in β cells, and underscores the unique potential of these cell clusters.

II. REVIEW OF THE LITERATURE

1. The Pancreas and its islets of Langerhans

1.1. Structure and Function of the pancreas

The pancreas is an organ composed of two endodermal main components: the exocrine and the endocrine compartment. The exocrine part of the pancreas accounts for more than 95% of the mass of pancreatic tissue and is made up mainly of acinar and ductal cells (TSUCHITANI et al., 2016). Acinar cells produce digestive enzymes such as amylase, lipase, and proteases, while duct cells form luminal structures to transport these enzymes to the duodenum. Additionally, duct cells secrete bicarbonate-rich fluids to neutralize the acidic chyme entering the duodenum from the stomach, thereby maintaining an optimal pH for enzymatic activity (GRAPIN-BOTTON, 2005; REICHERT & RUSTGI, 2011). The endocrine part comprises about ~2% of the total pancreatic cell mass, consists of the islets of Langerhans, and is distributed throughout the pancreatic organ (RAHIER et al., 1981; RENNER et al., 2016; TSUCHITANI et al., 2016).

The primary function of the islets of Langerhans (LANGERHANS, 1969) is the regulation of blood glucose levels. The islets contain several types of hormone-producing endocrine cells, with the main cell types being β cells, α cells, and δ cells. For the blood glucose homeostasis, insulin (INS)-producing β cells are the most crucial cell type. These cells secrete INS in response to rising blood glucose levels, enabling glucose uptake in tissues and thereby lowering blood sugar levels. Glucagon (GCG) is the direct counterpart of INS, secreted by α cells. GCG is secreted at low blood glucose levels, stimulating glycogenolysis and gluconeogenesis in the liver, thereby increasing blood sugar levels. δ cells contribute to blood glucose homeostasis by secreting somatostatin (SST), which acts as a tonic inhibitor of both INS and GCG secretion (KAILEY et al., 2012; XU et al., 2020). Besides these three main cell types, there are two other less abundant endocrine cell types: PP cells, which secrete pancreatic polypeptide (PPY), and ϵ cells, which secrete ghrelin. Both PPY and ghrelin appear to have inhibitory effects on other endocrine cells in the islets of Langerhans (KIM et al., 2014; ARAGÓN et

al., 2015; SAKATA et al., 2019; PEREZ-FRANCES et al., 2021).

Beyond the endocrine and exocrine compartments, the pancreas contains several other non-endocrine cell types, including endothelial cells, neurons, and mesenchymal cells. Endothelial cells form the inner lining of blood vessels and play a crucial role in nutrient and oxygen supply, while also directly affecting β -cell function (BURGANOVA et al., 2021). Furthermore, neurons innervate the pancreas and are involved in regulating pancreatic islet formation and function (AGERSKOV & NYENG, 2024). Mesenchymal cells serve as scaffold cells and produce extracellular matrix (ECM), both of which are crucial for proper tissue organization and function. Like in other organs, the ECM provides structural integrity to the pancreatic tissue and additionally delivers crucial signals for cell function. In islets, the ECM mainly consists of type IV collagen and the laminins 211 and 511, which are essential for the function of endocrine cells (WIELAND et al., 2021).

1.2. Development of pancreatic endocrine cells

The formation of the islets of Langerhans during embryogenesis is a highly orchestrated process that begins with the budding of the pancreatic epithelium from the foregut endoderm, driven by transcription factors (TFs) such as Pancreatic and Duodenal Homeobox 1 (PDX1) and Pancreas Associated Transcription Factor 1a (PTF1A). Multipotent progenitor cells (MPCs), expressing PDX1, SRY-Box Transcription Factor 9 (SOX9), GATA Binding Protein 4 (GATA4), and NK6 Homeobox 1 (NKX6-1), then segregate into tip and trunk domains (ZHOU et al., 2007; JENNINGS et al., 2013). The tip domain (GATA4⁺SOX9⁺) gives rise to acinar cells, while bipotent trunk cells (PDX1⁺SOX9⁺) later form ductal and endocrine cells (NAIR & HEBROK, 2015; NYENG et al., 2019).

The commitment to an endocrine fate is regulated by Neurogenin 3 (NGN3/NEUROG3) expression (BECHARD et al., 2016). After expression of high levels of NGN3, MPCs migrate from the ductal epithelium into the surrounding mesenchyme and commit to the endocrine lineage by expression of Fifth Ewing Variant Protein (FEV) (BASTIDAS-PONCE et al., 2019). By later expression of several TFs, like PDX1, NKX6-1, Aristaless Related Homeobox (ARX), Paired Box 6 (PAX6), Neuronal Differentiation 1 (NEUROD1), NK2 Homeobox 2 (NKX2-2), ISL LIM

Homeobox 1 (ISL1), and Regulatory Factor X6 (RFX6), the formation of the endocrine subtypes is orchestrated (AL-KHAWAGA et al., 2018; AIGHA & ABDELALIM, 2020; SIEHLER et al., 2021).

1.3. **β -cell properties and maturation**

After their development from precursor cells and commitment to the β -cell fate, β cells must undergo a maturation process to function properly. This maturation process involves the establishment of the cellular machinery necessary for glucose stimulated insulin secretion (SAKHNENY et al., 2021). This includes the production of insulin precursors, proper processing to mature insulin, storage of insulin in granules, and rapid but temporally limited release of insulin secretory granules upon glucose stimulus (KAESTNER et al., 2021).

The process of glucose-stimulated insulin secretion begins with glucose uptake via glucose transporters (GLUT), specifically GLUT1 (SLC2A1) and GLUT3 (SLC2A3) in humans (MCCULLOCH et al., 2011; BERGER & ZDZIEBLO, 2020). Once inside the cell, glucose is phosphorylated by glucokinase (GCK) and further metabolized in the mitochondria to generate adenosine triphosphate (ATP). An increased ATP to to adenosine diphosphate (ADP) ratio leads to the closure of potassium channels. The resulting depolarization opens voltage-gated calcium channels, allowing calcium ions to enter the cell. This influx of calcium triggers the release of mature insulin containing granules via exocytosis.

The expression of β -cell identity markers, such as PDX1, NKX6-1, and NEUROD1, along with maturation regulators like MAF BZIP Transcription Factor A (MAFA) and SIX Homeobox 3 (SIX3), as well as the absence of “disallowed genes” such as Solute Carrier Family 16 Member 1 (SLC16A1) and Lactate Dehydrogenase A (LDHA), are indicators for β -cell maturity (BARSBY & OTONKOSKI, 2022; JACOVETTI & REGAZZI, 2022).

1.4. **Differences and similarities between human, pig, and rodent islets**

In the realm of biomedical research, much of our understanding of islet biology and diabetes comes from experiments with rodents. However, significant differences exist in the development, morphology, and function of islets across species. Pigs, due to their genetic, anatomical, physiological, and developmental

similarities to humans, might serve as a valuable model to bridge these gaps (SCHOOK et al., 2015; RENNER et al., 2016; KIM et al., 2020; LICKERT et al., 2024).

While humans, pigs, and mice exhibit heterogeneous yet comparable islet size distributions, the cellular composition within the islets varies markedly (KIM et al., 2009). In rodents, α and δ cells are located in the periphery and β cells in the center. Conversely, human and pig islets display a more even distribution of endocrine cell types (HOANG et al., 2014). Although β cells constitute the largest proportion in all three species, their ratios differ significantly. In humans and pigs, β cells make up approximately 60%, while α cells account for around 30%. In mice, however, β cells represent about 75%, with α cells comprising only 20% (BRISSOVA et al., 2005; CABRERA et al., 2006; RENNER et al., 2016). These differences in cytoarchitecture lead to functional variations in Ca^{2+} -oscillatory activity, which is directly linked to beta cell function (CABRERA et al., 2006).

Furthermore, numerous mechanistic and functional disparities have been documented between human and rodent islets (SKELIN KLEMEN et al., 2017). These include differences in glucose transporters (GLUT1, GLUT2, and GLUT3) (MCCULLOCH et al., 2011; BERGER & ZDZIEBLO, 2020), ion channels (Na^+ , K^+ , and Ca^{2+} channels) (BRAUN et al., 2008), membrane potential oscillation patterns (BRAUN et al., 2009; RIZ et al., 2014), G-protein coupled receptors (AMISTEN et al., 2017), and citric acid cycle-associated pathways (MACDONALD et al., 2011)

Although the embryonic development of pancreatic endocrine cells in pigs is not as well-studied as in mice and humans, it has been shown that pigs exhibit islet-specific gene expression patterns more similar to humans, particularly in later developmental stages (LICKERT et al., 2024). Furthermore, porcine endocrine cells during embryonic and early postnatal development express specific islet TFs and maturation markers that resemble those of human cells, unlike those in mice (KIM et al., 2020).

These interspecies differences might impact the translatability of findings from rodent models to humans. Due to their closer resemblance to humans, particularly in the context of diabetes research, pigs might serve as a valuable model to bridge the gap between rodent and human.

2. Type 1 diabetes mellitus (T1DM)

2.1. Etiology, pathogenesis, symptoms, and complications

Type 1 diabetes mellitus (T1DM) is an autoimmune disorder characterized by the destruction of insulin-producing β cells in the pancreas, primarily mediated by T-cells. The etiology of T1DM involves a complex interplay of genetic predisposition and environmental factors, such as viral infections and diet (ZAJEC et al., 2022).

The pathogenesis of T1DM is marked by the presence of autoantibodies against insulin and other β -cell antigens (ILONEN et al., 2019), leading to progressive β -cell destruction and thereof to an absolute deficiency of insulin production and secretion. Without insulin, glucose uptake into cells is impaired, resulting in persistent hyperglycemia. The onset of T1DM is often marked by symptoms like polydipsia, polyuria, and weight loss (SYED, 2022). Additional clinical signs may include lack of energy or fatigue, blurred vision or constant hunger (MAGLIANO DJ, 2021).

T1DM is associated with both acute and chronic complications (NATHAN et al., 1993; JACOBSON et al., 2013; SABERZADEH-ARDESTANI et al., 2018). Severe blood glucose fluctuations complicate insulin treatment regime and can result in hypoglycemic episodes, typically caused by excessive insulin administration, or hyperglycemia due to insufficient insulin administration, which may progress to diabetic ketoacidosis - both of which can result in potentially life-threatening medical emergencies (CALIMAG et al., 2023). Long-term, even mild chronic hyperglycemia in T1DM can lead both to microvascular complications, such as retinopathy, nephropathies, and neuropathies, as well as macrovascular complications, including peripheral arterial disease or myocardial infarction (LIN et al., 2021; FUNG et al., 2022; LU et al., 2023).

2.2. Burden of T1DM

T1DM is a rapidly growing global health concern with significant implications for both individuals and healthcare systems. A meta-analysis of publications from January 1980 to September 2019 revealed an incidence of T1DM of 15 per 100,000 people, which has increased over time (MOBASSERI et al., 2020). In 2022, approximately nine million people worldwide were affected by T1DM, with an

estimated 182,000 deaths attributed to the condition (OGLE et al., 2022). By 2040, the worldwide prevalence of T1DM is projected to reach approximately 13.5 to 17.4 million cases, reflecting a 60% to 107% increase compared to 2021 (GREGORY et al., 2022). This projection underscores T1DM's status as one of the fastest-growing noncommunicable chronic diseases.

Health-care costs for people with T1DM are almost double for people without diabetes, and even higher than those for individuals with Type 2 diabetes mellitus (T2DM) (**Table 1**) (VOELTZ et al., 2024). The cost of care has shown a dramatic increase in recent years (CROSSEN et al., 2020) and is expected to rise to €1.5 billion in Germany, representing a 30% increase (VOELTZ et al., 2024).

Table 1: Average per capita health-care expenses in € in 2010 of non-diabetic patients and patients with T1DM or T2DM in Germany (VOELTZ et al., 2024).

	non-diabetic	T1DM	T2DM
women	2,316	4,889	3,889
men	2,360	4,285	3,868

Beyond the financial burden, T1DM significantly impairs the quality of life of affected people due to the need for continuous glucose monitoring, insulin administration, and the long-term risk of severe complications (JACOBSON et al., 2013).

2.3. Treatment and cure - status quo

In the early 20th century, numerous scientists endeavored to elucidate the mechanisms of blood-glucose regulation. This pursuit culminated in the landmark discovery of insulin by Banting, Macleod, Best, and Collip in 1921 (ROSENFELD, 2002; BALL & FEATHERSTONE, 2023). Before the discovery of insulin and the advent of insulin therapy, diabetes was a fatal disease. Patients often died from diabetic ketoacidosis due to high glucose levels or from severe undernutrition caused by "starvation diets" (MAZUR, 2011). The introduction of insulin derived from cattle and pig pancreas dramatically transformed the lives of diabetic patients when Eli Lilly and Company made it commercially available in 1923 (MALONE et al., 2020).

The standard treatment for T1DM nowadays remains the administration of exogenous insulin, now biotechnologically produced human insulin, delivered either through multiple daily subcutaneous injections or insulin pumps (CHANCE & FRANK, 1993; HOLT et al., 2021). While this approach effectively manages blood glucose levels, it remains purely symptomatic (HILL & HILL, 2024). Even innovative techniques such as insulin pumps or bi-hormonal treatment with insulin and glucagon cannot replicate the complex regulatory mechanisms of blood glucose homeostasis found in the islets of Langerhans (HOLT et al., 2021). In certain cases, despite meticulous monitoring of blood glucose levels and the conscientious use of insulin, severe dysregulations in blood glucose homeostasis still occur (HIRSCH & GAUDIANI, 2021). These dysregulations can lead to life-threatening complications such as hyperglycemic episodes or long-term morbidities like coronary heart disease (NATHAN et al., 1993; VANDERNIET et al., 2022; CALIMAG et al., 2023; LU et al., 2023).

For such cases, the only cure is the replacement of the endogenous but non-functional insulin source through transplantation. This can be performed either as pancreas transplantation or as islet transplantation. A milestone in islet transplantation was achieved with the introduction of the Edmonton protocol in 2000. This protocol established a standardized procedure for the isolation and transplantation of islets from deceased human donors and the introduction of a glucocorticoid-free immunosuppression regime (SHAPIRO et al., 2000).

Although islet transplantation reduces diabetes-related complications (REID et al., 2021), this approach is currently limited to individuals experiencing severe diabetic chronic kidney disease or severe metabolic complications, such as hypoglycemia unawareness, frequent life-threatening hypoglycemic episodes, or significant glycemic lability (HIRSCH & GAUDIANI, 2021; HOLT et al., 2021). The primary challenges of this therapy include the requirement for lifelong immunosuppression to prevent graft rejection, limited availability of donor pancreata, and the necessity for multiple transplants to achieve insulin independence (HOLT et al., 2021; MARFIL-GARZA et al., 2022).

2.4. Alternative treatment methods

Given the limitations of current treatments, intensive research is focused on developing innovative therapeutic strategies aimed at β -cell regeneration or replacement.

2.4.1. β -cell regeneration

One promising approach to restore physiological insulin production and secretion is the *in situ*-regeneration of β cells from endogenous cell populations. Several strategies are currently under investigation.

Despite prolonged diabetes progression, residual β cells persist even after decades (KEENAN et al., 2010; TAYLOR et al., 2022). Although these cells are not fully functional and are referred to as dedifferentiated β cells, they can be reactivated and serve as a source for functional cells (SACHS et al., 2020; SON & ACCILI, 2023). Additionally, the self-replication of β cells could expand the functional cell mass (KULKARNI et al., 2012; SAUNDERS & POWERS, 2016). This phenomenon is observed in neonates and as a response to insulin resistance, such as during pregnancy. It is also described as the primary source of new β cells in the adult pancreas (DOR et al., 2004).

Moreover, neogenesis from multipotent progenitors has been proposed as a mechanism for generating new β -cells in the adult pancreas. This process has been observed *in vivo* in diabetic rodent models (RAZAVI et al., 2015; GRIBBEN et al., 2021). However, the occurrence of β -cell neogenesis in the adult pancreas remains a topic of critical debate (MAGENHEIM et al., 2023). Transdifferentiation of other differentiated cell types into insulin-producing and secreting cells has also been reported (PURI et al., 2015). Studies have documented processes involving α cells (THOREL et al., 2010; BRAMSWIG et al., 2013) and pancreatic exocrine cells (BAEYENS et al., 2005; MINAMI et al., 2005).

Given that current research has yet to conclusively demonstrate the existence and underlying mechanisms of β -cell regeneration in the adult human pancreas, its clinical translation as a therapeutic option remains distant.

2.4.2. Usage of alternative β -cell sources for replacement therapy

Although β -cell replacement therapy through transplantation of isolated human islets is a clinically available treatment, its application is constrained by the scarcity of donor tissue (MANTOVANI et al., 2023). Therefore, intensive research is being conducted on alternative β -cell replacement strategies, like products derived from porcine pancreas and human induced pluripotent stem cells (hiPSCs), both already progressing towards clinical application (KIM et al., 2024; MATSUMOTO & MATSUMOTO, 2024; VERTEX, 2024).

hiPSCs can be generated from donor-derived mesenchymal cells by reprogramming them with the Yamanaka factors, which include the four transcription factors POU Class 5 Homeobox 1 (OCT3/4), SRY-Box Transcription Factor 2 (SOX2), KLF Transcription Factor 4 (KLF4), and MYC Proto-Oncogene (MYC) (TAKAHASHI & YAMANAKA, 2006). After achieving pluripotency, these cells undergo *in vitro* differentiation through a complex multi-step protocol leading to β -like cells. This protocol is guided by lineage checkpoints of embryonic β -cell development, such as Forkhead Box A2 (FOXA2), SRY-Box Transcription Factor 17 (SOX17), PDX1, NKX6-1, NGN3, MAFA, and INS (SIEHLER et al., 2021). Despite significant progress (REZANIA et al., 2014; RUSS et al., 2015; SIEHLER et al., 2021; BALBOA et al., 2022) and the initiation of clinical trials by Vertex (VX-880, Vertex NCT04786262) and ViaCyte (VC-02) (VERTEX, 2024), several challenges remain before these therapies can be widely implemented in the clinic.

One major issue is the purity of the cell products. Despite the goal of exclusively generating β -like cells, many of these products contain only 20-50% INS⁺ cells, alongside undesired cell types such as polyhormonal, pancreatic non-endocrine, and enterochromaffin-like cells (VERES et al., 2019; DOCHERTY et al., 2021; BALBOA et al., 2022). Furthermore, β -like cell products are not fully mature compared to native β cells and require further improvement to accurately reflect β -cell identity and physiological insulin responses to glucose stimuli (SIEHLER et al., 2021; BALBOA et al., 2022; JIANG & JIANG, 2023).

Further, safety concerns pose a significant challenge. Pluripotent stem cell-derived therapies require stringent safety measures to ensure the final product does not contain cells that are incompletely differentiated, which could retain

characteristics leading to tumor formation, including teratomas (HAN et al., 2022). Additionally, the large-scale and reproducible production of functional β cells remains technically challenging and expensive (CHOI et al., 2024).

In summary, while stem cell-based β -cell replacement therapies show great promise, issues related to cell purity, safety, scalability, and, most importantly, maturity must be addressed before these therapies can be widely implemented.

An alternative to these products are clusters generated from porcine pancreas (LIU et al., 2017). The significant similarity between human and porcine islets, particularly in their structure and the amino acid sequence of insulin, makes this approach generally feasible (HOANG et al., 2014; DAĞAŞAN, 2021). However, due to the species barrier, several modifications are necessary to prevent acute rejection reactions. Key strategies include the elimination of porcine antigens such as α -Gal, inhibition of the complement cascade, anticoagulatory strategies, and modulation of the immune system, all of which play a crucial role in graft survival (KEMTER et al., 2020; COWAN, 2022). Despite these challenges, porcine islets have successfully rendered diabetic non-human primates independent of exogenous insulin over the long term (SHIN et al., 2015).

3. Generation of porcine cell clusters for β -cell replacement therapy

To generate such clusters, donor pigs must be sacrificed and pancreatic tissue harvested and processed immediately post-mortem. Donors of various ages, including neonatal, juvenile, and adult pigs, are currently being investigated, with each age group presenting distinct advantages and limitations (SMITH et al., 2018).

3.1. Isolation of adult porcine islets

The isolation of islets from adult pig pancreas is similar to the process used for human islet isolation from deceased donor tissue. Due to anatomical differences between pig and human pancreases, donor selection is somewhat special.

Human islets are surrounded by a capsule that provides compact structural properties to the endocrine cell clusters. In contrast, pigs do not form a typical capsule structure around the islets of Langerhans. Only in sows with multiple pregnancies, where expansion and shrinkage occur due to metabolic reformation, a so-called pseudo capsule forms (MEYER et al., 1997; KRICKHAHN et al., 2002). This pseudo capsule enables islet isolation similar to the human procedure (RICORDI et al., 1989; STEFFEN et al., 2017).

For this procedure, the entire pancreas is retrieved from the donor animal and perfused with cold organ preservation solution (STEFFEN et al., 2017). Collagenase, neutral protease, and DNase are infused into the duct system via a catheter, and the pancreatic tissue is digested at 37°C by shaking in a Ricordi chamber. To enrich the islet-containing fraction within the digest, discontinuous gradient purification is performed. The cell clusters should be transplanted as soon as possible, like in the allotransplantation setting (human to human).

Islets derived from adult pigs contain fully differentiated β cells, which exhibit immediate functionality after transplantation. Additionally, the yield per pancreas is relatively high. However, the high costs associated with animal husbandry and the complex isolation technique make this process expensive and labor-intensive (VANDERSCHULDEN et al., 2019; COOPER et al., 2024). These factors limit the scalability and cost-effectiveness of this product.

3.2. **Generation of neonatal and juvenile islet-like clusters**

An alternative to adult porcine islets is clusters generated from the neonatal and juvenile pancreas. Compared to compact islets in adults, endocrine cell clusters are still developing in the neonatal and juvenile pig pancreas. Here the endocrine cells are present as single cells or small clusters (NAGAYA et al., 2019). This makes traditional islet isolation techniques inapplicable. Korbitt and colleagues addressed this issue in the 1990s and developed a relatively easy protocol to generate functional clusters from the developing pig pancreas (KORBUTT et al., 1996).

3.2.1. **General procedure**

Therefore, tissue is cut into ~1-2mm pieces and gently digested with collagenase.

As this process does not isolate compact endocrine clusters, like in human islet isolation, enrichment for endocrine cells is achieved by *in vitro* culture for several days. For this purpose, Korbitt et al. developed a Ham's F10 based medium supplemented to final concentrations of 10 mmol/L glucose, 50 μ mol/L 3-Isobutyl-1-methylxanthin (IBMX), 0.5% bovine serum albumin, 2 mmol/L L-Glutamine, 10 mmol/L nicotinamide. After 9 days of culture, clusters consisted of 35% endocrine cells and corrected hyperglycemia in diabetic mice within 8 weeks after transplantation.

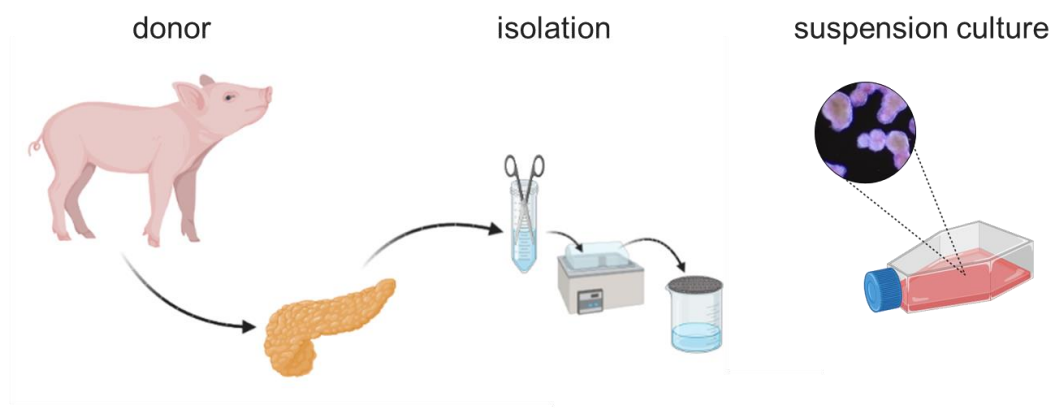


Figure 1: Procedure of cluster generation from neonatal pancreatic tissue. Created with BioRender.com.

3.2.2. *In vitro* maturation

Since the introduction of this protocol, various research groups have attempted to optimize *in vitro* conditions to enhance the functionality of clusters. These efforts have focused on the effects of donor age (NAGARAJU et al., 2015; AREFANIAN et al., 2022), culture duration (JIMENEZ-VERA et al., 2015), and particularly, various media conditions.

Regarding media conditions, different basal media, glucose concentrations, protein sources, compounds for cell recovery/protection, compounds for *in vitro* maturation, and the addition of extra cellular matrix components or other cells have been tested.

The basal media used range from Ham's F10 (ELLIS et al., 2016) and Ham's F12 (LUCA et al., 2005), to RPMI1640 (LI et al., 2018) and EGM2 (MA et al., 2018), and further to M199 (KEMTER et al., 2017) und DMEM F12 (HASSOUNA et al., 2018). These media differ significantly in their amino acid composition, vitamins,

inorganic salts, and other additives. The glucose concentrations used range from 7.8 mmol/L (KEMTER et al., 2017) to 17.5 mmol/L (HASSOUNA et al., 2018), the latter being significantly within the diabetic blood glucose range. The protein sources include serum-free options such as bovine serum albumin and human albumin, as well as human, porcine, or fetal calf serum (LOPEZ-AVALOS et al., 2001), which contain undefined amounts of growth factors, hormones, lipids, and minerals.

Commonly used additives can be categorized into protective additives like aprotinin, Pefabloc, necrostatin, and protease inhibitors (LAMB et al., 2014; LAU et al., 2021) and additives that promote the maturation of endocrine cells, such as nicotinamide, IBMX, or oncostatin (ELLIS et al., 2016; HASSOUNA et al., 2018; LI et al., 2018). Additionally, various ECM components like fibrin or decellularized tissue (SALAMA et al., 2020; CITRO et al., 2023) and cells such as endothelial or multipotent stromal cells are used (MONTANARI et al., 2021; HONARPISHEH et al., 2025).

In summary, the media conditions used are highly heterogeneous, and there is no consensus on the optimal conditions. This diversity reflects the complexity of *in vitro* optimization and underscores the need for further research to develop standardized and effective protocols.

3.3. Neonatal islet-like clusters vs adult porcine islets

While donors for adult islet isolation are ideally 2-3 years old (STEFFEN et al., 2017), clusters from neonatal pancreas can be isolated within the first days of life (AREFANIAN et al., 2022). This results in significant cost differences, as younger donors can be produced quickly and at substantially lower costs. Given that donor animals must be genetically modified for transplantation into humans (BOTTINO et al., 2014; HAWTHORNE et al., 2014; KEMTER et al., 2018), this issue is exacerbated. Additionally, the isolation of islets from adult pancreas involves higher material costs and greater technical and personnel effort due to the more complex isolation technique, leading to significantly higher costs compared to pNPCs (STEFFEN et al., 2017). Despite the necessary *in vitro* maturation, pNPCs are relatively easy and cost-effective to generate. These factors not only impact costs

but also make neonatal islets scalable compared to adult islets (ELLIS et al., 2016).

Adult porcine islets have been shown to immediately restore normoglycemia in non-human primates (SHIN et al., 2015; SHIN et al., 2018). In contrast, pNPCs require several weeks to achieve functionality despite prior *in vitro* maturation (AREFANIAN et al., 2022; HONARPISHEH et al., 2025).

Although adult islets provide immediate functionality, and neonatal clusters exhibit higher resistance to hypoxia, it remains unclear which type is more advantageous in terms of long-term survival and function (NAGARAJU et al., 2015; KEMTER & WOLF, 2018)

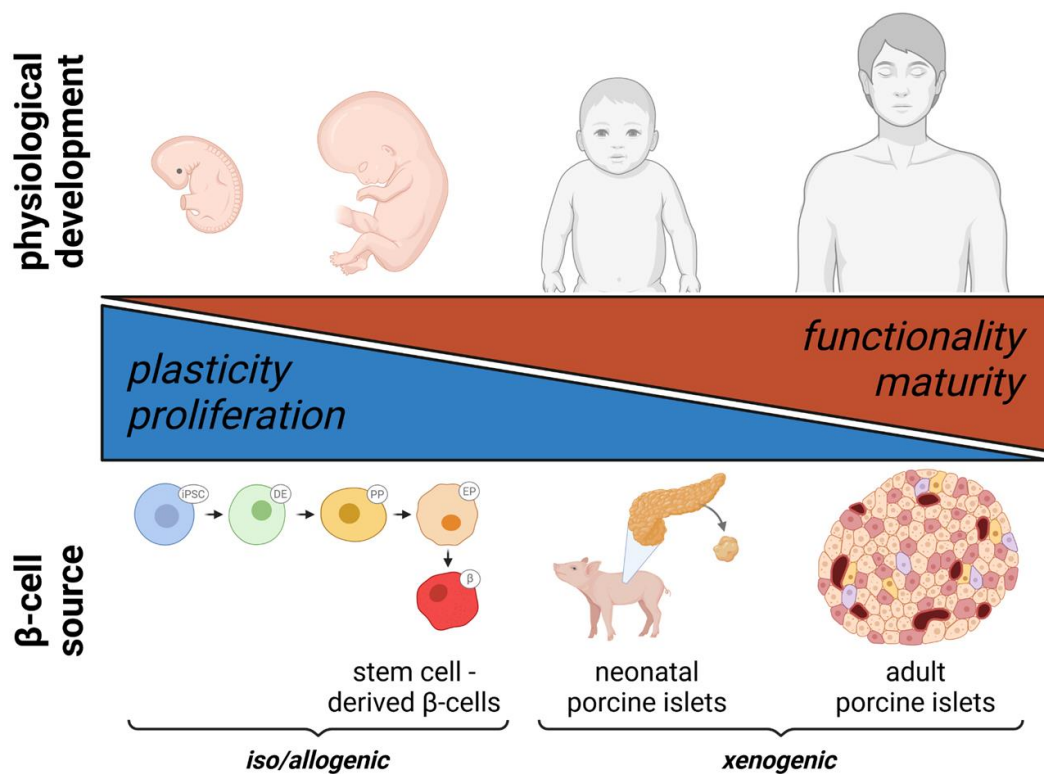


Figure 2: Schematic illustration of the relationship between cell plasticity & proliferation and functionality & maturity in the context of physiological development and β -cell sources for replacement therapy. Created with BioRender.com.

III. OBJECTIVES

This study aimed to elucidate the processes occurring during the *in vitro* maturation of clusters derived from porcine neonatal pancreas, which are essential for their functionality post-transplantation. The objectives were as follows:

1. Characterization of cellular dynamics of clusters isolated from neonatal pig pancreas throughout the culture period.
2. Evaluation of molecular characteristics of endocrine cells throughout culture.
3. Assessment of plastic processes involved in β -cell proliferation, neogenesis, and differentiation.

IV. ANIMALS, MATERIALS AND METHODS

1. Animals

All animal procedures were conducted according to the German Animal Welfare Act §4 Abs.3. All efforts were made to reduce the quantity of animals required for this study.

Three- to five-day-old piglets (German hybrid pigs) from a farm with consistent breeding genetics and environmental factors were used as organ donors.

2. Materials

2.1. Devices

Axioscan 7 Microscope Slide Scanner	Zeiss; Germany
Biorep Perifusion System (Peri 4.2)	Biorep Technologies; USA
BVC control Fluid aspiration system	VACUUBRAND GMBH + CO KG; Germany
Centrifuge 5804 R	Eppendorf SE; Germany
CO2 Incubator CB 260	Binder GmbH; Germany
CryoStar NX50	Thermo Fisher Scientific; USA
Embedding molds #10505	PLANO GmbH; Germany
Excelsior AS A82310100	Thermo Fisher Scientific; USA
FACS ARIA III	BD Bioscience; USA
Grant Sub 14 water bath	CLF; Germany
Heating Thermoshaker HTM	HTA-BioTec; Germany
Herasafe 2030i	Thermo Electron LED GmbH; Germany
Illumina NovaSeq6000	Illumina; San Diego
Incubator ED056-230V	Binder GmbH; Germany

Incubator ED056-230V	Binder GmbH; Germany
InoLab pH meter 7110	Thermo Fisher Scientific; USA
Lauda Aqualine AL12	LAUDA DR. R. WOBSEER GMBH & CO. KG; Germany
Leica TCS SP5 II	Leica Microsystems; Switzerland
Microm HM 325 rotary microtome	Thermo Fisher Scientific; USA
Microplate reader Spark	Tecan Austria GmbH; Austria
Microwave MS-196VUT	LG; South Korea
Milli-Q water system	Millipore; USA
Olympus microscope model BX43F	Olympus; Japan
Perifusion chamber	Biorep Technologies; USA
Pipets Pipetman	Gilson; USA
Spectrafuge 24D Microcentrifuge	Labnet International Inc.; USA
Stemi SV 6	Carl Zeiss AG; Germany
Stereo microscope SMZ-171	MOTICEUROPE, S.L.U.; Spain
TBS 88 Paraffin Embedding System	Thermo Fisher Scientific; USA
TES 99 modular paraffin embedding system	Medite Medical GmbH; Germany
Thermomixer 5436	Thermo Fisher Scientific; USA
Tissue cool plate COP 30	Medite Medical GmbH; Germany
Tissue float bath 1052	GFL; Germany
Vortexer MS1 minishaker	IKA-Works Inc.; USA

2.2. Consumables

10cm cell culture dish	Sarstedt; Germany
5 mL Polystyrene Tube, with Cell Strainer	Corning Incorporated; USA
Cover slips 24 x 40 mm	Epredia; USA
Embedding cassettes UniLink	Engelbrecht Medizin- & Labortechnik; Germany

Falcon 50 ml	Greiner Holding; Austria
HistoGel	Thermo Fisher Scientific; USA
Histoplast PE Paraffin	Epredia; Netherlands
Microtome blades S35	FEATHER Safety Razor Co Ltd.; Japan
Needles	Braun; Germany
Parafilm	Bemis; USA
Periclips	Biorep Technologies; USA
PERI-NOZZLE	Biorep Technologies; USA
Pipette tips (2 µL, 10 µL, 200 µL, 1000 µL)	Sarstedt AG & Co. KG; Germany
PluriStrainer Mini 40 µm	PluriSelect Life Science UG & Co.KG; Germany
Safe-Lock reaction tubes	Eppendorf; Germany
Serological pipettes (5 ml, 10 ml)	Sarstedt AG & Co. KG; Germany
StarFrost microscope slides	Engelbrecht Medizin- & Labortechnik; Germany
Stop tubing with connectors (PERI-TUBSET)	Biorep Technologies; USA
Syringes	Braun; Germany
Tissue-Tek O.C.T.	PLANO GmbH; Germany
Tubing (PERI-TUB-040)	Biorep Technologies; USA
Y connectors (Peri – FITTING -3)	Biorep Technologies; USA
2.3. Drugs	
Azaporc 40 mg/mL	Serumwerk Bernburg AG; Germany
Fentadon 50 µg/mL	Dechra; UK
Ursotamin 100 mg/mL	Serumwerk Bernburg AG; Germany

2.4. Chemicals and reagents

4',6-diamidino-2-phenylindole (DAPI)	Biotium; USA
7-Aminoactinomycin D (7-AAD) #A1310	Thermo Fisher Scientific; USA
BD Horizon Fixable Viability Stain 780	BD Bioscience; USA
Caustic soda (NaOH)	Carl Roth; Germany
Collagenase V #C9263	Sigma-Aldrich; USA
Disodium hydrogen phosphate (Na_2HPO_4)	Carl Roth; Germany
Eosin, 2%	Morphisto; Germany
Ethanol denatured, >99.8% (EtOH)	Carl Roth; Germany
Ethylenediaminetetraacetic acid (EDTA)	VWR; USA
Glycin	Carl Roth; Germany
Hematoxylin	Morphisto; Germany
Histokitt	Karl Hecht GmbH & Co KG; Germany
Hydrochloric acid 25% (HCl)	Carl Roth; Germany
Meyer's Hemalum	Sigma-Aldrich; USA
Sodium chloride (NaCl)	Carl Roth; Germany
Neutral serum	Biozol; Germany
Paraformaldehyde (PFA)	Carl Roth; Germany
Potassium chloride (KCl)	Carl Roth; Germany
Potassium dihydrogen phosphate (KH_2PO_4)	Carl Roth; Germany
Proteinase K	Dako; Denmark
Tris ($\text{C}_4\text{H}_{11}\text{NO}_3$)	Carl Roth; Germany
Tri-sodium citrate dihydrate ($\text{C}_6\text{H}_5\text{Na}_3\text{O}_7$)	Carl Roth; Germany
Triton X100	Carl Roth; Germany
TrypL Express	Thermo Fisher Scientific; USA
Tween20	Carl Roth; Germany
Xylol	VWR; USA

2.5. Kits

3,3'-diaminobenzidine (DAB) Substrate Kit (HRP), with Nickel	Vector Laboratories Inc.; USA
Chromium Single Cell 3' Reagent Kits v3.1	10x Genomics; USA
HTRF Insulin Ultra Sensitive Detection Kit	Cisbio Bioassays; Frankreich
Vectashield Vibrance	Vector Laboratories Inc.; USA

2.6. Buffers, Medium and Solutions

2.6.1. Pancreas procurement and cluster isolation and culture

Organ preservation solution

Custodiol (HTK)	Dr. Franz Köhler Chemie GmbH; Germany
100 U/mL penicillin-streptomycin #15140122	Gibco, Thermo Fisher Scientific; USA
2.5 µg/mL Amphotericin B #15290026	Gibco, Thermo Fisher Scientific; USA

Wash solution

Hanks' Balanced Salt solution (HBSS) #H6648	Sigma-Aldrich; USA
0.25% Bovine Serum Albumin #A9418	Sigma-Aldrich; USA
10 mM HEPES #15630056	Gibco, Thermo Fisher Scientific; USA
100 U/mL penicillin-streptomycin #15140122	Gibco, Thermo Fisher Scientific; USA

Adjust pH to 7.4

Collagenase solution

Hanks' Balanced Salt solution (HBSS) #H6648	Sigma-Aldrich; USA
10 mM HEPES #15630056	Gibco, Thermo Fisher

Scientific; USA

2 mg/mL Collagenase type V #C9263

Sigma-Aldrich; USA

Adjust pH to 7.4

Stop solution

Hanks' Balanced Salt solution (HBSS) #H6648

Sigma-Aldrich; USA

0.75% Bovine Serum Albumin #A9418

Sigma-Aldrich; USA

10 mM HEPES #15630056

Gibco, Thermo Fisher
Scientific; USA

100 U/mL penicillin-streptomycin #15140122

Gibco, Thermo Fisher
Scientific; USA

Adjust pH to 7.4

Culture medium

Ham's F10 #N6908

Sigma-Aldrich; USA

0.5% Bovine Serum Albumin #A9418

Sigma-Aldrich; USA

10 mM glucose #G7021

Sigma-Aldrich; USA

2 mM L-glutamine #G8540

Sigma-Aldrich; USA

50 μ M IBMX #I5879

Sigma-Aldrich; USA

10 mM nicotinamide #N0636

Sigma-Aldrich; USA

100 U/mL penicillin-streptomycin #15140122

Gibco, Thermo Fisher
Scientific; USA

1.6 mM CaCl_2 #C7902

Sigma-Aldrich; USA

2.6.2. Solutions for histology, immunostaining and perfusion

10x Phosphate-buffered salt solution (PBS), pH 7.4

79.5 g NaCl

Carl Roth; Germany

14.4 g $\text{Na}_2\text{HPO}_4 \cdot 2 \text{H}_2\text{O}$

Carl Roth; Germany

2.0 g KCl

Carl Roth; Germany

2.0 g KH_2PO_4 Carl Roth; Germany

In 1L Aqua bidest.

10x Tris-buffered salt solution (TBS), pH 7.6

83.33 g NaCl Carl Roth; Germany

60.57 g Tris Carl Roth; Germany

1 l Aqua bidest

Adjust to pH 7.6.

PBS-buffered 4% Paraformaldehyde (PFA), pH 7.4:

40 g Paraformaldehyde Carl Roth; Germany

100 mL 10x PBS

850 mL Aqua bidest

200 μl 5 M NaOH Carl Roth; Germany

Mix and dissolve with a magnetic stirrer at 50°C. Cool down to room temperature (RT), then adjust the pH to 7.4.

Add Aqua bidest to 1L. Store at 4°C.

Tris-EDTA-0.5% Tween20 buffer, pH 9.0 for immunohistochemistry (TRIS)

1.21 g Tris Carl Roth; Germany

2 mL 0.5 M EDTA (pH 8.0) VWR; USA

Adjust to pH 9.0. Add Aqua bidest to 1L. Add 0.5 mL Tween20

Acid ethanol

24.4 mL 100% EtOH Carl Roth; Germany

15.6 mL 25% HCl Carl Roth; Germany

Store at -20°C

Perm-block buffer

Permeabilisation buffer #00-8333-56 eBioscience, Thermo Fisher Scientific; USA

5% donkey Serum #P30-0101 PAN-Biotech GmbH; Germany

1% Bovine Serum Albumin #A9418

Sigma-Aldrich; USA

Donkey block

Phosphate buffered saline

10% FCS #F9665

Sigma-Aldrich; USA

0.1% Bovine Serum Albumin #A9418

Sigma-Aldrich; USA

3% donkey Serum #P30-0101

PAN-Biotech GmbH;
Germany

0.1% Tween20

Carl Roth; Germany

Krebs-Ringer buffer (KRB)

137 mM NaCl

Carl Roth; Germany

5.36 mM KCl

Carl Roth; Germany

0.34 mM Na₂HPO₄ · 2 H₂O

Carl Roth; Germany

0.81 mM MgSO₄

Carl Roth; Germany

1.26 mM CaCl₂ · 2 H₂O

Carl Roth; Germany

0.44 mM KH₂PO₄

Carl Roth; Germany

4.17 mM NaHCO₃

Carl Roth; Germany

10 mM HEPES

Carl Roth; Germany

0.1% BSA

Carl Roth; Germany

Adjust pH to 7.3.

2.7. Antibodies

Primary antibodies for Flowcytometry:

Mouse-anti-Cytokeratin 7 mAb #NBP3-12013 (1:1000)	Novus biologicals; UK
Mouse-anti-Glucagon mAb #565860 (1:50)	BD Bioscience; USA
Mouse-anti-Glucagon mAb #565891 (1:100)	BD Bioscience; USA
Mouse-anti-Insulin mAb #565689 (1:100)	BD Bioscience; USA
Mouse-anti-Ki67 mAb #570280 (1:800)	BD Bioscience; USA
Mouse-anti-Nkx6.1 mAb #563023 (1:50)	BD Bioscience; USA
Mouse-anti-Nkx6-1 mAb #567608 (1:25)	BD Bioscience; USA
Mouse-anti-PDX1 mAb #562161 (1:100)	BD Bioscience; USA
Mouse-anti-PDX1 mAb #563436 (1:50)	BD Bioscience; USA
Mouse-anti-Somatostatin mAb #566032 (1:200)	BD Bioscience; USA
Mouse-anti-Vimentin mAb #562337 (1:2000)	BD Bioscience; USA
Rabbit-anti-Synaptophysin pAb #17785-1-AP (1:4000)	Proteintech; USA
Sheep-anti-Neurogenin 3 pAb #AF3444 (1:200)	R&D Systems; USA

Primary antibodies for Immunohistochemistry:

Rabbit-anti-Amylase pAb #12540-1-AP (1:4000)	Proteintech; USA
--	------------------

Primary antibodies for Immunofluorescence:

Goat-anti-PPY pAb #SAB2500747 (1:300)	Sigma-Aldrich; USA
Guinea pig-anti-GCG pAb #M182 (1:4000)	Takara Bio; Japan
Mouse-anti-CK7 mAb #M7018 (1:200)	Dako; Denmark
Mouse-anti-INS mAb #I2018-2ML (1:400)	Sigma-Aldrich; USA
Mouse-anti-SST mAb #sc-55565 (1:800)	Santa Cruz Biotechnology; USA
Mouse-anti-Synaptophysin mAb #ab8049 (1:500)	Abcam; UK

Mouse-anti-Vimentin mAb #AMF-17b (1:400)	DSHB; USA
Rabbit-anti-INS mAb #3014 (1:400)	Cell Signaling Technology; USA
Rabbit-anti-KI67 mAb #ab16667 (1:300)	Abcam; UK
Rabbit-anti-Synaptophysin pAb #17785-1-AP (1:4000)	Proteintech; USA
Sheep-anti-NGN3 pAb #AF3444 (1:200)	R&D Systems; USA

Secondary antibodies

AF405 donkey-anti-rabbit IgG pAb #ab175649 (1:500)	Abcam; UK
AF488 donkey-anti-mouse IgG pAb #A21202 (1:500)	Invitrogen; USA
AF488 donkey-anti-rabbit IgG pAb #A21206 (1:500)	Invitrogen; USA
AF488 donkey-anti-sheep IgG pAb #713-546-147 (1:500)	Dianova; Germany
AF555 donkey-anti-goat IgG pAb #A21432 (1:500)	Invitrogen; USA
AF555 donkey-anti-mouse IgG pAb #A31570 (1:500)	Invitrogen; USA
AF555 donkey-anti-rabbit IgG pAb #A31572 (1:500)	Invitrogen; USA
AF647 donkey-anti-guinea pig IgG pAb #706-605-148 (1:500)	Dianova; Germany
AF647 donkey-anti-rabbit IgG pAb #A31573 (1:500)	Invitrogen; USA
DL755 donkey-anti-mouse IgG pAb #SA5-10171 (1:500)	Life technologies; Germany
HRP goat-anti-rabbit IgG pAb #111-035-046 (1:300)	Dianova; Germany

Isotype control antibodies:

BV421 mouse-anti-mouse IgG1, k isotype ctrl mAb #562438	BD Bioscience; USA
AF488 mouse-anti-mouse IgG2b, k isotype ctrl mAb #565383	BD Bioscience; USA
PE mouse-anti-mouse IgG1, k isotype ctrl mAb #554680	BD Bioscience; USA
AF647 mouse-anti-mouse IgG1, k isotype ctrl mAb #565571	BD Bioscience; USA
PerCP-Cy5.5 mouse-anti-mouse IgG1, k isotype ctrl mAb #550795	BD Bioscience; USA

2.8. Software

Biorender	BioRender Inc.; Kanada
CellSens Dimension	Olympus; Japan
DeepL Version 24.11.4.14424 (used for language and grammar revision)	DeepL GmbH; Germany
FACSDiva software v.6.1.3	BD Bioscience; USA
FlowJo v10.10	BD Bioscience; USA
GraphPad Prism 10.4.1	Graphpad Software; USA
ImageJ 1.54f	National Institute of Health; USA
Microsoft 365 Copilot (used for language and grammar revision)	Microsoft Corporation; USA
Microsoft Office Professional Plus 2019 (Version 1808)	Microsoft Corporation; USA
MotiConnect	Motic; Hongkong
perplexity 2.42.0 (used for literature search)	Perplexity AI Inc.; USA
QuPath 0.5.1	The University of Edinburgh; Scotland
SAS 9.4	SAS Institute Inc.; USA

3. Methods

3.1. Organ retrieval and cluster isolation and culture of porcine neonatal pancreatic organoids

Three- to five-day-old piglets (German hybrid pigs) were anesthetized by intramuscular injection of azaperone (4 mg/kg body weight (BW); Azaporc; Serumwerk Bernburg AG) and ketamine (20 mg/kg BW; Ursotamin; Serumwerk Bernburg AG). Analgesia was provided by intramuscular injection of fentanyl (10 µg/kg BW; Fentadon; Dechra). To ensure the procurement of high-quality donor tissue, euthanasia was performed via exsanguination. The pancreas was surgically excised within a maximum warm ischemia time of 10 min. Subsequently, the organs were preserved in organ preservation solution at 4°C, with a maximum cold ischemia time of 2 h.

All subsequent procedures were conducted under sterile conditions within a laminar flow hood or closed sterile sample tubes. Centrifugation was performed at 150 × g for 3 min at room temperature (RT) with reduced brake.

Connective, adipose, and lymphatic tissues were gently trimmed from the pancreata, transferred into cold wash solution, and mechanically cut into approximately 1 mm³ fragments. After a washing step with wash solution, tissue fragments were enzymatically digested with collagenase-V (Sigma-Aldrich) by manual shaking for 20 min at 37°C in a water bath. Digestion was terminated by adding stop solution, and the digest was gently homogenized by pipetting. The resulting cell suspension was passed through a 500 µm filter mesh and subsequently washed with wash solution.

Cell clusters were seeded in a Ham's F10-based medium (Table 2), initially cultured in T175 suspension flasks (30 mL per flask) from culture day 0-3 and subsequently transferred to 10 cm suspension dishes (10 mL per dish). Cultures were maintained at 37°C in a humidified atmosphere of 5% CO₂.

Isolation was performed by Christina Blechinger and Florentine Stotz.

Day of isolation was defined as day 0 of culture. Sampling for analysis was performed on days 0, 1, 3, and 9.

Table 2: Culture medium.

final conc.	Medium / Supplement
	Ham's F10
0.5%	BSA
10 mM	Glucose
10 mM	Nicotinamid
50 μ M	IBMX
2 mM	Glutamine
1.6 mM	CaCl ₂ x2H ₂ O

A complete media exchange was performed on culture days 1 and 3. Therefore, cell clusters were collected from the culture vessels and washed twice with washing solution before resuspension in fresh medium. On days 5, 7, and 9, a half-media exchange was conducted by removing half of the culture medium and replacing it with fresh medium. All isolates were processed separately during media changes and subsequent analyses.

3.2. Cell cluster size and volume

To quantify cell cluster volume, one-quarter of the total isolation mass from three independent isolates was cultured separately. From day 3 to day 9, cultures were imaged daily using a stereomicroscope (SMZ-171; MOTICEUROPE). Imaging was not performed before day 3 due to the known loss of exocrine tissue and the impracticality of capturing a large number of cell clusters at earlier time points while ensuring a sufficient number remained at the end of the culture period.

Image analysis was conducted using a custom automated ImageJ script, which measured the cell cluster areas. Based on the measured area, the cluster radius was calculated, and cell clusters were categorized into size intervals of 50 μ m, ranging from 50 μ m to >350 μ m. Corresponding to human islet procedures, cluster volume was subsequently determined using standard conversion factors for islet equivalents (IEQ) (Table 3). One aggregate equivalent (AEQ) corresponds to an average-sized human islet with a diameter of 150 μ m.

Table 3: Conversion factors for islet/aggregate equivalents (IEQ/AEQ).

islet diameter	IEQ conversion factor
50-100	0.167
101-150	0.648
151-200	1.685
201-250	3.5
251-300	6.315
301-350	10.352
>350	15.833

3.3. Flow cytometry

Cell clusters were randomly picked on the day of isolation (day 0) and during media changes on days 1, 3, and 9. Between all processing steps, cells were washed twice with wash solution. Centrifugation was performed at $300 \times g$ for 3 min at RT.

Cell clusters were enzymatically dissociated using TrypLE Express (Gibco) in a thermoshaker at 400 rpm and 37°C for 12-15 min. Gentle pipetting with a coated pipette tip every 2–3 min facilitated digestion into single cells, which was monitored using a stereomicroscope (Stemi SV 6, Zeiss). Digestion was terminated by adding ice-cold wash solution, and the resulting single-cell suspension was passed through a 40 μm filter. A small aliquot was retained for blanks and controls.

The remaining cells were stained with a fixable viability dye (BD Biosciences) at a 1:2000 dilution for 30 min at 4°C, followed by fixation with 4% PFA for 20 min at 4°C. Cells were subsequently stored in 1% BSA in HBSS until analysis. After sample collection, cells were counted, and 200,000 cells were used per staining condition in a final volume of 100 μL . To block unspecific binding and permeabilize cells, cells were resuspended in perm-block buffer and incubated for 20 min at 4°C.

Primary antibody staining was performed in perm-block buffer overnight at 4°C using antibody combinations and concentrations described in (Table 4). Secondary antibody staining was conducted for 1 h at 4°C. All antibodies were titrated for optimal concentrations and specificity validated using isotype or secondary-antibody controls.

Before analysis, cells were passed through a 35 μm filter into polystyrene tubes. Compensation for multicolor flow cytometry panels was performed using unstained and single-stained compensation controls in BD FACSDiva™ Software. Per sample, 10,000–50,000 events were acquired using BD FACSAria™ III (85 μm nozzle).

Raw data were analyzed using FlowJo. Gating strategies were based on live, single cells, pre-gated using forward scatter and side scatter (FSC-A vs. SSC-A, SSC-H vs. SSC-W, FSC-H vs. FSC-W), and exclusion of dead cells.

Table 4: Staining panels for flow cytometry. * indicates primary fluorophore labeled antibody was used; # indicates fluorophore labeled secondary antibody was used.

Antigen		Fluorophore	Dilution	Company	Order-ID
Synaptophysin	#	AF647	1:4000	Proteintech	17785-1-AP
Cytokeratin 7	*	AF405	1:1000	Novus biologias	NBP3-12013AF405
Neurogenin 3	#	AF488	1:200	R&D Systems	AF3444
Vimentin	*	PE	1:2000	BD Bioscience	562337
Ki67	*	RB705	1:800	BD Bioscience	570280
Synaptophysin	#	AF647	1:4000	Proteintech	17785-1-AP
Insulin	*	AF647	1:100	BD Bioscience	565689
Nkx6-1	*	AF488	1:25	BD Bioscience	567608
PDX1	*	PE	1:100	BD Bioscience	562161
Insulin	*	AF647	1:100	BD Bioscience	565689
Glucagon	*	BV421	1:100	BD Bioscience	565891
Somatostatin	*	AF488	1:200	BD Bioscience	566032
Nkx6.1	*	PE	1:50	BD Bioscience	563023
PDX1	*	PerCP-Cy5.5	1:50	BD Bioscience	563436
Synaptophysin	#	AF405	1:4000	Proteintech	17785-1-AP
Insulin	*	AF647	1:100	BD Bioscience	565689
Glucagon	*	PE	1:50	BD Bioscience	565860
Somatostatin	*	AF488	1:200	BD Bioscience	566032

3.4. Immunostaining of sections

For paraformaldehyde-fixed paraffin-embedded (PFPE) samples, tissue was fixed in 4% paraformaldehyde at 4°C for 24 h, while cultured cell clusters were fixed for 1 h under the same conditions. Cell clusters were subsequently embedded in

HistoGel (Thermo Fisher Scientific) according to the manufacturer's instructions. Fixed tissue and embedded cell clusters were processed using an automated tissue processor (Excelsior AS; Thermo Fisher Scientific) and embedded in paraffin (Epredia). Paraffin blocks were sectioned at 3 μm using a microtome (HM 325; Thermo Fisher Scientific), mounted on microscope slides (Engelbrecht Medizin- & Labortechnik) and stored at 37°C until staining.

For cryopreserved samples, tissue was snap-frozen in Tissue-Tek O.C.T. (PLANO GmbH) and stored at -80°C. Cultured cell clusters were fixed in 4% paraformaldehyde for 30 min at 4°C, followed by cryopreservation in a sucrose gradient (7.5% for 1 h at RT, 15% for 1 h at RT, and 30% overnight at 4°C). The cryopreserved cultured cell clusters were embedded in Tissue-Tek O.C.T. (PLANO GmbH) and stored at -80°C. Cryo blocks were sectioned at 10 μm using a CryoStar NX50 (Thermo Fisher Scientific), mounted on microscope slides (Engelbrecht Medizin- & Labortechnik), and fixed in 4% paraformaldehyde for 10 min at 4°C.

Histological examination of cultured clusters and age-matched tissue was performed, including hematoxylin and eosin staining, immunohistochemistry and immunofluorescence.

All immunohistochemical stainings and the four-hormone immunofluorescence panel were performed on PFPE samples, while all other Immunofluorescence panels were conducted on cryopreserved samples.

3.4.1. Hematoxylin and eosin staining

The slides were deparaffinized with xylol (20 min) and rehydrated in decreasing ethanol row (2 x 100%, 2 x 96%, 1 x 70% ethanol, 2 min each). The slides were then washed with aqua bidest for 10 sec. Staining was done with hematoxylin (Morphisto) for 5 min, followed by washing with floating tap water for 5 min. Differentiation was carried out using 0.5% HCl-EtOH for 2 sec, followed by another wash with floating tap water for 5 min. Counterstaining was performed with 2% eosin (Morphisto) for 2 min, followed by washing with aqua bidest for 10 sec. Dehydration was done using increasing ethanol row (1 x 70%, 2 x 96%, 2 x 100% ethanol, 2 min each). Clearing was performed with xylol for at least 5 min. Slides were mounted using Histokitt (Karl Hecht GmbH & Co KG).

3.4.2. Immunostaining with PFPE samples

The slides were deparaffinized with xylol (2x for 20 min) and rehydrated in decreasing ethanol row (100%, 96%, 70% EtOH, 10 sec each). After washing with aqua bidest (10 sec), antigen retrieval was performed using TRIS buffer (20 min sub-boiling). Slides were cooled for 30 min on ice and washed with TBS (10 min). Blocking was performed with 5% neutral serum in TBS (1 h at RT). The primary antibody was incubated overnight at 4°C in TBS. After washing with TBS (2x for 10 min), the secondary antibody was incubated for 1 h at RT in TBS, followed by washing with TBS (2x 10 min).

For immunohistochemistry, staining was performed with DAB (Vector Laboratories Inc.), followed by washing with tap water (5 min). Counterstaining with Meyer's Hemalum (Sigma-Aldrich) (~30 sec) was followed by washing with tap water (5 min) and aqua bidest (10 sec). Dehydration was done using increasing ethanol row (1 x 70%, 2 x 96%, 2 x 100% ethanol, 2 min each). Clearing was performed with xylol for at least 5 min. Slides were mounted using Histokitt (Karl Hecht GmbH & Co KG).

For immunofluorescence stainings, nuclear staining was performed with DAPI (Biotium) at a dilution of 1:500 in PBS for 20 min. Finally, the slides were washed once with PBS and mounted using Vectashield Vibrance (Vector Laboratories Inc.).

3.4.3. Immunostaining with cryopreserved samples

The slides were first warmed to RT for 30 min. Following this, they were washed for 10 min in 1x PBS. The sections were then permeabilized using a solution of 0.25% Triton X-100 (Carl Roth) in PBS with 0.1 M glycine (Carl Roth) for 15 min at RT. After permeabilization, the slides were washed three times for 5 min each with PBS-Tween 0.1% (PBS-T). To block unspecific binding, the slides were incubated with donkey block for 1 h at RT. The primary antibody was then applied in donkey block and incubated for 48 h. Post-incubation, the slides were washed three times for 10 min each with PBS-T. Subsequently, the secondary antibodies were applied at a dilution of 1:500 in donkey block and incubated for 1 h at RT. The slides were then washed twice for 10 min each with PBS-T, followed by a single wash for 10 min with PBS. For nuclear staining, the slides were incubated with DAPI (Biotium)

at a dilution of 1:500 in PBS for 20 min. Finally, the slides were washed once with PBS and mounted using Vectashield Vibrance (Vector Laboratories Inc.).

3.5. **scRNA-seq**

Two experiments, each involving three isolates, were conducted. All isolates were cultured separately, and clusters were collected for single-cell ribonucleic acid (RNA) sequencing (scRNA-seq) on culture days 0, 1, 3, and 9. These experiments were carried out in collaboration with the scRNA-seq unit at the Institute of Diabetes and Regeneration Research (Prof. Heiko Lickert) at the Helmholtz Center Munich.

3.5.1. **Sample preparation**

Cell clusters were enzymatically dissociated using TrypLE Express (Thermo Fisher Scientific) in a water bath at 37°C for 12-15 min. Gentle pipetting with a coated pipette tip every 2-3 min facilitated digestion into single cells. Digestion was terminated by adding ice-cold wash solution, and the resulting single-cell suspension was passed through a 40 µm filter. Cells were stained with 7-Aminoactinomycin D (7-AAD) (Thermo Fisher Scientific) and sorted for living cells using a BD FACSAria III. Sorting was performed by Anika Böttcher and Mireia Molina van den Bosch.

3.5.2. **Library preparation and sequencing**

The following steps were performed by Michael Sterr and Ines Kunze

Cells were then washed with PBS containing 2% fetal calf serum (FCS) and diluted to a final concentration of ~1,000 cells/µl in PBS containing 2% FCS. After quality control and counting, the cell suspension was immediately used for scRNA-seq library preparation with a target recovery of 10,000 cells.

Libraries were prepared using the Chromium Single Cell 3' Reagent Kits v3.1 (10x Genomics, 1000268) according to the manufacturer's instructions. Libraries were pooled and sequenced on an Illumina NovaSeq6000 with a target read depth of 50,000 reads/cell.

3.5.3. Improved genome annotation for *Sus scrofa*

All following steps of scRNA-seq data processing were performed by Minas Schwager

As the gene annotation for *Sus scrofa* is incomplete, Beiki et al. (BEIKI et al., 2019) generated an annotation for the pig genome by integrating poly (A) selected single-molecule long-read isoform sequencing (Iso-seq) and Illumina (short read) RNA sequencing (RNA-seq). By combining these transcripts generated by Beiki et al. with the latest Ensembl annotation (version 101), a new annotation for *Sus scrofa* was created. The data provided by Beiki et al. (iso-seq annotation) was downloaded via <https://github.com/hamidbeiki/Porcine-PacBio> and annotated with the transcripts with gffcompare (PERTEA & PERTEA, 2020) using the Ensembl version 101 as reference. Then, “pseudogene” and “processed_pseudogene” biotypes genes were removed from the Ensembl annotation and the associated same strand transcripts from the iso-seq annotation were added to the Ensembl annotation. Furthermore, the gene bodies were extended if required. If a transcript was added, -iso was added as a suffix to the respective gene ID. Additionally, an “extension gene” downstream of the gene body was added, where its length was defined by the maximum possible region of 1-10kb (in 1kb steps) that does not overlap with any other same strand gene. The extension genes were named by adding the suffix -ext’x’kb to the name of the original genes, whereby ‘x’ stands for the integer length of the addition from 1-10.

In the end, the final gene counts were obtained by summing the -iso and -ext’x’kb versions of each gene.

3.5.4. Pre-processing of droplet-based scRNA-seq data

The pre-processing of the data was performed using Python 3.8.12 and the Scanpy package (WOLF et al., 2018) as described below. All samples were processed separately, and filtering thresholds were set individually for each sample.

3.5.4.1. Data preparation

The raw data obtained from Cell Ranger was pre-filtered by using the Scanpy `pp.filter_cells` and `pp.filter_genes` function, to remove cells with less than 10 count and genes detected in less than 10 cell.

3.5.4.2. Ambient gene detection

The R package DropletUtils (LUN et al., 2019) was used in R 4.3 for the detection of ambient genes. The p-value cutoff for ambient genes was set to 0.00065 after visual inspection. These genes were not removed from the analysis but marked as being ambient, as they could still hold informational value.

3.5.4.3. Empty Droplets

To identify empty droplets, DropletUtils was used in the same R version 4.3 as above. The output obtained from DropletUtils was intersected with the "barcodes.tsv" available from the "filtered_feature_bc_matrix" provided by the Cell Ranger pipeline and only the intersection between these two methods was counted as real cells.

3.5.4.4. Quality Control

Quality control and cell filtering were done according to published best practice guidelines (LUECKEN & THEIS, 2019). In brief, cells with very low or high number of counts were excluded, as well as cells with very low numbers of genes. In addition, cells with a high fraction of mitochondrial genes were excluded. As the mitochondrial genome of *Sus scrofa* is also not fully annotated, the threshold was set lower than for samples from other organisms.

3.5.4.5. Doublet detection

For the detection of doublets, droplets that contain two or more cells, a total of 5 different programs were used. In this process, each cell received a score between 0 and 5, depending on how many of the programs used identified it as a doublet. The programs used in this step were Scrublet (WOLOCK et al., 2019) with an expected_doublet_rate of 0.9 and a manual threshold of 0.4 and DoubletDetection (GAYOSO et al., 2019) with a parameter of p_thresh=1e-6 and voter_thresh=0. In R 4.3 scDbtFinder (GERMAIN et al., 2021) with a dbr of 0.1, scds (BAIS & KOSTKA, 2020) with a manual set cut-off of 0.8 and DoubletFinder (MCGINNIS et al., 2019) with default parameters were used. The thresholds for the doublets were set relatively permissible. At this step, the doublets identified were scored and added to the dataset as a category, but not removed from the analysis.

3.5.4.6. Concatenation and normalization

After doublet detection the samples were concatenated. For genes the intersection between the samples was kept, meaning, that genes missing in one sample lead to the loss of said genes in all other samples. The thus concatenated object was then normalized to account for differences in sequencing depth using the package `scran` in R 4.3 (LUN et al., 2016). Subsequently, the values were log-transformed ($\log(\text{expr} + 1)$).

3.5.4.7. Integration

The samples were integrated using `scvi-tools` (GAYOSO et al., 2022). First, the top 4,000 highly variable genes (HVGs) were identified using `Scanpy` with "seurat" selection flavor and each individual sample as batch. Then genes that were earlier marked as ambient genes (see section 2. Ambient gene detection) were then removed from the HVGs. Next, a `scvi` model was trained on the filtered HVGs with the parameters as follows: `batch_key = "sample"`, `layer = "raw_counts"`, 20 latent dimensions and 256 hidden layers, `gene_batch` as dispersion, `zinb` as `gene_likelihood` and a normal latent distribution.

3.5.4.8. Single-cell manifolds and visualization

For the generation of a Uniform Manifold Approximation and Projection (UMAP) (BECHT et al., 2018), a neighborhood graph of the individual cells was computed using the latent representation of the dataset that was used for the integration on the full dataset containing all genes, the `pp.neighbors` function in the `Scanpy` implementation with `n_neighbors=25`, `n_pcs = 20` and `metric=correlation`. Then the UMAP was calculated with `Scanpy` using the default parameters.

3.5.4.9. Doublet Removal

To exclude the doublets identified earlier from further analysis, a high-resolution `leiden` clustering (BECHT et al., 2018), as implemented in `Scanpy`, was performed (`resolution = 2`). Clusters that had more than 70% of the cells identified as doublets by at least one method, and more than 30% identified as doublets by at least two methods were excluded from the further analysis. Next, all individual cells that were identified as doublets by three or more methods were excluded. Afterwards, the UMAP was recalculated using the `Scanpy` standard parameters.

3.5.4.10. Clustering and Cell Type annotation

The package clustree (ZAPPIA & OSHLACK, 2018) was used in R 4.3 to compare different resolutions of leiden clustering. After visual inspection, a resolution of 1.3 was chosen for the annotation. Cycling cells were identified using the Scanpy implementation `tl.score_genes_cell_cycle` to calculate gene scores associated with the S and G2M phase of the cell cycle respectively (SATIJA et al., 2015). The cell types were annotated on the basis of the leiden cluster and known marker genes which were scored using the Scanpy function `tl.score_genes`.

3.5.4.11. Differential gene expression

Differential gene expression between the different cultivation days were compared using Delegate, a wrapper for the R package edgeR in the Version 3.40.2. First pseudo-bulks were generated by summing the raw counts per sample, whereas samples with less than 30 cells were excluded and a total number of 3 pseudoreplicates were generated. The threshold for the p-value, fold-change an expression was set automatically. The gene set enrichment analysis was done using Erichr.

3.6. **Perifusion Assay for Dynamic Glucose-Stimulated Insulin Secretion**

The perifusion of clusters for dynamic glucose-stimulated insulin secretion assays was conducted in collaboration with Libera Valla, due to the delicate nature of sample and machine handling. This system enables continuous perifusion of cell clusters in perifusion chambers with varying fluids at 37°C and automated sampling of their metabolic products by collecting eluates from the chambers.

3.6.1. **Machine preparation**

Tubing was mounted onto a perifusion system with automated tray handling (Peri 4.2; Biorep Technologies). Cassettes with tubing were clipped onto the peristaltic pump, and unused channels were blocked with dead-end tubing to prevent leakage. Pre-heated perifusion solutions were placed in the tube holder unit. The system was heated to 37°C, except for the tray holder, which was maintained at 4°C, and then flushed.

3.6.2. Sample equilibration and perfusion experiment

After 2 h of equilibration at 37°C in a humidified atmosphere of 5% CO₂ in Krebs-Ringer buffer (KRB) with 3 mM glucose, 100 cell clusters per sample were placed into perfusion chambers (Biorep Technologies) and connected to the system. Pre-priming and priming of all tubes were done to eliminate air bubbles and fill the tubing completely with perfusion solution. Once the protocol started, the system was monitored to ensure proper filling of the chambers without air bubbles. The system was maintained at 37°C, except for the sample tray, which was kept at 4°C.

Cultured clusters were perfused at a flow rate of 100 µL/minute. Samples were collected in 96-well plates at 120-second intervals. Clusters were flushed for 60 min with 3 mM glucose KRB to equilibrate them to the new environment. Then, clusters were perfused with KRB buffer containing 3 mM glucose for 10 min, followed by 30 min with 16.7 mM glucose, 30 min with 3 mM glucose, 20 min with 16.7 mM glucose and 60 mM KCl, and finally 10 min with 3 mM glucose. After perfusion, clusters were gently removed from the columns and transferred to 500 µL acid ethanol. All samples were frozen at -20°C until assayed for insulin content using an ultra-sensitive insulin HTRF assay. Samples were analyzed according to the manufacturer's instructions.

3.7. Statistics

The statistical analysis was performed with the support of Eckhard Wolf.

Longitudinal data for proportions of positive gated events, median fluorescence intensity (MFI) for fluorophores, and side scatter area or height (SSC/A, SSC/H) from flow cytometry were analyzed using a general linear mixed model (GLM) (PROC MIXED, SAS 8.2). The model accounted for the effects of batch (n=3), replicate within batch (n=3), timepoint (culture days 0, 1, 3, and 9), and the interaction between batch and timepoint. Means and standard errors of means (SEM) were calculated for each timepoint and compared individually using the general linear mixed model.

Data for cell-type groups at specific timepoints were also analyzed using GLM, considering the effects of batch (n=3), replicate within batch (n=3), cell-type group, and the interaction between batch and cell-type group. Means and SEM

were calculated for each timepoint and compared individually using the GLM.

Additionally, data on cell cluster size distribution and volume were analyzed using GLM, accounting for the effects of replicate ($n=3$), timepoint or cluster size, and their interaction. Means and SEM were calculated for each timepoint or cluster size and compared individually using the GLM.

V. RESULTS

1. From pancreatic aggregates to islet-like cell clusters

Piglets are born with a functionally immature pancreas, where endocrine cells are predominantly solitary or assembled in small clusters, with no endocrine cell clusters resembling the typical morphology of islets of Langerhans (NAGAYA et al., 2019). Cell clusters isolated from a newborn pancreas require a recovery and maturation culture period before responding to a glucose stimulus with insulin secretion *in vitro* and achieving normoglycemia after transplantation into a diabetic recipient (JIMENEZ-VERA et al., 2015).

A commonly used medium for this *in vitro* maturation period is based on Ham's F10, supplemented with glucose, IBMX, BSA, L-glutamine, and nicotinamide. This medium was developed alongside the isolation procedure of clusters from porcine neonatal pancreas by Korbitt et al. (KORBUTT et al., 1996). The optimal culture duration is reported to be 7–12 days (JIMENEZ-VERA et al., 2015; ELLIS et al., 2016; AREFANIAN et al., 2022).

To improve this product for xenotransplantation, a more detailed understanding of the cellular dynamics and molecular changes during the *in vitro* culture period is essential. Therefore, these aspects were investigated in Ham's F10-based medium over a culture duration of 9 days, as outlined in the following chapters.

1.1. Significant reduction in cell cluster volume and changes in size distribution during culture period

Mass loss is a common phenomenon observed during the recovery and maturation period of porcine neonatal pancreatic clusters (pNPCs). Pellet-volume per isolate drastically decreases, especially in the first 3 days of culture. To evaluate mass loss followed by this initial phase, cluster volume - measured in Aggregate Equivalent (AEQ; 1 AEQ corresponds to a cell aggregate with a diameter of 150 μm , corresponding to Islet Equivalent (IEQ) in human allotransplantation, based on an average-sized human islet) - was quantified using stereomicroscopy and automated image analysis. Due to the distinct mass loss and

the limitation in imaging large numbers of clusters at once, mass loss was first evaluated from day 3 onwards.

On average, the volume decreased significantly from 43,000 AEQ on culture day 3 to 13,000 AEQ on day 9 (general linear mixed model (GLM); $p < 0.0001$), corresponding to a volume loss of 71% (**Figure 3** and **Table 5**). Following a substantial initial loss in early culture, with daily losses of up to 28%, the relative daily volume loss decreased and showed signs of plateauing towards the end of the culture period, stabilizing at approximately 10%. It should be noted that quantification might be underestimated in early culture due to the presence of many clusters in a confined space, resulting in potential overlap.

Table 5: Distinct loss of cluster volume of pNPCs between culture days 3 and 9. Absolute cluster volume is measured in AEQ (corresponds to a cell cluster with a diameter of 150 μm). Relative daily loss is the loss compared to the previous day.

day	absolute volume (in AEQ)		relative daily loss (in %)	
	Mean	SEM	Mean	SEM
3	43064	2259		
4	34464	1466	19.89	0.88
5	25319	800	26.47	0.88
6	19351	867	23.61	1.7
7	15673	876	19.09	0.89
8	14003	619	10.54	1.05
9	12619	866	10.07	2.44

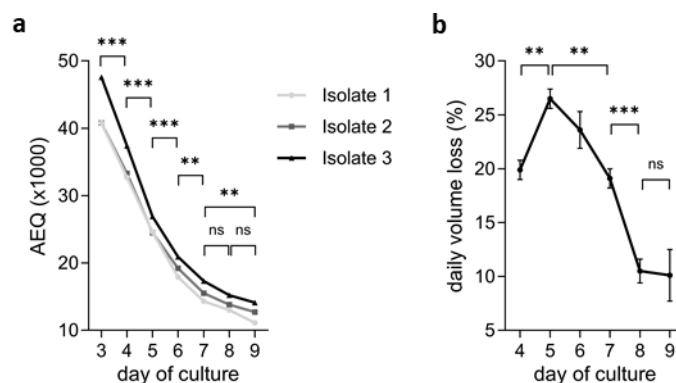


Figure 3: Distinct loss of cluster volume between culture days 3 and 9. **a:** absolute volume per isolate in 1,000 AEQs; 3 biological replicates. **b:** loss of volume compared to previous day per isolate; all values are means, error bars indicate SEM, $n=3$. GLM: * $p < 0.05$, ** $p < 0.01$, *** $p < 0.001$.

With increasing cluster size, especially above 150 μm , oxygen and nutrient supply

by diffusion is insufficient and below the demand of the cells in the cluster center (KOMATSU et al., 2017). Therefore, the size distribution of pNPCs throughout the culture period was examined in size categories of 50 μm , ranging from 50 to >350 μm .

Throughout the entire culture period, the size distribution of pNPCs was heterogeneous (**Figure 4**). The number of clusters in each size category decreased significantly throughout the culture period (day 3 vs day 9: $p < 0.0001$) (**Figure 4a**). Small clusters with a diameter of less than 100 μm were the predominant size, comprising approximately 30% of all pNPCs present between days 3 and 9 (**Figure 4b**). Examining the proportion of each size category relative to the total particle count (relCount - **Figure 4b**) and the total volume (relVolume - **Figure 4c**) from days 3 to 9 of culture reveals the following observations. Due to larger clusters containing more cells, the relVolume differed from the relCount within the size categories. Although most pNPCs were smaller in size, the majority of the cluster volume (relVolume) was found in large pNPCs (>350 μm), starting at 20% on day 3, increasing to 40% by day 5, and plateauing at a maximum of 45% by the end of the culture period. The relCount and relVolume in all other categories either decreased or did not significantly change.

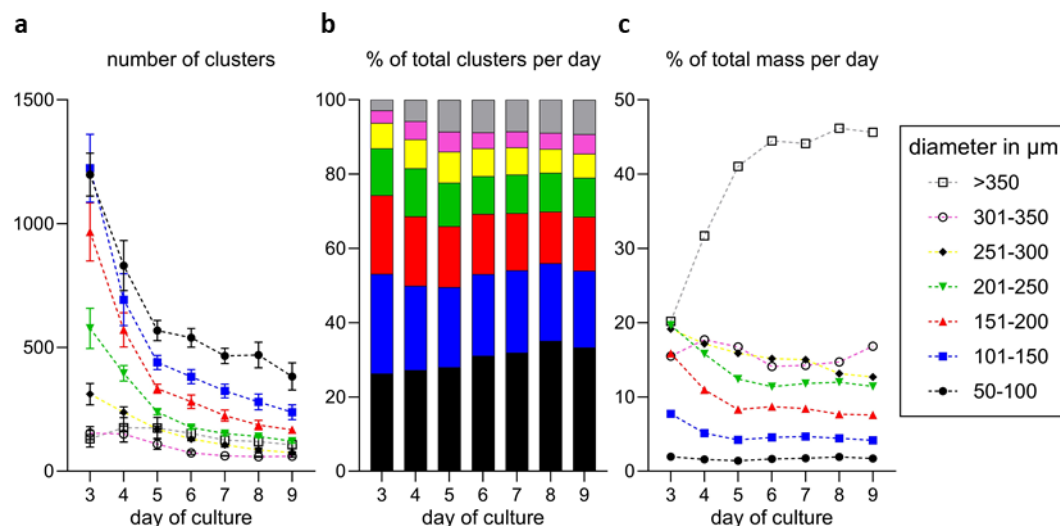


Figure 4: Dynamic of cluster size categories and corresponding volume between culture days 3 and 9. **a:** Number of clusters per size category. **b:** Proportion per cluster size category on total cluster number per day (relCount). **c:** Proportion per cluster size category on total volume per day (relVolume). Colors represent the size categories as indicated. $n=3$, error bars indicate SD.

1.2. **Gross morphology of pNPCs during the cultivation period: From structural integrity to cellular adaptation**

To gain a general impression of morphology, native pNPCs were examined by stereomicroscopy, and fixed clusters were stained with Hematoxylin and Eosin (H&E), both directly after isolation of clusters (culture day 0) and on culture days 1, 3, and 9.

Consistent with the particle analysis, stereomicroscopy analysis, and histological examination by H&E staining of cluster sections confirmed a heterogeneous size distribution of pNPCs throughout the culture period (**Figure 5**). On the day of isolation, pNPCs consisted of irregular cell clusters with a grape-shaped surface and of numerous solitary cells (**Figure 5a**). Within the clusters, morphological structures were apparent resembling acini and ducts from neonatal pig pancreas (**Figure 5b** and **c**). By day 1 after isolation, pNPCs exhibited a smooth surface with a compact, homogeneous appearance and a round to oval shape. Solitary cells and cell debris were largely removed during the washing step of the media change. Initial signs of cell death became apparent, characterized by pyknosis (nuclear shrinkage) and karyorrhexis (nuclear fragmentation). On day 3, an increased number of cells showed signs of cell death, and areas with accumulated debris from dead cells started to develop. Larger clusters seemed more likely to be affected by cell death. Despite these changes, pNPCs remained mostly compact and roundish. By day 9, numerous areas with dying cells or debris were present (**Figure 5b** and **c**).

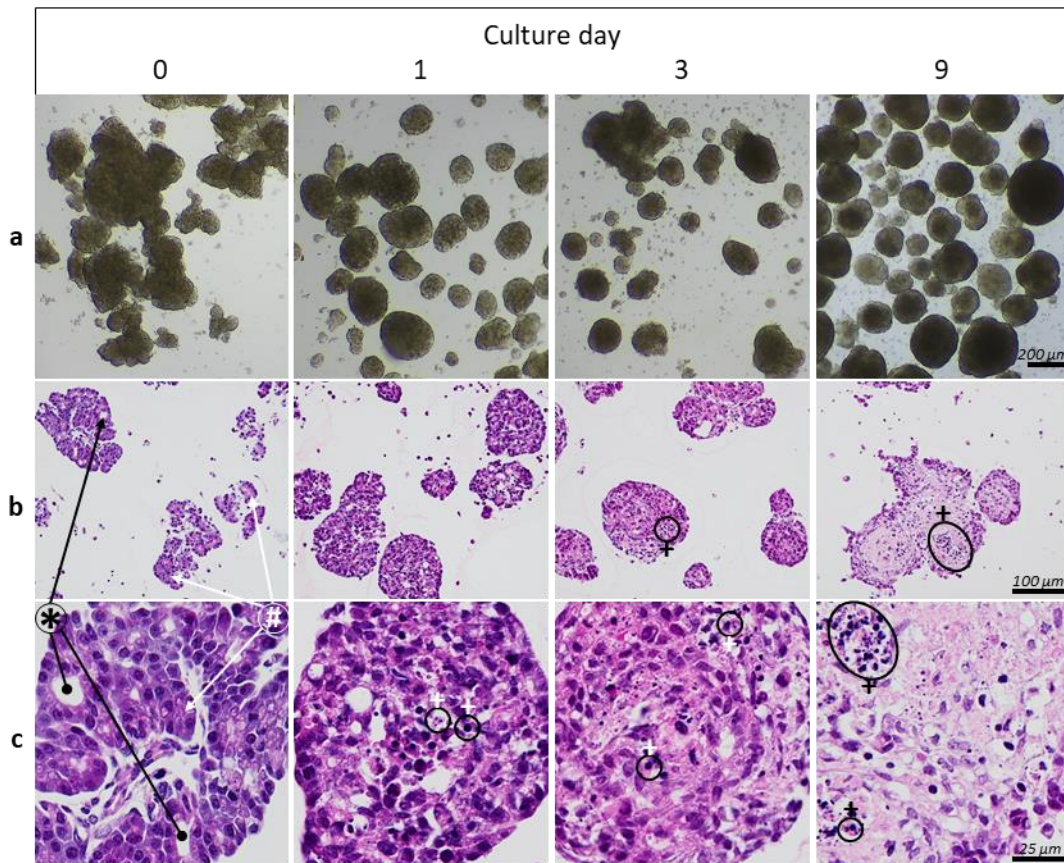


Figure 5: Morphology of pNPCs on culture days 0, 1, 3, and 9. **a:** Stereomicroscopic images of native clusters, scale bar 200 μm . **b** and **c:** H&E staining of cluster section. **b:** General view, scale bar 100 μm . **c:** Detailed view, scale bar 25 μm . Typical acinus-structures are indicated by #, and ductal by *, and nuclear signs of cell death by +.

1.3. Early pNPCs consist of all pancreatic cell types

To assess the cell type composition of pNPCs during the early culture period, immunostainings of pNPCs on culture days 0 and 1 were performed for amylase (AMY, a marker for acinar cells), cytokeratin 7 (CK7, a marker for ductal cells), vimentin (VIM, a marker for mesenchymal and endothelial cells), and synaptophysin (SYP, a marker for endocrine cells).

Immunostaining of pNPCs confirmed the presence of AMY⁺, CK7⁺, VIM⁺, and SYP⁺ cells, both at day 0 and day 1 (**Figure 6**). Of note, staining intensities showed high variability and cell morphology that was distinctly different to findings in pancreatic tissue of age matched pigs.

Staining for AMY showed low staining intensity on culture day 0 and uncommon staining pattern on day 1. Both might be a sign for acinar cells releasing their digestive enzymes (**Figure 6a**).

In both, tissue and cultured clusters on days 0 and 1, positive cells for SYP, CK7, and VIM were present (**Figure 6b**).

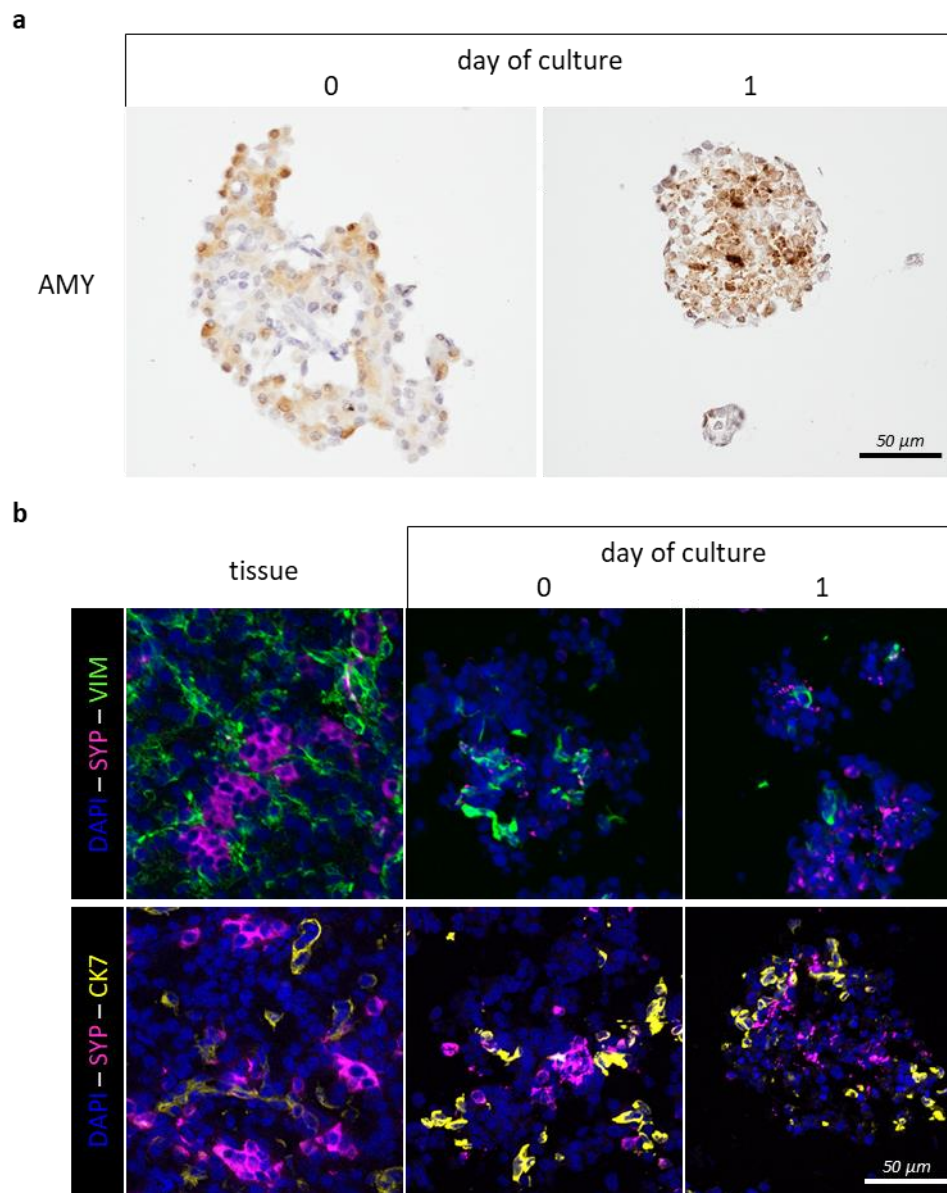


Figure 6: Immunostaining for acinar, ductal mesenchymal, and endocrine cells in pNPCs on culture days 0 and 1. **a:** Immunohistochemistry staining for AMY of pNPCs. **b:** Immunofluorescence staining for SYP (magenta), VIM (green), and CK7 (yellow) of pancreatic tissue of age-matched animals and cultured pNPCs; nuclei are stained with DAPI (blue); scale bar 50 μ m.

In the early stage of culture, as expected, cells exhibited no double-positivity for SYP, CK7, and/or VIM (**Figure 7b**). No significant differences were observed in the proportions of endocrine and ductal cells between culture day 0 and day 1 by flow cytometry (SYP⁺ mean \pm SEM: d0=13.3 \pm 1.2%, d1=11.6 \pm 3.1%; GLM: p=0.5759; CK7⁺SYP⁻ mean \pm SEM: d0=6.6 \pm 1.8%, d1=2.0 \pm 0.6%; GLM: p=0.2238) (Figure 7c).

However, mesenchymal and endothelial cells showed a significant decrease ($VIM^+CK7^-SYP^-$ mean \pm SEM: d0=16.5 \pm 4.6%, d1=8.3 \pm 2.0%; $p=0.003$). The majority of cells in the clusters were $SYP^-CK7^-VIM^-$ and encompassing cell types other than endocrine, ductal, mesenchymal, or endothelial cells, such as exocrine cells (**Figure 7d**).

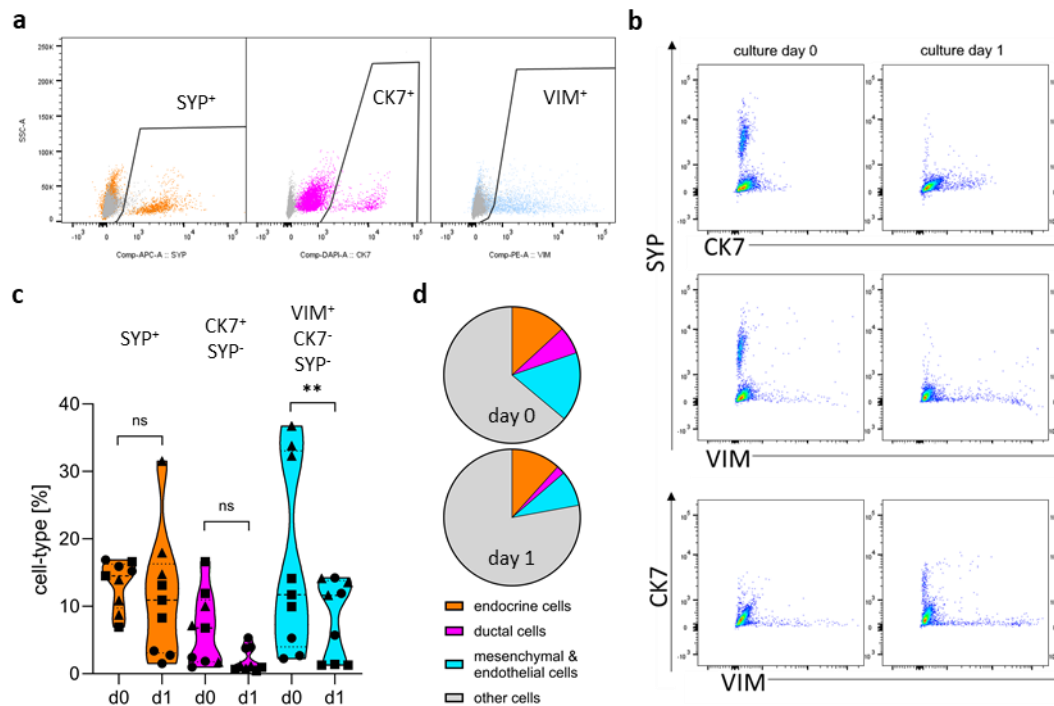


Figure 7: Quantification of pancreatic cell types by flow cytometry on culture days 0 and 1. **a:** Representative gating plots for cells positive for SYP, CK7, and VIM (samples are colored and antibody controls in grey). **b:** Representative dual-plots for SYP, CK7, and VIM. **c:** Proportions of endocrine (SYP^+), ductal ($CK7^+SYP^-$), and mesenchymal ($VIM^+CK7^-SYP^-$) cells on culture days 0 and 1; all values are means; $n=9$ (3 independent experiments with 3 isolates each); $*p < 0.05$, $**p < 0.01$, $***p < 0.001$; circles indicate Batch1, squares Batch2, and triangles Batch3. **d:** Relative distribution of endocrine (SYP^+), ductal ($CK7^+SYP^-$) and mesenchymal/endothelial ($VIM^+CK7^-SYP^-$) cells, and other cell types ($VIM^-CK7^-SYP^-$) on culture days 0 and 1. Values are means from c.

To further characterize the endocrine compartment, pNPCs were analyzed for the proportion of the 3 main hormone-producing cell types for glucose homeostasis by flow cytometry, that are Insulin (INS)-producing β cells, glucagon (GCG)-producing α cells, and somatostatin (SST)-producing δ cells. The group/category “other endocrine cells” was defined as cells being positive for SYP but negative for INS, GCG and SST. These could be either PP cells or low abundant cell types like ghrelin-producing cells, but also neuronal cells.

On day 0 pNPCs consisted of (mean \pm SEM) 12.5 \pm 1.1% SYP⁺ endocrine cells with 5.1 \pm 0.5% β , 2.3 \pm 0.4% α , 1.5 \pm 0.2% δ cells, and 4.1 \pm 0.7% other endocrine cells (**Figure 8b**). For none of these cell types, a significant change in the proportion occurred between d0 and d1 (mean \pm SEM day 1: 12.5 \pm 3.0% endocrine cells, 4.2 \pm 0.4% β cells, 3.1 \pm 0.4 α cells, 1.2 \pm 0.2% δ cells. GLM d0 vs d1: endocrine cells, $p=0.9938$; β cells, $p=0.3259$; α cells, $p=0.1528$; δ cells, $p=0.1936$).

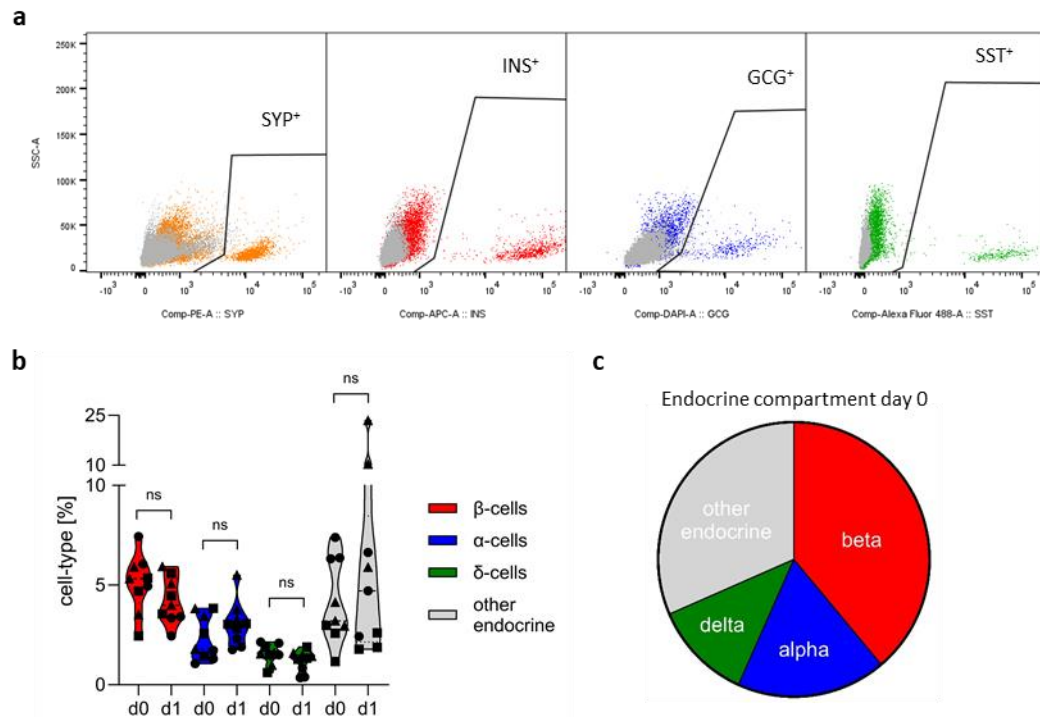


Figure 8: Quantification of endocrine cell types by flow cytometry on culture days 0 and 1. **a:** Representative gating plots for cells positive for SYP, INS, GCG and SST. **b:** Absolute proportions of β (INS⁺), α (GCG⁺), δ (SST⁺), and other endocrine cells (cells positive for SYP, but negative for INS, GCG or SST) on culture days 0 and 1; * $p<0.05$, ** $p<0.01$; *** $p<0.001$. Circles indicate Batch1, squares Batch2, and triangles Batch3. **c:** Relative distribution of cell types within the endocrine compartment on culture day 0. Values are means from **b**.

1.4. Enrichment of the endocrine cell fraction and depletion of non-endocrine cell types during *in vitro* culture of pNPCs

To analyze the changes in the cellular composition of pNPCs throughout the culture period, the abundance of endocrine, ductal, mesenchymal/endothelial, β , α , δ , and other endocrine cells was further evaluated at days 3 and 9 of culture and compared to the cluster composition at day 1. Additionally, four-hormone immunofluorescence staining for INS, GCG, SST and pancreatic polypeptide (PPY, PP cells), was performed on culture days 0, 1, 3, and 9.

The analysis revealed significant changes in endocrine, ductal, and mesenchymal cells after day 1 of culture (**Figure 9a** and **b**). The proportion of endocrine cells (SYP⁺) increased from 11.6±3.1% (mean±SEM) on day 1 to 41.0±1.7% on day 3 and further to 59.48±2.9% at day 9, representing a five-fold increase of the endocrine cell fraction during the culture period of 9 days. Ductal cells (CK7⁺SYP⁻) showed a significant increase from 2.0±0.6% at day 1 to 16.7±4.4% and 37.4±2.9% on culture days 3 and 9, respectively. Mesenchymal and endothelial cells (VIM⁺CK7⁻SYP⁻) also increased from 8.3±2.0% on culture day 1 to 20.4±2.7% on culture day 3, but decreased to 8.6±1.6% on culture day 9 (for all cell types, day 1 vs day 3 and day 3 vs day 9, $p < 0.0001$). The GLM indicated no significant differences between isolation rounds (batch) or biological replicates within isolations (replicate(batch)) for the proportions of endocrine and ductal cells on culture days 0, 1, 3, and 9 (endocrine cells: batch $p = 0.2032$, replicate(batch) $p = 0.8183$; ductal cells: batch $p = 0.096$, replicate(batch) $p = 0.93$). For proportions of mesenchymal/endothelial cells GLM showed significant differences for batch ($p = 0.0137$) but not replicate(batch) ($p = 0.4241$).

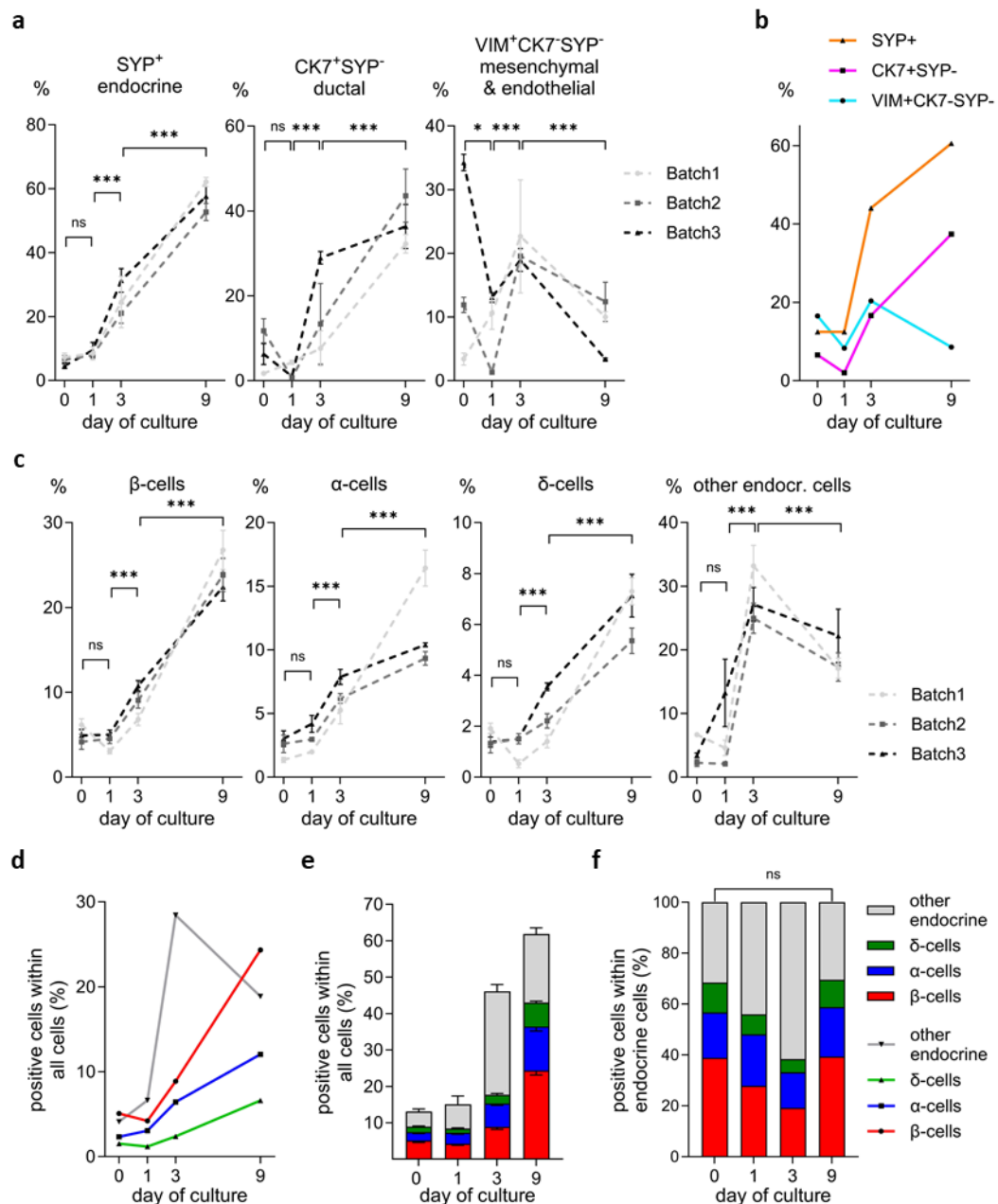


Figure 9: Quantification of pancreatic cell types by flow cytometry on culture days 0, 1, 3, and 9. **a, b:** Proportions of endocrine (SYP⁺), ductal (CK7⁺SYP⁻), and mesenchymal/endothelial (VIM⁺SYP⁻CK7⁻) cells. **c-f:** Proportions of endocrine cell types detected by the expression of their respective hormone. Other endocrine cells, are SYP⁺INS⁻GCG⁻SST⁻. **a, c:** Proportions per batch; all values are means; n=9 (3 independent experiments with 3 isolates each). **b, d, e:** Mean values of a and c of cell types per day. **f:** Relative proportions of cell types within the endocrine compartment. All values are means; error bars indicate SEM; n=9 (3 independent experiments with 3 isolates each); *p<0.05, **p<0.01, ***p<0.001.

Examining the endocrine compartment in more detail, we observed that the proportions of all endocrine cells increased after day 1 of culture (**Figure 9c, d** and **e**). The proportion of β cells increased from 4.2±0.4% (mean±SEM) on culture

day 1 to $8.9\pm 0.7\%$ on culture day 3 ($p<0.0001$) and further to $24.3\pm 1.2\%$ on culture day 9 ($p<0.0001$). The proportion of α cells rose from $3.1\pm 0.4\%$ on culture day 1 to $6.4\pm 0.5\%$ on culture day 3 ($p<0.0001$), and to $12.1\pm 1.2\%$ on day 9 ($p<0.0001$). Similarly, δ cells increased from $1.2\pm 0.2\%$ on culture day 1 to $2.4\pm 0.3\%$ on culture day 3 ($p=0.0003$), and to $6.6\pm 0.5\%$ on culture day 9 ($p<0.0001$). In summary, β , α , and δ cells increased between culture days 1 and 9 by factors of 5.8, 4.0, and 5.6, respectively. Other endocrine cells increased between culture days 1 and 3 from $6.6\pm 2.3\%$ to $28.4\pm 1.9\%$ ($p<0.0001$), but decreased to $18.9\pm 1.7\%$ ($p=0.0008$) on culture day 9. The proportion of this population decreased, in contrast to β , α , and δ cells that continued to increase between culture days 1 and 9.

When comparing the composition within the endocrine compartment, GLM revealed significant differences between timepoints except for days 0 and 9 (**Figure 9f**). There were no significant differences in the fractions (mean \pm SEM) of β -, α -, δ -, and other endocrine cells ($p=0.87$, 0.79 , 0.11 , 0.97). β cells were the predominant endocrine cell type ($39.1\pm 1.2\%/39.5\pm 1.5\%$), followed by α cells ($18.9\pm 2.8\%/19.4\pm 1.5\%$), and δ cells ($11.7\pm 0.5\%/10.6\pm 0.4\%$). On days 1 and 3, the proportions of β cells ($31.4\pm 3.5\%/19.4\pm 1.6\%$, p -values <0.007) and δ cells ($8.5\pm 1.4\%/5.2\pm 0.7\%$, p -values <0.004) were lower compared to days 0 and 9. The proportion of α cells decreased only on day 3 of culture ($13.9\pm 1.0\%$, p -values <0.02). Regarding "other endocrine cells" (SYP⁺INS⁻GCG⁻SST⁻), the proportions at days 0, 1, and 9 showed no significant differences, with $30.3\pm 3.4\%$, $38.0\pm 6.4\%$, and $30.5\pm 2.1\%$, respectively. Only an increased proportion of $61.5\pm 2.9\%$ occurred on day 3 (all p -values <0.0001). This relative increase on day 3 might indicate immature endocrine cells that do not produce high levels of hormones but contain granules.

While the absolute proportion of endocrine cells increased to approximately 60% (**Figure 9e**), the composition within the endocrine compartment remained the same when comparing days 0 and 9 (**Figure 9f**). This suggests that prolonged culture enriches for endocrine cells, but the cell composition, even though it changes distinctly during culture, returns to its initial state.

4-hormone immunofluorescence staining of pNPCs revealed an increase in hormone-positive cells throughout the culture, which is in line with the findings in

flow cytometry analyses (**Figure 10**). Furthermore, PPY⁺ PP cells were identified.

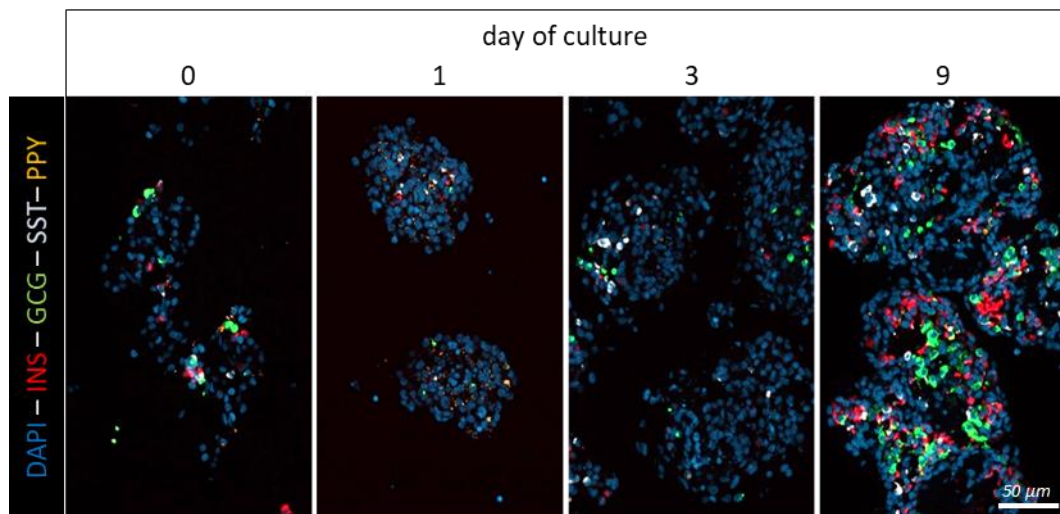


Figure 10: Immunofluorescence staining for INS (red), GCG (green), SST (white), and PPY (orange) of pNPCs on culture days 0, 1, 3, and 9; nuclei are stained with DAPI (blue); scale bar 50 μm.

1.5. Molecular characterization of pancreatic cell types

To determine molecular changes in different cell types, single-cell RNA sequencing (scRNA-seq) of clusters cultured for 1, 3, and 9 days was performed. In addition, scRNA-seq from pig β-cell atlas (SCHWAGER et al., Manuscript in prep) was included in the analysis and served as a d0 reference. In this pig β-cell atlas, due to the low proportions of endocrine cells and high proportion of acinar cells on culture day 0, only β cells isolated from *INS*-eGFP transgenic pig (KEMTER et al., 2017) clusters were characterized by scRNA-seq.

ScRNA-seq successfully identified pancreatic cell types via Leiden-Algorithm-based clustering and expression of common marker genes for pancreatic cell types (**Figure 11**). In addition to acinar and ductal cells, which represent the exocrine compartment, mesenchymal and endothelial cells were also present. Endocrine cell types included β, α, δ, and PP cells, as well as endocrine progenitor-like cells marked as NGN3_FEV. For all subsequent analyses, only annotated clusters containing at least 100 cells were considered. Due to the low cell numbers for individual culture days, endothelial cells were excluded.

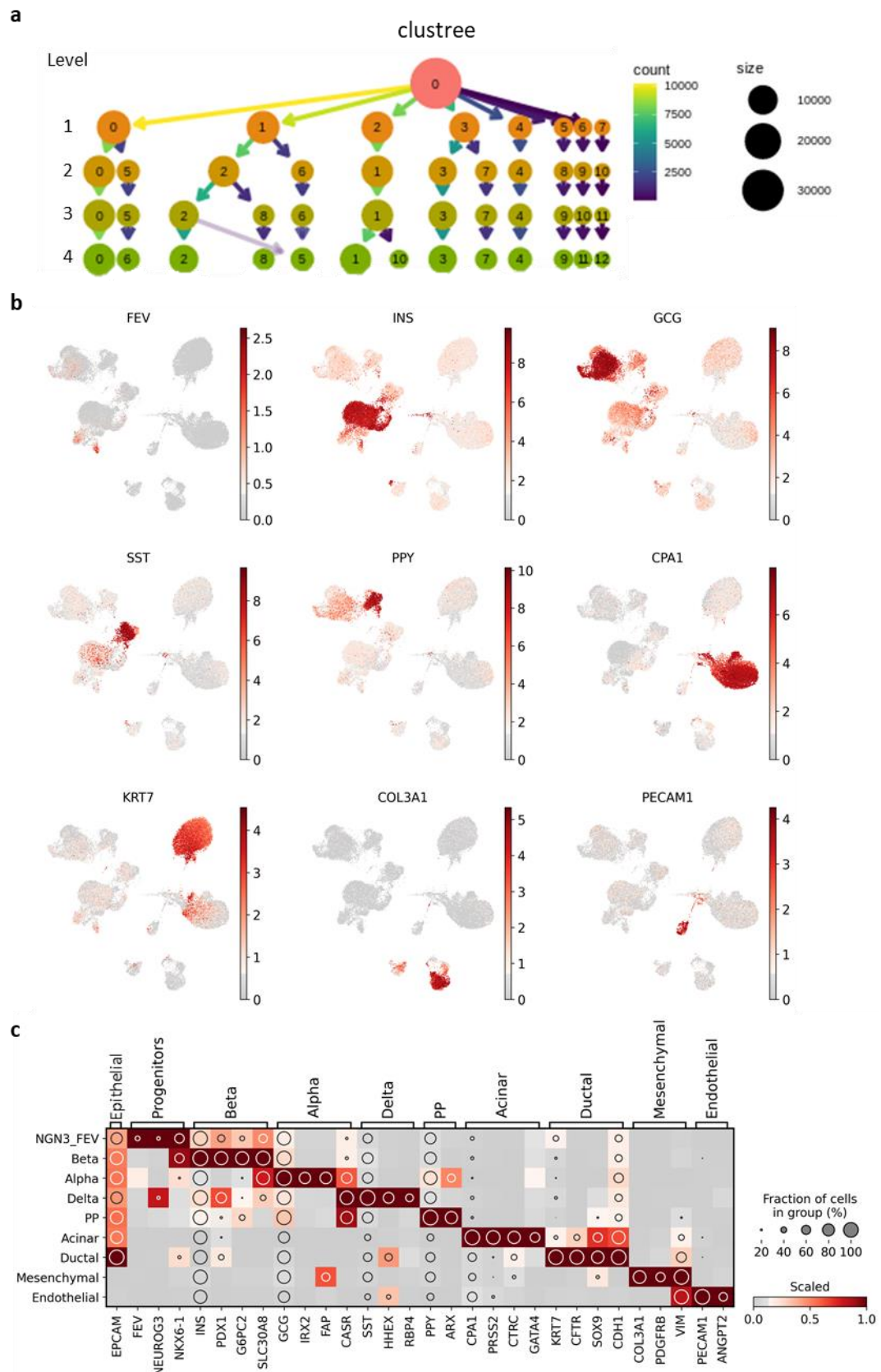


Figure 11: Annotation of pancreatic cell types by Leiden-clustering and expression of marker genes (scRNA-seq). **a:** Clustree-visualized clustering of different resolutions generated by Leiden-Algorithm. **b:** Neighborhood graphs showing the expression levels of selected pancreatic cell type markers. **c:** Expression levels of marker genes in clustered cell types. The color intensity indicates the expression

level. The circle size indicates the fraction of positive cells.

In line with the previous findings by flow cytometry analyses, scRNA-seq analysis revealed similar changes in the cell composition during culture (means, n=2). While acinar cells were depleted over time (d1=55.1%, d3=22.0%, d9=0.8%), mesenchymal cells first showed an increase from 5.7% at day 1 to 10.6% at day 3, followed by a drop to 7% at day 9 (**Figure 12b**). Contrary to the findings in flow cytometry, ductal cells didn't show a continuous increase, but first an increase from 15.8% at day 1 to 44.9% at day 3, followed by a drop to 13.2% at day 9. The only compartment that rose to day 9 was the endocrine compartment. Proportions stayed relatively similar between days 1 and 3 (β cells: 8.9 and 8.7%, α cells: 5.2 and 6.3%, δ cells: 2.4 and 2.7%, PP cells: 1.8 and 1.5%, endocrine progenitors: 2.6/2.4%, respectively) but rose distinctly to day 9. At day 9 the proportion of β cells was 28.4%, α cells 29.0%, δ cells 7.5%, PP cells 7.3%, and endocrine progenitors 6.0%, which is a 3.3-, 4.6-, 2.8-, 4.8-, and 2.5-fold increase, respectively.

All pancreatic cell types exhibited distinct changes throughout the culture period. This is evident in the localization of cells within the neighborhood graph for different culture days based on overall transcriptome (**Figure 12c**), and in the changes of expression levels and fractions of positive cells of individual cell type markers (**Figure 12d**), indicating a distinct influence of the *in vitro* culture conditions.

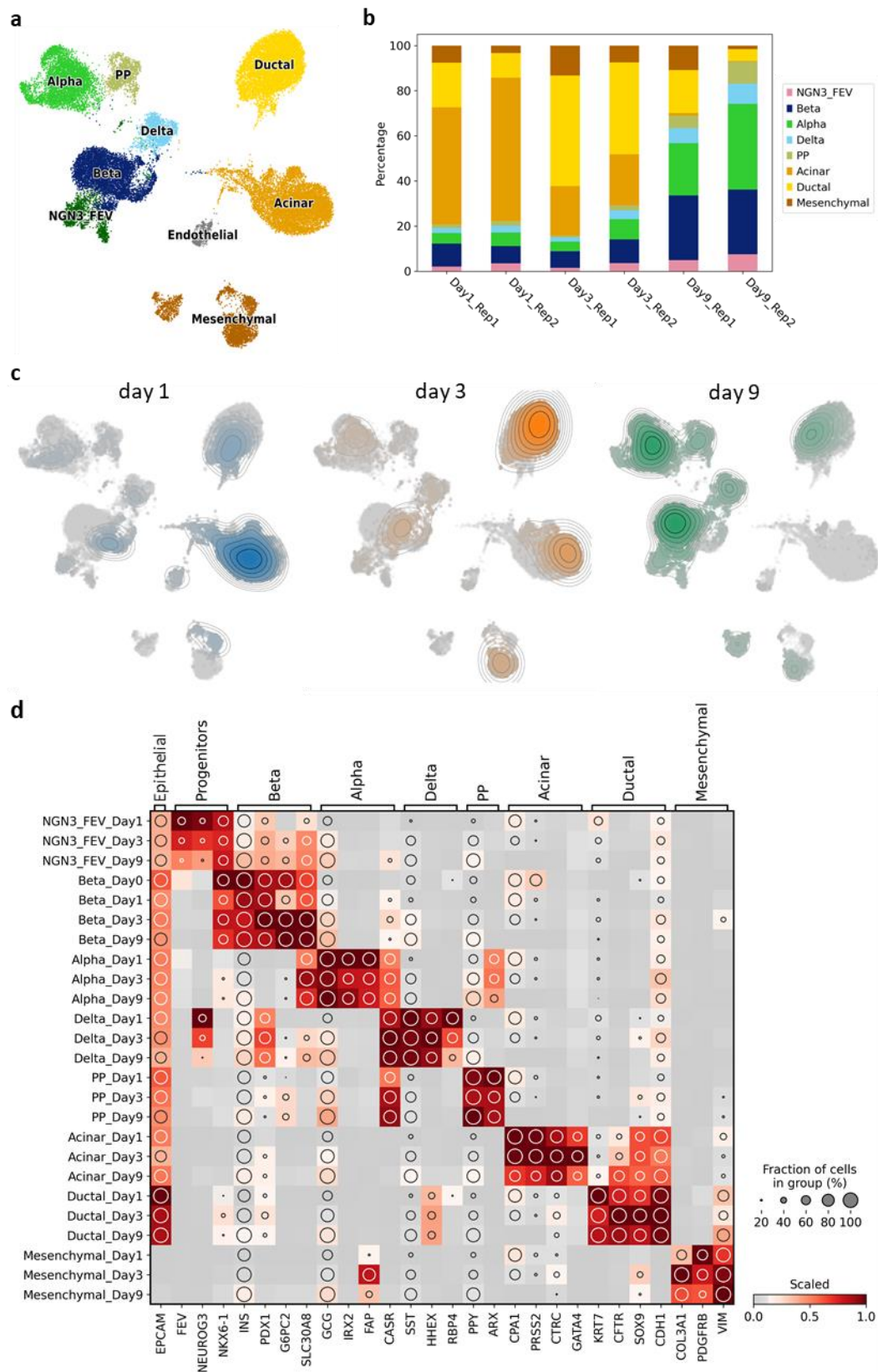


Figure 12: Cellular composition and characteristics of pNPCs on transcriptome level (scRNA-seq). **a:** Neighborhood graph of annotated cell types. **b:** Proportions of detected cell types for culture days 1, 3, and 9 from 2 experiments (3 biological replicates equally mixed each). **c:** Neighborhood graph showing the cell distribution on culture days 1, 3, and 9. **d:** Expression levels of marker genes specific for pancreatic cell types in annotated clusters on culture days 1, 3, and 9; the color intensity indicates the expression level and the circle size the fraction of positive cells.

2. Signs of stress recovery and maturation in endocrine cells

2.1. Endocrine cells gain endocrine-lineage transcription factors during culture and exhibit typical expression patterns in β , α , and δ cells

Endocrine cells in the neonatal pancreas are not fully mature yet and undergo an *in vivo* maturation during postnatal pancreatic development (SAUNDERS et al., 2024). In β cells this process is marked by the expression of several transcription factors (TFs), like PDX1, NKX6-1, neuronal differentiation 1 (NEUROD1), and MAFA (TAYLOR et al., 2015; JACOVETTI & REGAZZI, 2022). Furthermore, the lack of certain TFs like NKX6-1, can lead to non-functional polyhormonal β cells (AIGHA & ABDELALIM, 2020). Therefore, we focused our analysis next on TFs of endocrine lineage differentiation and maturation.

ScRNA-seq revealed distinct expression patterns of TFs across the endocrine cell types (**Figure 13a**). *FEV* was exclusively expressed in the NGN3_FEV cluster and showed a decrease during the culture period, similar to *NEUROG3*. *NEUROG3*⁺ cells were only found in the NGN3_FEV cluster and in δ cells. *NKX6-1* was present in both the NGN3_FEV cluster and β cells, with a low proportion of cells and low expression levels in α cells. *PDX1* was predominantly expressed in β cells, with lower levels in δ cells and even lower levels in the NGN3_FEV cluster. *PAX6* was expressed in all endocrine cell types at varying levels, with the highest expression levels in β cells at day 0. *NEUROD1*, *FOXA2*, *NKX2-2*, and *FOXO1* were also present in all cell types, albeit at lower proportions, with the highest expression levels in β cells. *RFX6* was expressed in all cell types, with the highest levels in α cells, while *RFX3* was also present in all cell types, with the highest expression levels in the NGN3_FEV cluster and δ cells. *ISL1* was expressed in all cell types except the NGN3_FEV cluster, with the highest levels in δ cells. *ARX* was exclusively expressed in α - and PP cells, with lower expression levels and proportions of positive cells in α cells compared to PP cells. *IRX* was exclusively expressed in α cells. Other commonly used markers like *UCN3* or *MAFA* could not be detected or were only present in a small proportion of cells. In general, most TFs showed the highest expression levels at days 3 or 9, except for β cells, where day 0 exhibited the highest expression levels. As some of these markers are associated with improved β -cell function (AIT-LOUNIS et al., 2010; JACOVETTI & REGAZZI, 2022; VAN GURP

et al., 2022), this suggests an *in vitro* maturation process during culture. However, since data for β cells were only available for day 0 and expression appears higher at this time point, this might merely indicate recovery from an initial decrease rather than true maturation.

The expression of most TFs in cultured pNPCs corresponded with descriptions in the literature and our observations in the pig pancreas atlas (SCHWAGER et al., Manuscript in prep). For instance, *ARX* was restricted to α and PP cells, while β cells were positive for *PDX1* and *NKX6-1*. However, some observations initially appeared inconsistent with the literature. For instance, the expression of *NKX6-1* in α cells. According to the literature, *NKX6-1* is a repressor of *ARX*, the main driver for differentiation into α cells (SCHAFFER et al., 2013), and thus should not be present in α cells. Data from healthy pigs of different ages suggest that the expression of *NKX6-1* in α cells appears to be physiological up to the juvenile age (SCHWAGER et al., Manuscript in prep). Therefore, abundance of *PDX1* and *NKX6-1*, both relevant for β -cell development and identity, was validated also at protein level by flow cytometry.

In contrast to transcriptome data, no distinguishable population of *PDX1*⁺ or *NKX6-1*⁺ cells could be detected up to day 3 of culture (**Figure 13b**). By day 9 of culture, three distinct populations of cells emerged: a double-positive population (*PDX1*⁺*NKX6-1*⁺) and two single-positive (*PDX1*⁺*NKX6-1*⁻ and *PDX1*⁻*NKX6-1*⁺) populations. These populations largely aligned with hormone-positive cells: *INS*⁺ β cells were positive for both TFs, while *GCG*⁺ α cells were single-positive for *NKX6-1*, and *SST*⁺ δ cells were single-positive for *PDX1*, both at lower levels compared to β cells (**Figure 13c**). This observation is consistent with the findings from scRNA-seq. To evaluate protein abundance, median fluorescence intensity (MFI) of fluorophore labeled antibodies bound to their specific target was evaluated by flow cytometry. The abundance of *PDX1* and *NKX6-1* in β cells increased for both TFs (p-values: <0.0001) (**Figure 13d**).

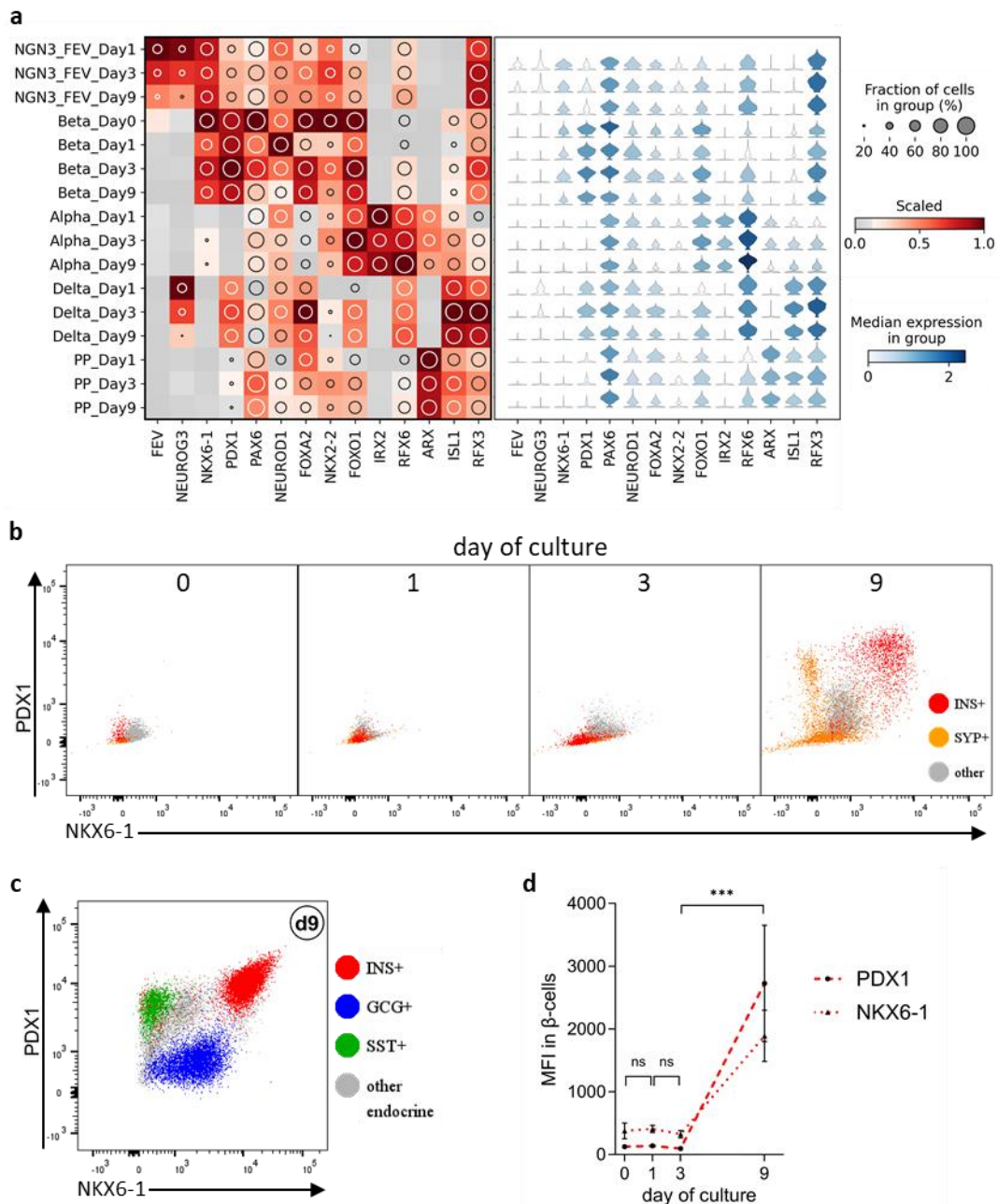


Figure 13: Expression of endocrine lineage specific markers in endocrine cells of pNPCs during culture. **a:** Expression levels and distribution of markers for endocrine lineage differentiation and maturation in endocrine cell types on culture days 1, 3, and 9 (scRNA-seq); $n=2$; the color intensity indicates the expression level; the circle size indicates the fraction of positive cells; violin plots indicate distribution of expression. **b, c, and d:** Prevalence of PDX1 and NKX6-1 evaluated by flow cytometry. **b:** Representative dual-plots for PDX1 and NKX6-1 of β cells (INS⁺), endocrine cells (SYP⁺), and INS-SYP⁻ cells (other) on culture days 0, 1, 3, and 9. **c:** Representative dual-plot for PDX1 and NKX6-1 of β (INS⁺), α (GCG⁺), δ (SST⁺), and other endocrine (SYP⁺INS⁻GCG⁻SST⁻) cells on culture day 9. **d:** MFI of PDX1 and NKX6-1 in β cells on culture days 0, 1, 3, and 9; All values are means; error bars indicate SEM; $n=9$ (3 independent experiments with 3 isolates each); * $p<0.05$, ** $p<0.01$, *** $p<0.001$.

2.2. Few multihormonal cells during *in vitro* culture

To investigate whether *in vitro* culture conditions promote polyhormonal cells, as often described in the generation of stem cell-derived β -like cells (CUESTA-GOMEZ et al., 2022), and due to the lack of NKX6-1 detection in β cells before culture day 9 by flow cytometry (**Figure 13b**), which can lead to non-functional polyhormonal β cells (AIGHA & ABDELALIM, 2020), pNPCs were next examined for polyhormonality.

The proportion of double- or triple-positive cells for INS, GCG, and/or SST within all cells increased from $0.11\pm 0.02\%$ on culture day 0 to $0.42\pm 0.08\%$ on day 9 of culture ($p < 0.0001$), as determined by flow cytometry (**Figure 14a** und **b**). Examining the relative proportion of double- or triple-positive cells among the hormone-positive cells, the proportion initially increased from $1.26\pm 0.20\%$ on day 0 to $2.28\pm 0.32\%$ on day 1 ($p = 0.0014$) and subsequently decreased back to $1.08\pm 0.21\%$ on day 9 ($p = 0.0003$). This indicates that there was an absolute increase in hormone double- or triple-positive cells, but this was primarily driven by an overall increase in hormone-positive cells. The increase of these cells between days 0 and 1 was less than two-fold, and their proportion of the total cell count was below 1% in all samples.

levels. The proportion of endocrine cells expressing additional hormones increased with prolonged culture, with increasing but low expression levels. Interestingly, acinar, ductal, and mesenchymal cells showed the same pattern of increase in fraction and expression level (**Figure 14d**). As this occurs consistently across all cell types and as early as culture day 1, when cells have not had sufficient time to gain the capacity to form transcripts of other cell types, it might be an artifact. Possible explanations include technical artifacts during data processing, such as dropout correction (QIU, 2020) or biological artifacts like RNA incorporated from other cells, known as ambient RNA (YANG et al., 2020). Alternatively, it could indicate increased polyhormonality at a low level. However, given the similar pattern across all cell types in scRNA-seq data and the low proportions of hormone-double/triple positive cells in flow cytometry, this seems rather unlikely.

2.3. **Distinct early drop and subsequent recovery in hormone abundance and granularity in endocrine cells during culture period**

To characterize endocrine cells in more detail, we further evaluated the abundance of the hormones INS, GCG, and SST, in β , α , and δ cells, respectively on the protein level. Therefore, MFI of fluorophore labeled antibodies bound to their specific target was evaluated by flow cytometry.

MFIs decreased significantly during the early culture period. When examining the abundance of hormones on different culture days compared to their levels on day 0 (relMean), less than half of the initial hormone levels remained by day 1 (relMeans: INS 42.7%, GCG 44.1%, SST 41.4% %, all p-values <0.0001) (**Figure 15a and b**). This decline continued to day 3 in β cells (relMean INS: 11%, p<0.0001), but not in α cells (relMean GCG: 39%, p=0.6293) and δ cells (relMean SST: 33%, p=0.3309). While α and δ cells recovered by day 9 (relMeans: GCG 104%, SST 85%, both p<0.0001), β cells did not show a similar recovery of insulin levels (relMean INS: 14%, p=0.5325).

Similar to the protein expression, though less pronounced, scRNA-seq data revealed decreased expression levels of *INS* in β cells with continued culture with minimal recovery by day 9 (**Figure 15c**). α , δ , and PP cells exhibited relatively

constant expression levels of their respective hormones on culture days 1, 3, and 9 (**Figure 15c**). Furthermore, small populations of hormone low-expressing cells were present in all endocrine cell types during culture.

Examining markers associated with hormone production and processing, it appears that upregulation of these genes occurred in all endocrine cell types after day 1. Interestingly, β cells also showed higher expression levels on day 0, which - like in developmental markers (**chapter 2.1**) - indicates an initial decrease followed by recovery.

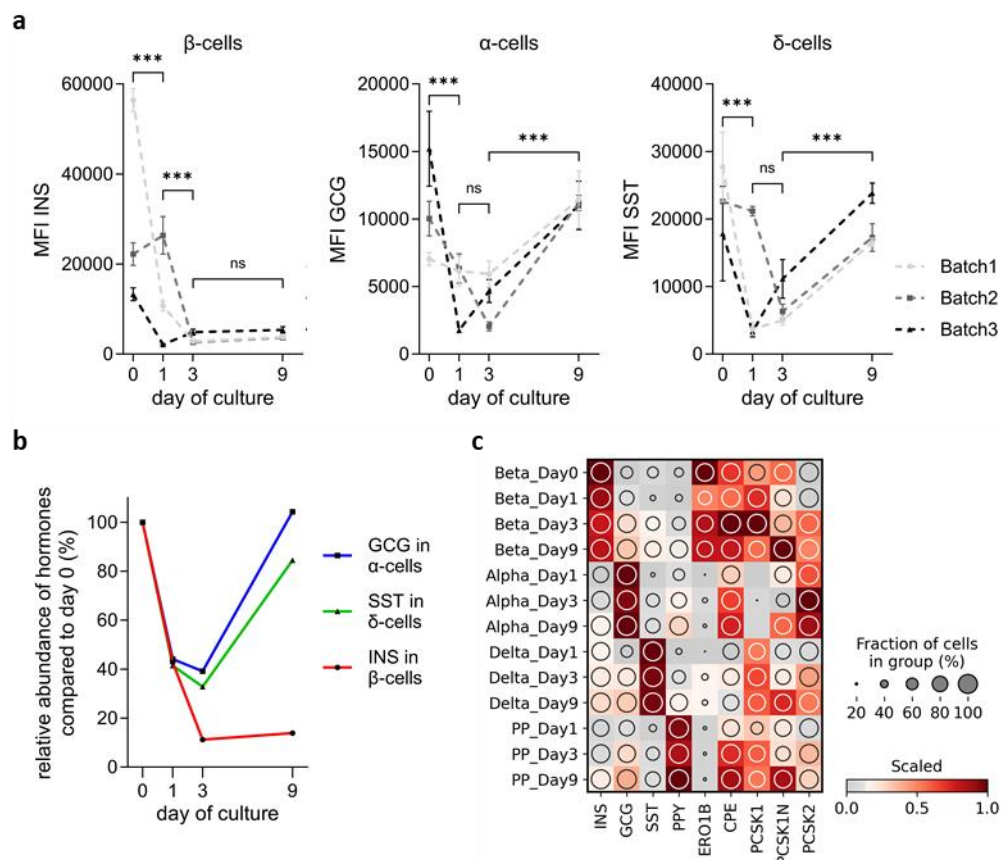


Figure 15: Characterization of hormone-associated markers in endocrine cells of pNPCs during culture. **a, b:** Abundance of INS, GCG, and SST in respective endocrine cell types evaluated by flow cytometry on culture days 0, 1, 3, and 9; all values are means; error bars indicate SEM; $n=9$ (3 independent experiments with 3 isolates each); $*p<0.05$, $**p<0.01$, $***p<0.001$. **a:** Absolute MFI separate per batch. **b:** Means of relative abundance compared to day 0 (based on a). **c:** Expression levels of markers associated with hormone synthesis and processing in endocrine cell types on culture days 1, 3, and 9 (scRNA-seq); $n=2$; the color intensity indicates the expression level; the circle size indicates the fraction of positive cells.

As a readout for functionality, granularity was evaluated by flow cytometry, using side scatter area and height (SSC-A / SSC-H). Both are commonly used measures

of internal cell complexity, which are expected to reflect granules in endocrine cells. As this method did not give conclusive results (**Figure 16**), the abundance of synaptophysin (SYP), a membrane integral protein in microvesicles and secretory granules (NORRIS et al., 2024), was examined.

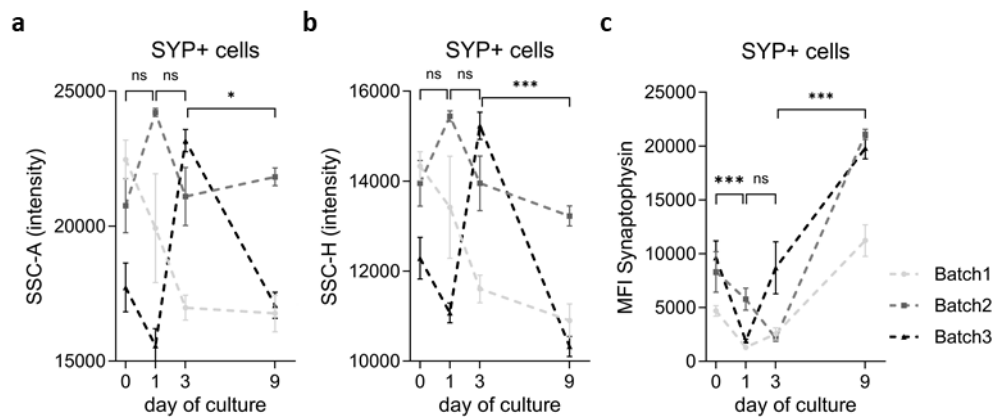


Figure 16: Comparison of different methods to evaluate granularity in vesicle containing cells (SYP⁺) on culture days 0, 1, 3, and 9 by flow cytometry. **a:** Intensity of SSC-A. **b:** Intensity of SSC-H. **c:** MFI of SYP. All values are means; error bars indicate SEM; $n=9$ (3 independent experiments with 3 isolates each); * $p<0.05$, ** $p<0.01$, *** $p<0.001$.

β , α , and δ cells exhibited a significant drop in granularity from day 0 to day 1, with reductions of 63.5%, 60.8%, and 65.8%, respectively, compared to day 0 (**Figure 17a and b**). By day 3, granularity began to recover (all p -values <0.007), reaching levels similar to day 0 (β cells: 94.5%, α cells: 77.5%, δ cells: 81.1%). By day 9, SYP abundance exceeded the initial levels observed at the beginning of the culture period (all p -values <0.0001), with increases to 257% in β cells, 215% in α cells, and 183% in δ cells, compared to day 0. Notably, in the early culture period, β , α , and δ cells showed similar granularity (day 0 and 1: all p -values >0.05). However, by day 9, β and α cells exhibited significantly higher granularity than δ cells, with β cells showing even higher granularity than α cells (all p -values <0.0001) (**Figure 17c**).

The scRNA-seq data showed an increase in the expression levels of genes related to secretory granules, granule trafficking, and exocytosis across all endocrine cell types (**Figure 17d**). In β cells, a few genes, such as Synaptosome Associated Protein 25 (SNAP25) and Secretogranin II (SCG2), exhibit a decrease in expression levels from day 0 to day 1, while most others continued to increase until day 3. As noted

in previous chapters regarding islet-developmental and hormone-processing genes, several markers for vesicles and exocytosis showed a decrease in expression levels from day 3 to day 9 across all cell types. Chromogranin A (*CHGA*) is the only marker that continuously decreases throughout the culture period. Interestingly, in β cells, this is opposite to the expression pattern of Chromogranin B (*CHGB*). While CHGB is known to be involved in the processing of early insulin granules (BEARROWS et al., 2019), the functional roles of CHGA remain largely unknown. To assess the maturity of granules, transcriptome and protein analyses do not provide a sufficient basis. Instead, electron microscopy studies are necessary to distinguish mature from immature containing granules based on their dense core of crystalline insulin (RAO et al., 2020)

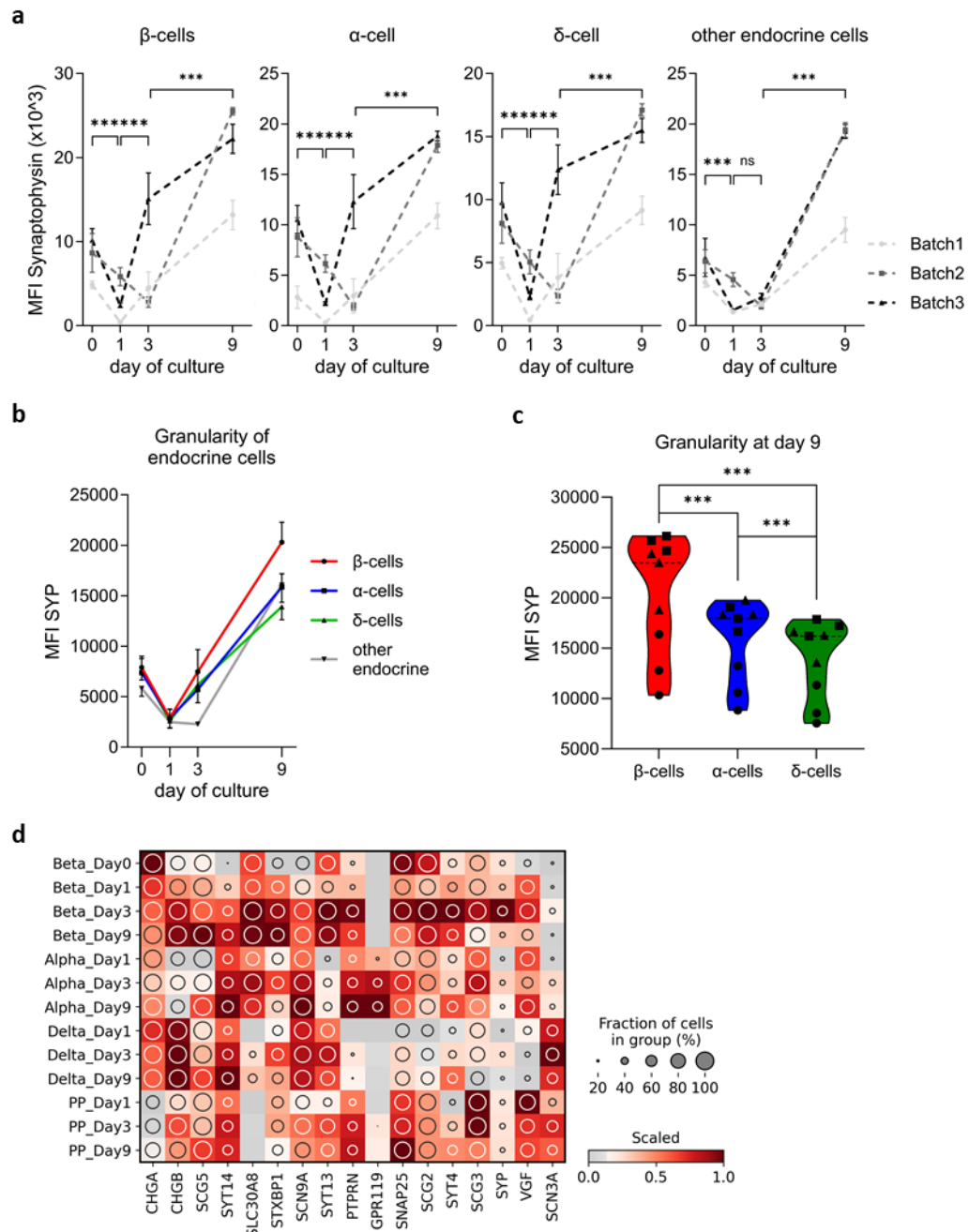


Figure 17: Characterization of vesicle-associated markers in endocrine cells of pNPCs during culture. **a - c:** Abundance of SYP in β (INS^+), α (GCG^+), δ (SST^+), and other endocrine ($SYP^+INS^-GCG^-SST^-$) cells evaluated by flow cytometry; all values are means; $n=9$ (3 independent experiments with 3 isolates each); $*p<0.05$, $**p<0.01$, $***p<0.001$. **a, b:** MFI of SYP on culture days 0, 1, 3, and 9; error bars indicate SEM. **c:** MFI of SYP on culture day 9; circles indicate Batch1, squares Batch2, and triangles Batch3. **d:** Expression levels of markers associated with secretory granules in endocrine cell types on culture days 1, 3, and 9 (scRNA-seq); $n=2$; the color intensity indicates the expression level; the circle size indicates the fraction of positive cells.

2.4. Insulin secretory profile of β cells

To assess the capacity to release insulin in response to glucose stimulation, β cells were evaluated for the expression of marker genes linked to glucose sensing and calcium signaling in the scRNA-seq dataset. Additionally, the *in vitro* functionality of clusters to respond to increased glucose levels with insulin secretion was assessed by dynamic glucose-stimulated insulin secretion on culture day 9 (dGSIS).

In scRNA-seq data distinct changes in markers for glucose sensing and calcium signaling in β cells were present (**Figure 18a and b**). Solute Carrier Family 2 Member 2 (*SLC2A2*, also known as GLUT2) was exclusively detected in β cells, but its expression was lost during culture. As reduced expression levels of *SLC2A2* is also described in offspring from hyperglycemic mothers (KEMTER et al., manuscript in preparation), this could indicate receptor downregulation due to glucose overabundance. Glucokinase (*GCK*), relevant for glucose sensing in β cells (ABU AQEL et al., 2024), showed an increase in expression level and fraction of cells by day 3, followed by a decrease by day 9. In contrast, ATP Binding Cassette Subfamily C Member 8 (*ABCC8*) and Potassium Inwardly Rectifying Channel Subfamily J Member 11 (*KCNJ11*), both genes encoding potassium channels relevant for insulin secretion via ATP-induced depolarization (DE FRANCO et al., 2020) and Glucose-6-Phosphatase Catalytic Subunit 2 (*G6PC2*), an antagonist of *GCK* (BOSMA et al., 2020), exhibited an opposite pattern: a decrease in expression levels by day 1, followed by an increase. This might also indicate initial stress followed by a maturation process.

For dGSIS, pNPCs were continuously perfused with fluids containing either 3 mM glucose, 16.7 mM glucose, 16.7 mM glucose and the secretagogue forskolin, or 16.7 mM glucose and potassium chloride (KCl) to fully depolarize the β cells. During dGSIS pNPCs exhibited low insulin secretion in response to 3 mM glucose stimulus. Upon stimulation with 16.7 mM glucose, pNPCs showed a biphasic insulin secretion response, returning to basal levels after reverting to 3 mM glucose. Insulin secretion was further enhanced by 16.7 mM glucose combined with forskolin, achieving similar insulin secretion levels as obtained with maximal depolarization using 16.7 mM glucose and potassium chloride. This indicates the general capacity of β cells within the cell clusters to release insulin in response to

glucose stimulation, with further enhancement by secretagogues, basically resembling the response of an islet *in vivo*.

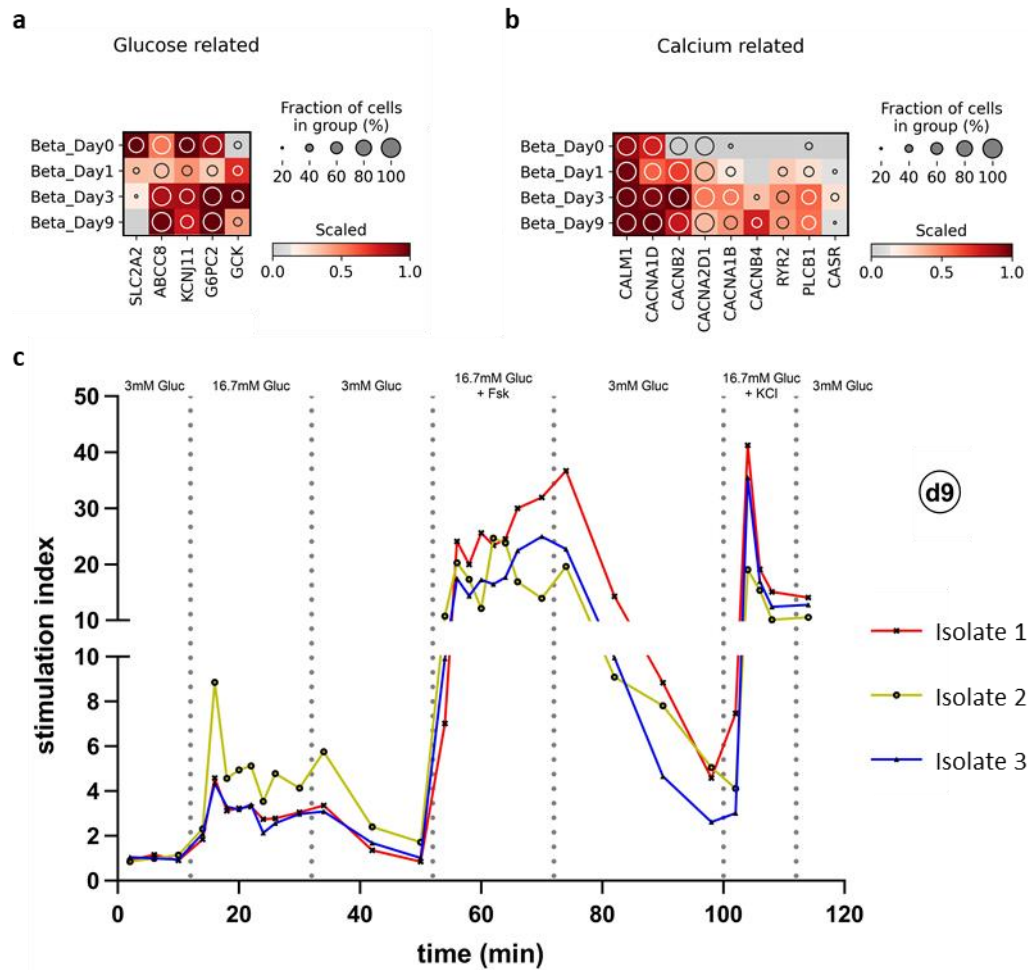


Figure 18: Evaluation of markers for glucose stimulated insulin secretion. **a, b:** Expression levels of markers associated with glucose (a) and calcium (b) in β cell on culture days 1, 3, and 9 (scRNA-seq); $n=2$; the color intensity indicates the expression level and the circle size the fraction of positive cells. **c:** dGSIS evaluating β -cell functionality *in vitro*; insulin release compared to basal secretion (at 3 mM glucose) from pNPCs on stimulus by 16.7 mM glucose, 16.7 mM glucose and forskolin, and 16.7 mM glucose and KCl on culture day 9 *in vitro*; $n=3$.

3. Evaluation of proliferation and other dynamic processes

The neonatal pancreas undergoes a postnatal developmental process characterized by the proliferation of the endocrine compartment, differentiation of cells into mature endocrine cells, and the formation of islets (NAGAYA et al., 2019; SAUNDERS et al., 2024). Cell clusters isolated from neonatal pancreas must undergo a maturation process to achieve functional capacity, enabling them to respond with insulin secretion specifically to a glucose challenge *in vitro* and to engraft and restore normoglycemic control in diabetic recipients post-transplantation. Our analysis showed a relative increase in endocrine cells within the clusters during the maturation process (**Figure 9**). Consequently, we aimed to determine whether this increase in endocrine cells resulted solely from the depletion of other cell types or also from the generation of new endocrine cells. Additionally, we sought to explore the molecular characteristics of developmental processes in this dynamic culture system.

3.1. Self-replication of endocrine cells / Changes in cell proliferation with higher proliferation in endocrine cells

Postnatal expansion of β cells is a physiological process during islet development (TAYLOR et al., 2015). Therefore, products derived from the neonatal pancreas hold substantial potential in this regard. To evaluate proliferation in endocrine cells expression of the Marker of Proliferation Ki-67 (MKI67) was assessed by flow cytometry. Furthermore, scRNA-seq data was analyzed focusing on cell-cycle genes and proliferative cell populations.

In flow cytometry analysis, only a few MKI67 positive cells were detected until day 3 (**Figure 19b**). On day 9, the proportion of MKI67⁺ cells increased to 18.6±2.6% (mean±SEM) (p<0.0001). Endocrine cells (SYP⁺) showed a higher proportion of proliferating cells compared to non-endocrine cells (SYP⁻) on day 9 (mean±SEM: SYP⁺=24.7±5.4%, SYP⁻=9.3±1.6%; p<0.0001) (**Figure 19d**). The proportion of proliferative β cells (INS⁺) did not show a significant difference compared to non- β cells (INS⁻) at day 9 (mean±SEM: INS⁺=21.1±4.2%, INS⁻=17.8±2.3%; p=0.2757). As β cells were not more proliferative at day 9, but endocrine cells were, compared to non-endocrine cells, this suggests that

endocrine cells, that are not β cells, are more proliferative than β cells. These could be α cells, as they are the largest endocrine population after β cells.

In general, these results indicate that endocrine enrichment occurs not only through the depletion of other cell types but also due to proliferation. Despite being less proliferative than other endocrine cells, β cells exhibit the greatest relative increase in number during the culture period (**Figure 9**). This might indicate that β cells are less affected by cell death compared to other endocrine cells. In immunofluorescence staining the presence of proliferating α and β cells on day 9 were confirmed.

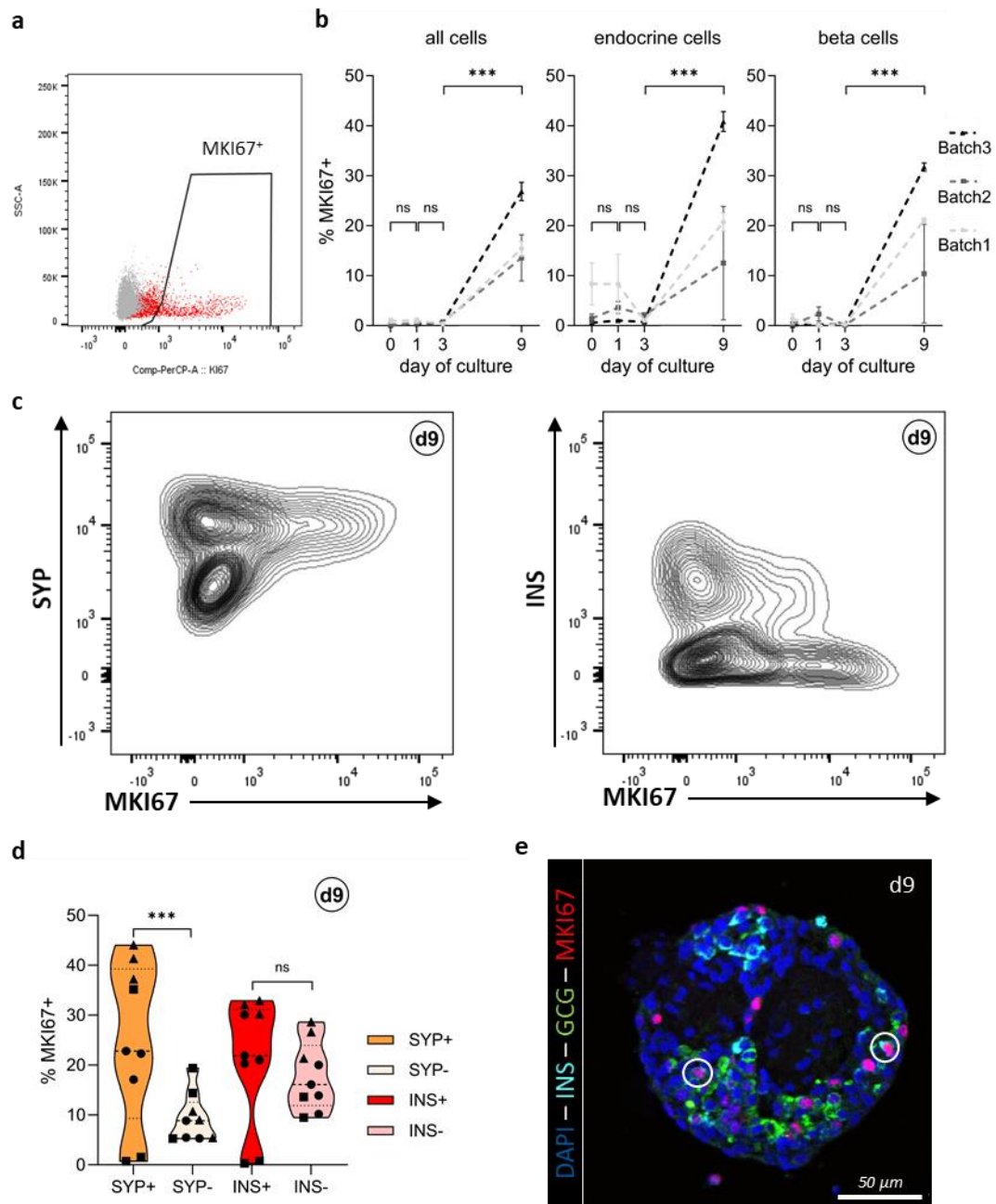


Figure 19: Evaluation of proliferation in pNPCs via MKI67 in pNPCs. **a - d:** Evaluated by flow cytometry. **a:** Representative gating plot for the detection of MKI67 positive cells (sample in red and antibody control in grey). **b:** Proportions of MKI67⁺ cells on culture days 0, 1, 3, and 9; all values are means; error bars indicate SEM; $n=9$ (3 independent experiments with 3 isolates each); * $p<0.05$, ** $p<0.01$, *** $p<0.001$. **c:** Representative dual-plots for MKI67/SYP and MKI67/INS on culture day 9. **d:** Proportion of MKI67⁺ cell within endocrine (SYP⁺), non-endocrine (SYP⁻), β (INS⁺), and non- β (INS⁻) cells on culture day 9; $n=9$ (3 independent experiments with 3 isolates each); * $p<0.05$, ** $p<0.01$, *** $p<0.001$; circles indicate Batch1, squares Batch2, and triangles Batch3. **e:** Immunofluorescence staining for INS (turquoise), GCG (green), and MKI67 (red) of pNPCs on culture day 9; nuclei are stained with DAPI (blue); scale bar 50 μ m.

The scRNA-seq data revealed that all pancreatic cell types expressed various cell cycle-associated genes of the S-phase (DNA replication phase) and the G2M-phase (cell growth phase followed by mitosis) throughout the culture period (**Figure 20a**). More detailed examination of cell cycle genes in endocrine cells reveals dynamic changes. When assigning cells to different cycle phases, the proportion of S-phase cells changed distinctly across all endocrine cell types, showing a decrease after day 1, while the proportion of cells in the G2M phase remained relatively constant (**Figure 20b**). β , α , δ , and PP cells exhibited generally higher proportions of cycling genes compared to NGN3_FEV cells on culture day 1. A similar pattern was observed when looking at the expression levels of cell cycle genes, especially for the S-phase (**Figure 20a**). Corresponding to the decrease in cycling cells during culture, the expression levels of cell cycle-associated genes also declined. β cells showed an increase in proliferating cells (S and G2M phases) between day 0 and 1. Due to the lack of cells, this could not be evaluated for other endocrine cell types. Furthermore, a β -cell subcluster of proliferative cells was detected (**Figure 20c**). This cluster contained most of the β cells with a proliferative signature and exhibited a shift from cells being predominantly in the S-phase on day 0 to mostly in the G2M phase from day 3 onwards (**Figure 20d and e**). MKI67 was not detected at the transcriptome level, thus precluding a direct comparison between transcript and proteome levels.

In summary, both the transcriptome and proteome indicate significant signs of proliferating cells. While these signs decreased at the RNA level after day 1, proliferating cells were detectable by flow cytometry and immunofluorescence only at the end of the culture period. This might be due to the dynamics of MKI67 during the cell cycle (MILLER et al., 2018). Generally, MKI67 is expressed from the middle of the G1 phase until mitosis. It accumulates during the S and G2 phases, and mitosis, and is degraded in the G1 and G0 phases. In this context, the increase of β cells in the G2M phase during culture observed in scRNA-seq data, together with the delay between RNA and protein, seems to correspond with the rising number of MKI67⁺ β cells.

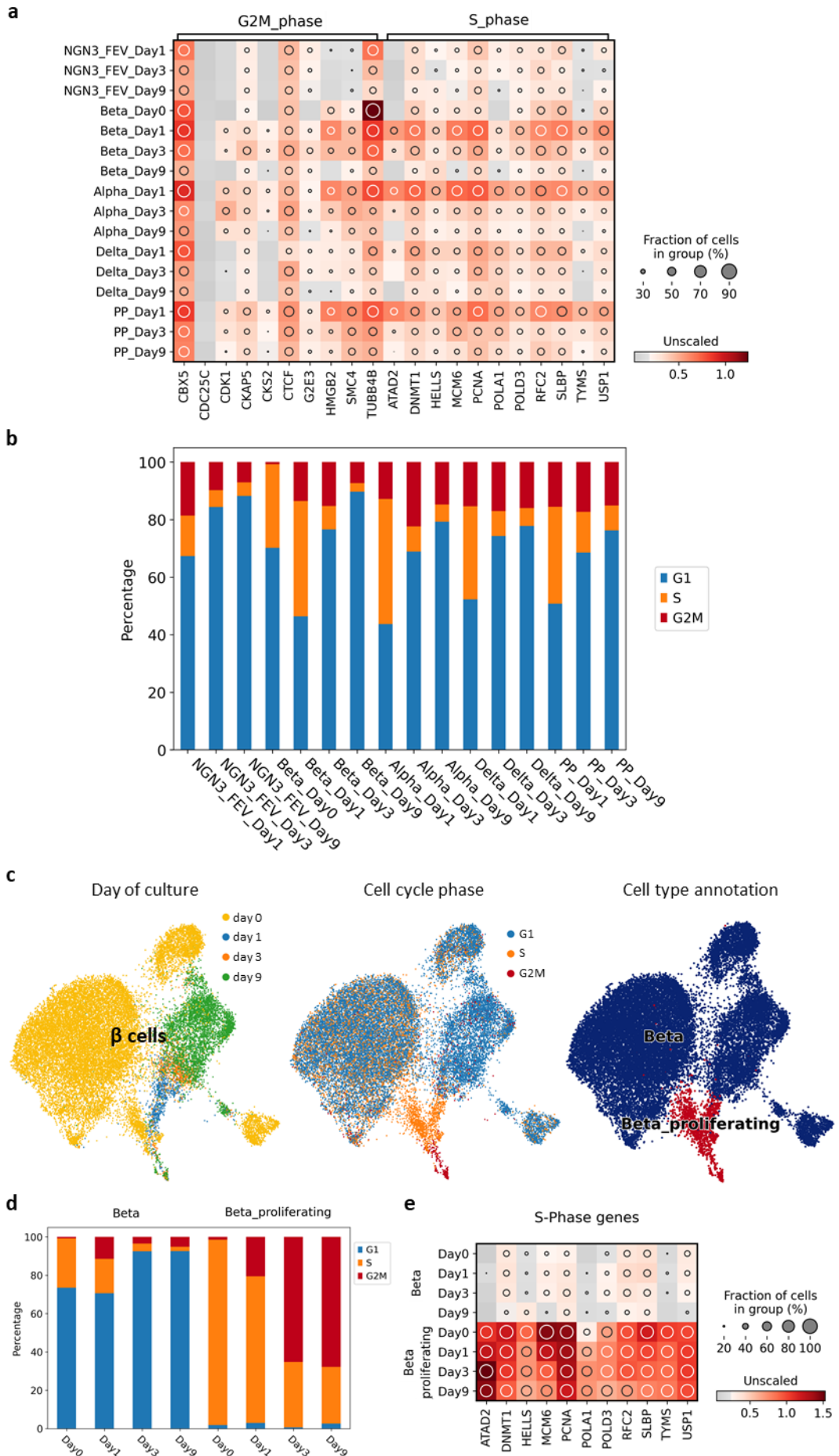


Figure 20: Prevalence of proliferation in endocrine cells of pNPCs during culture (scRNA-seq); $n=2$. **a, d:** Proportions of cells assigned to cell cycle phases G1, S, and G2M in endocrine cell types (a) or β -cell subtypes (d). **b, e:** Expression levels of cell cycle phase associated genes in endocrine cell types (b) or β -cell subtypes (e); the color intensity indicates the expression level and the circle size the fraction of positive cells. **c:** Neighborhood graphs of β cells showing the distribution according to culture day, cell cycle phase, and β -cell subtype.

3.2. Potential for β -cell neogenesis: Presence of endocrine progenitor-like cells

During the growth and maturation of the pancreas in early postnatal life, neogenesis of endocrine cells occurs, and it is assumed that they differentiate from a pool of endocrine progenitors, which transiently express NGN3 and FEV. Therefore, we next focused on the prevalence and characteristics of this cell population.

The scRNA-seq cluster analysis showed a population of cells, partly positive for NGN3, but also positive for FEV (cluster name NGN3_FEV) (**Figure 21a**). A high fraction of cells of this population expressed endocrine lineage TFs like Paired Box 6 (PAX6), Neuronal Differentiation 1 (NEUROD1), Regulatory Factor X3 (RFX3), FOXA2, NKX6-1, NK2 Homeobox 2 (NKX2.2), PDX1, at medium to high expression levels (**Figure 13a**), but no markers of non-endocrine or mature endocrine cells (**Figure 11b** and **c**). This suggests that these cells are committed to the endocrine lineage, but have not differentiated to a certain cell type yet. The proportion of these cells rose from approximately 2.5% on day 1 and 2.4% on day 3 to 5.7% on day 9 (**Figure 12b**).

Immunofluorescence staining revealed no NGN3⁺ cells at days 0 and 1, but positive cells were found on days 3 and 9. No cells positive for both, SYP and NGN3, were detected (**Figure 21b**).

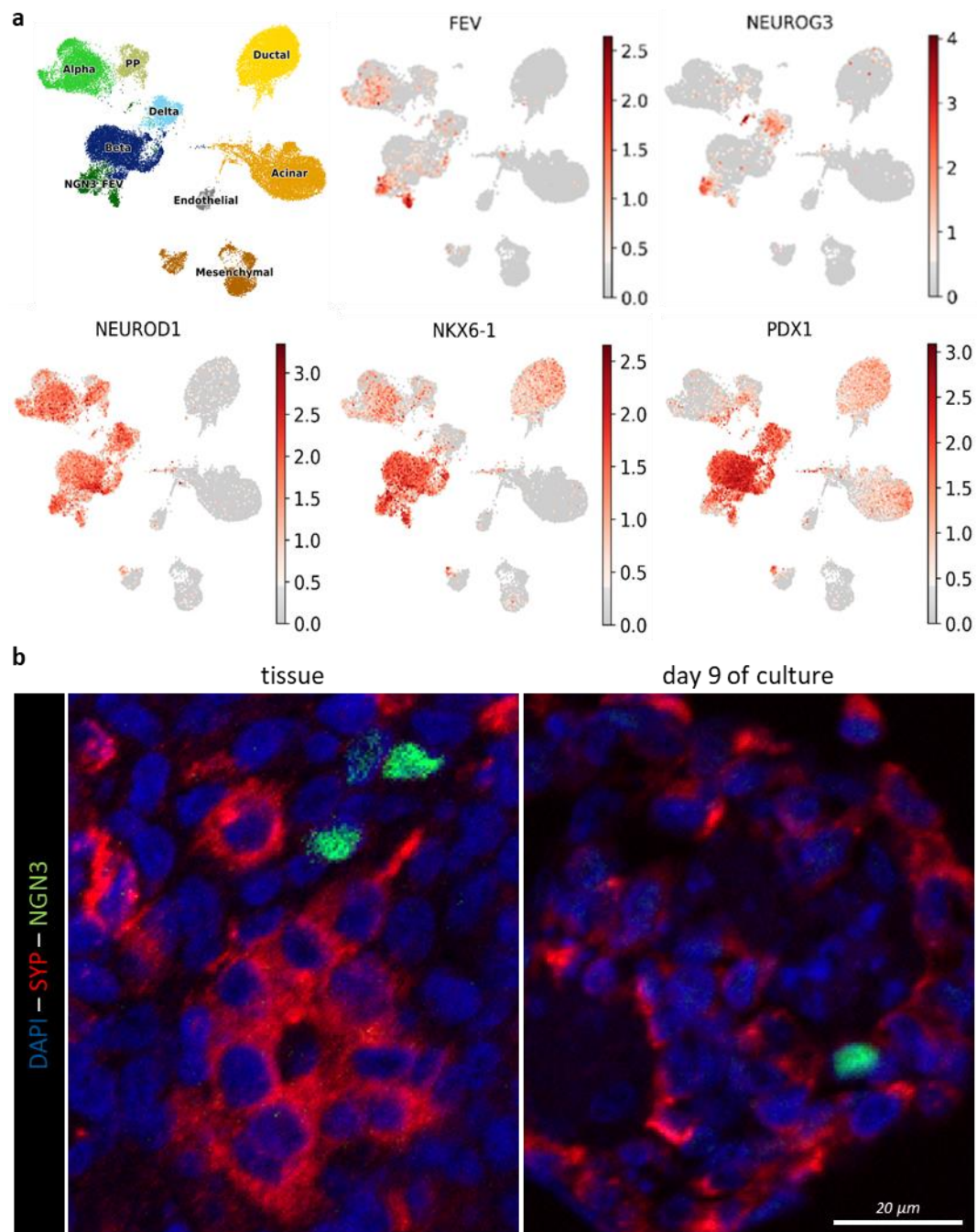


Figure 21: Characterization of endocrine progenitor-like cells in pNPCs. **a:** Neighborhood graphs showing the expression levels of endocrine progenitor markers FEV, NEUROG3, NEUROD1, NKX6-1, and PDX-1 (scRNA-seq). **b:** Immunofluorescence staining for NGN3 (green) and SYP (red) of age matched pancreatic tissue and pNPCs on culture day 9, demonstrating NGN3⁺ nuclear staining in few SYP⁻ cells. Nuclei are stained with DAPI (blue); scale bar 20 μ m.

Flow cytometry revealed a proportion of $18.3 \pm 2.2\%$ NGN3⁺ cells on culture day 0 (**Figure 22b**). Afterwards the proportion dropped to $4.4 \pm 0.9\%$, $6.2 \pm 1.0\%$, and $4.4 \pm 0.8\%$, at days 1, 3, and 9 of culture, respectively, with no significant difference between days (4-6%, p-values > 0.075). Of note, flow cytometry analysis of NGN3 in early culture was limited due to technical issues, including high background signal and indications of nonspecific binding in antibody controls. High proportions of NGN3⁺ cells are described in early culture (LAU et al., 2021), but must be seen critical considering proportions of other cell populations and no NGN⁺ cells being detected by Immunofluorescence at days 0 and 1. Thus it is difficult to draw conclusions for these timepoints. In conclusion, our findings proofed the presence of approximately 5% of Ngn3⁺ endocrine progenitor-like cells in *in vitro* matured pNPCs at the end of the culture period.

Examining the endocrine lineage markers PDX1 and NKX6-1 in combination with the hormones INS, GCG, and SST using flow cytometry, a population of PDX1⁺NKX6-1⁺ but hormone-negative cells became apparent at day 3 and 9 of culture (**Figure 10c and d**). The fact that these cells were hormone-negative but positive for endocrine developmental markers suggests that they were on the path to differentiate into endocrine cells but have not yet committed to one of the hormone-producing cell types. While these cells could theoretically also be other endocrine cells, such as PP cells, this seems unlikely given their very low abundance. These cells might also overlap with those described in the previous paragraph. Co-staining with NGN3 would be necessary to confirm this, but it was not technically possible due to the antibodies used. Furthermore, NGN3 is only transiently expressed, making co-staining likely less informative. The scRNA-seq data also supported this theory, as a significant proportion of the cells in the NGN3-FEV cluster are positive for both PDX1 and NKX6-1 and their numbers increase over the course of the culture (**Figure 12b and d**).

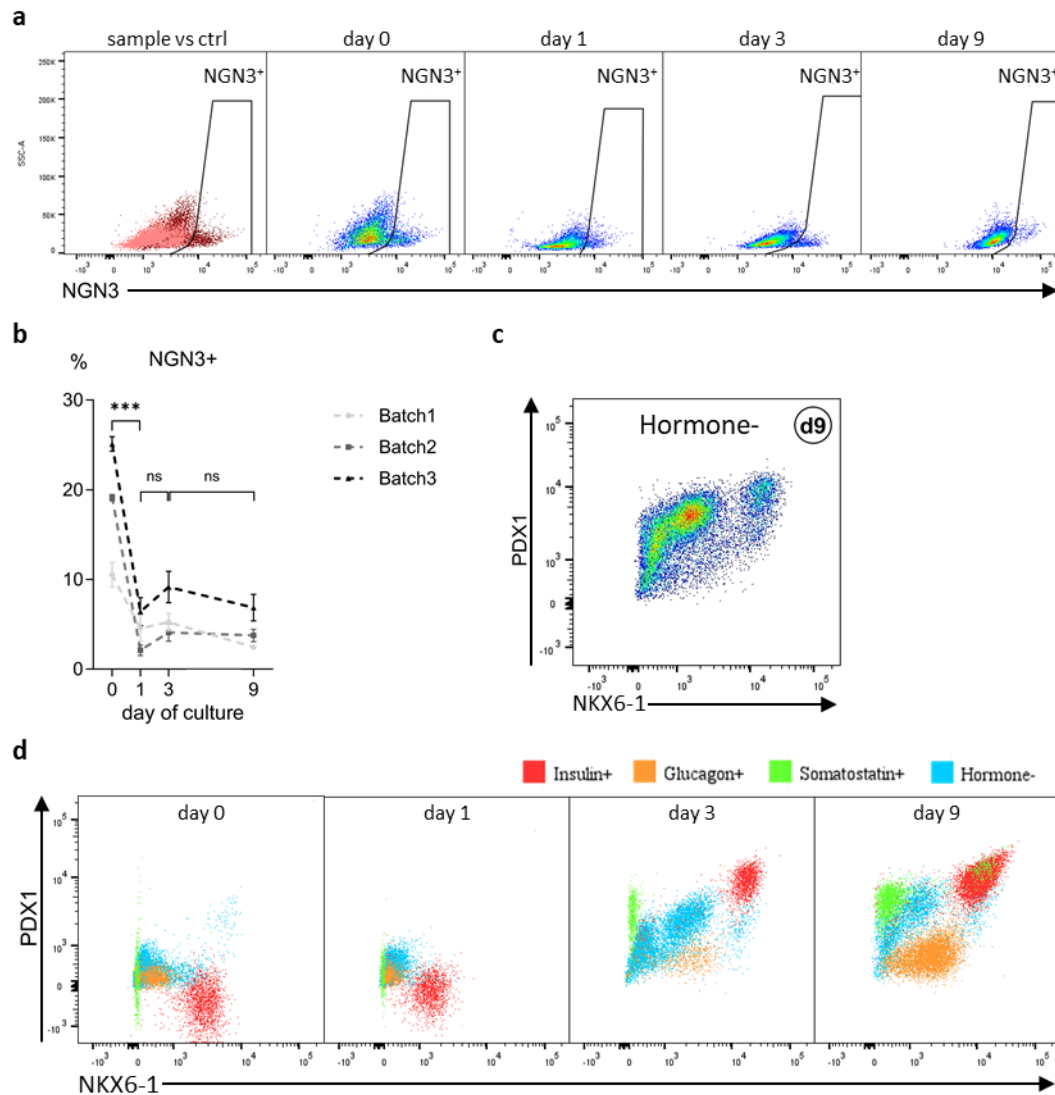


Figure 22: Prevalence of endocrine progenitor-like cells in pNPCs evaluated by flow cytometry. **a:** Representative gating plots for detection of NGN3 positive cells during culture (sample is colored dark red and antibody controls in light red). **b:** Proportions of NGN3⁺ cells; all values are means; error bars indicate SEM; n=9 (3 independent experiments with 3 isolates each); *p<0.05, **p<0.01, ***p<0.001. **c:** Dual-plot for NKX6-1 and PDX1 of hormone negative cells (INS⁻GCG⁻SST⁻) on culture day 9. **d:** Representative dual-plots for NKX6-1 and PDX1 of β (INS⁺, red), α (GCG⁺, orange), δ (SST⁺, green), and hormone⁻ (INS⁻GCG⁻SST⁻ blue) cells.

3.3. Occurrence of cells with multi-lineage molecular pattern

While examining the abundance of markers for endocrine and non-endocrine cells, we observed dual positive cells expressing both types of lineage markers simultaneously.

For instance, a distinct cell population exhibiting a pattern of SYP⁺CK7⁺ (endocrine and ductal marker) and SYP⁺VIM⁺ (endocrine and mesenchymal marker) was

detected by flow cytometry analysis at day 3 in all samples analyzed, only differing in the ratio of occurrence (**Figure 23a**). Such a population was not detected in samples before or after culture day 3. Dual SYP-VIM positive cells were also detected in immunofluorescence staining on slides, but only in clusters of culture day 9 (**Figure 23b**). In co-staining for SYP and CK7 two staining intensities were observed on culture day 9: SYP⁺CK7^{+(low)} dual positive cells with weak CK7 staining intensity and SYP⁻CK7^{+(high)} positive cells with strong CK7 staining intensity. These findings were in line with the completely shifted CK7 intensity observed in flow cytometry at day 9.

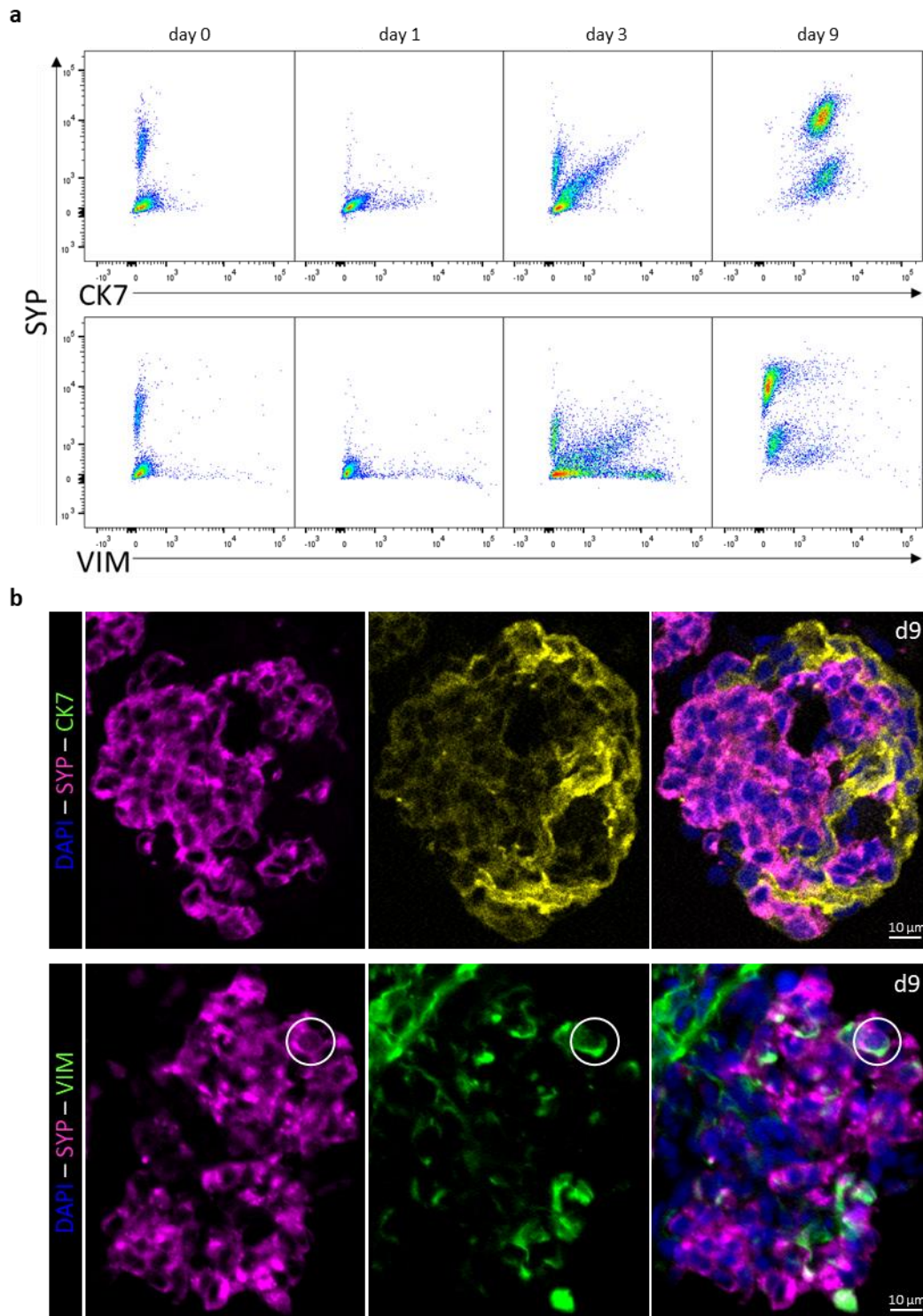


Figure 23: Cells with dual properties. **a:** Representative dual-plots for SYP and CK7/VIM of pNPCs on culture days 0, 1, 3, and 9 evaluated by flow cytometry. **b:** Immunofluorescence staining for SYP (magenta) and CK7 or VIM (both green) on culture day 9.

These signatures are an effect of *in vitro* culture, as they are not found *in situ*, and might indicate transdifferentiation of cells or cells with dual lineage properties. Therefore, we evaluated marker expression levels of pancreatic cell type specific markers and markers for the endocrine developmental process using scRNA-seq data. In detail, we focused on the question whether endocrine cells acquire non-endocrine properties or vice versa during the *in vitro* culture period.

The scRNA-seq data revealed minimal expression of non-endocrine markers in endocrine cells (**Figure 24**). For instance, a small proportion of all endocrine cell types, particularly the NGN3_FEV cluster on day 1, expressed KRT7 (ductal marker CK7). This expression exhibited a decreasing trend during culture and was significantly lower compared to ductal cells. This phenomenon may be a remnant of the developmental processes of endocrine cells originating from bipotent progenitors, which differentiate into both ductal and endocrine cells (NAIR & HEBROK, 2015). Consistent with flow cytometry observations, a subset of β cells on culture day 3 expressed VIM. Additionally, low expression levels of Carboxypeptidase A1 (CPA1) and Serine Protease 2 (PRSS2), both acinar markers, were detected across all cell types. As the fraction and expression levels decreased in correlation with the proportion of acinar cells, this may be an artifact caused by ambient RNA (see chapter 2.2). In summary expression of non-endocrine markers in endocrine cells was relatively low, and only in few endocrine cells present.

When examining non-endocrine cells, several atypical expression patterns were prominent (**Figure 24**). A portion of ductal cells expressed the endocrine lineage TFs PDX1 and NKX6-1, with the highest expression levels observed on day 3. Acinar cells exhibited a similar pattern, but only for PDX1. Additionally, acinar cells showed increasing proportions and expression levels of the ductal markers KRT7, Cystic Fibrosis Transmembrane Conductance Regulator (CFTR), and SOX9 throughout the culture period. The increase in ductal markers, coupled with the decrease in acinar cells and a significant rise in ductal cells by day 3 (**Figure 9a** and **Figure 12b**), suggests potential transdifferentiation from acinar to ductal cells.

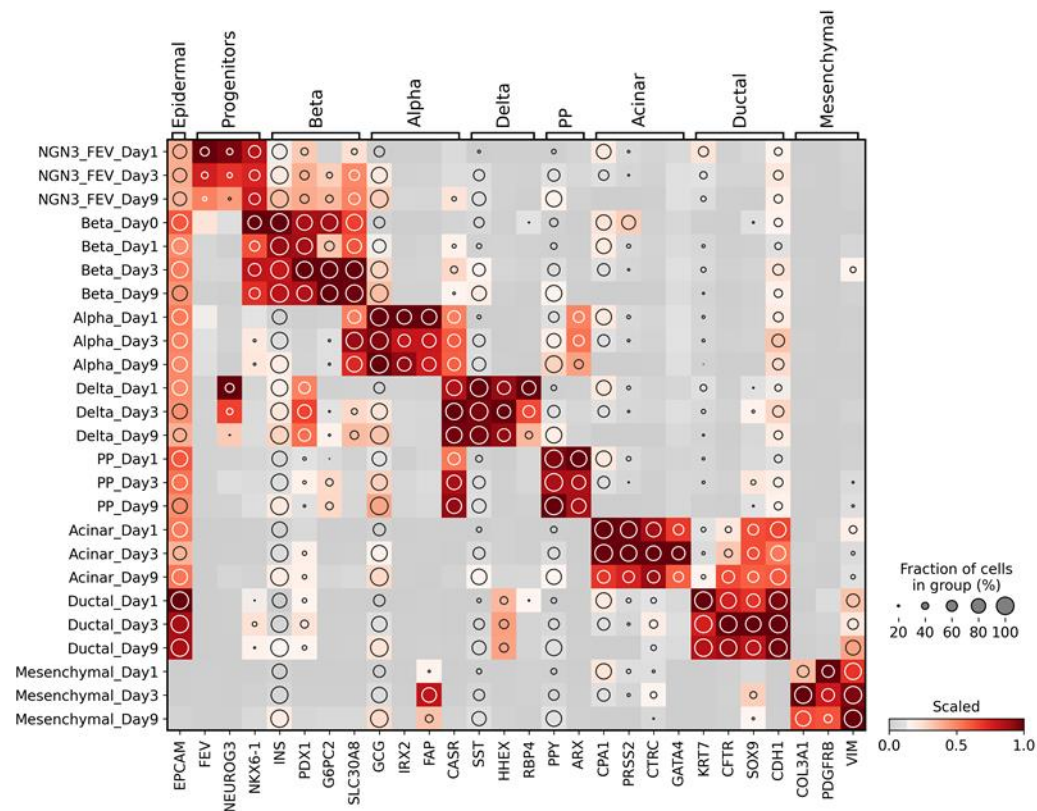


Figure 24: Expression levels of marker genes specific for pancreatic cell types from scRNA-seq data in pancreatic cell types of pNPCs during culture; $n=2$; the color intensity indicates the expression level and the circle size the fraction of positive cells (corresponding to Figure 10d).

Atypical SOX9 expression was detected not only in acinar cells but also in a subset of mesenchymal cells on day 3. Since SOX9 is a marker for multipotent pancreatic progenitor cells during development, from which acinar, ductal, and endocrine cells originate (NAIR & HEBROK, 2015), this could indicate the reprogramming of mesenchymal cells towards an epithelial-like state. Further evidence for mesenchymal cells transitioning towards an endocrine lineage was found in a subpopulation on culture day 9 (Figure 25). These cells expressed at relatively high levels hormone-processing and vesicle-associated genes such as Carboxypeptidase E (CPE), Proprotein Convertase Subtilisin/Kexin Type 2 (PCSK2), Secretogranins III and V (SCG3/SCG5), and CHGA, which are typically expressed exclusively in endocrine cells. Taken together, these observations suggest the presence of plastic processes in subsets of non-endocrine cells towards endocrine fate.

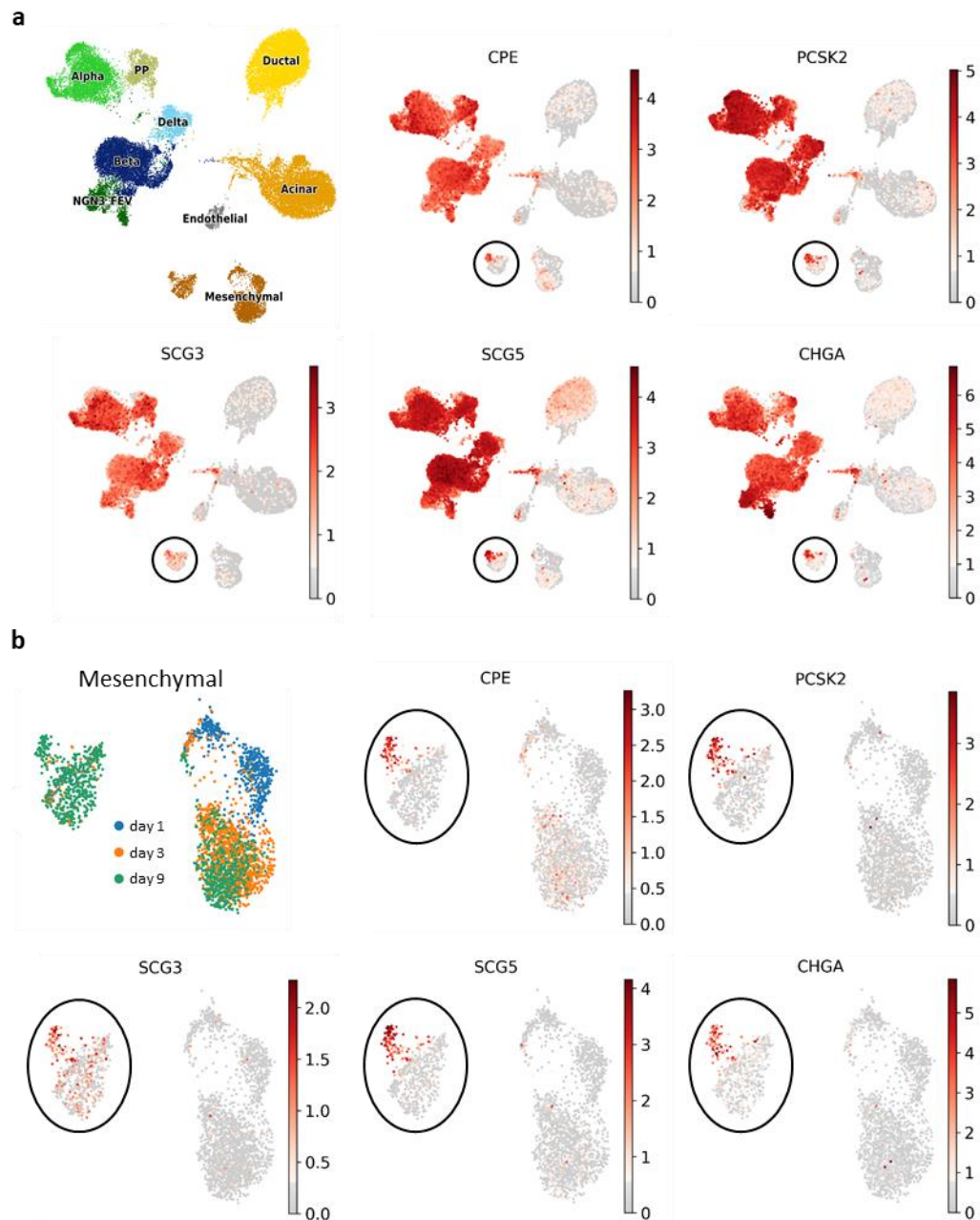


Figure 25: Neighborhood graphs showing the expression level and distribution of selected endocrine cell markers from scRNA-seq data of pNPCs; $n=2$; the color intensity indicates the expression level. **a:** In pancreatic cell types. **b:** In mesenchymal cells. Population of mesenchymal cells exhibiting endocrine properties marked by circles.

All of these findings indicate processes in which subsets of cells acquire atypical characteristics during culture, primarily non-endocrine cells transitioning to a more endocrine-like state. These *in vitro* patterns need to be validated by other methods in a follow-up study. Nevertheless, these findings support the hypothesis that *in vitro* matured pancreatic clusters have a high capacity for plastic processes.

3.4. Cell-cell interaction & matrix

The interaction of endocrine cells with other cells and the extracellular matrix (ECM) is essential for preserving *in vivo* function, as well as for the differentiation and maturation of pancreatic endocrine cells (WIELAND et al., 2021). Consequently, the expression of ECM and cell-cell interaction molecules in the pancreas and islets of Langerhans was evaluated using scRNA-seq data.

Markers were predominantly expressed by non-endocrine cells, with a general trend of increased expression levels during culture (**Figure 26**). Integrins, which are cell adhesion molecules vital for pancreatic tissue integrity and β -cell function (AROUS & WEHRLE-HALLER, 2017) showed the highest expression levels in non-endocrine cells. Integrin subunits Beta 1 (ITGB1), Alpha V (ITGAV), and Alpha 6 (ITGA6) were also expressed in endocrine cell types, albeit at lower levels and fractions compared to non-endocrine cells. In β cells, ITGB1, ITGAV, and ITGA6 exhibited peak expression levels on day 3 of culture. Laminins, essential components of the islet basement membrane and important for β -cell function (SIGMUNDSSON et al., 2018), were primarily expressed in mesenchymal or exocrine cell types, similar to integrins. Laminin subunits Beta 1 (LAMB1) and Gamma 1 (LAMC1) were also expressed by endocrine cells, with the highest expression levels observed in β cells on day 3 of culture.

Markers primarily expressed in endocrine cells included Ephrin A5 (EFNA5), relevant for cell-cell communication, and Neural Cell Adhesion Molecule 1 (NCAM1), a cell adhesion molecule, both associated with β -cell function (ESNI et al., 1999; BERNARD-KARGAR et al., 2001; KONSTANTINOVA et al., 2007). β cells exhibited a drop and recovery pattern for EFNA5 and an increase in expression levels of NCAM1. The expression of these markers, which are crucial for β -cell function, in various cell types underscores the importance of cell heterogeneity as a foundation for a functional product in β -cell replacement therapy.

Cell-cell and cell-matrix interaction

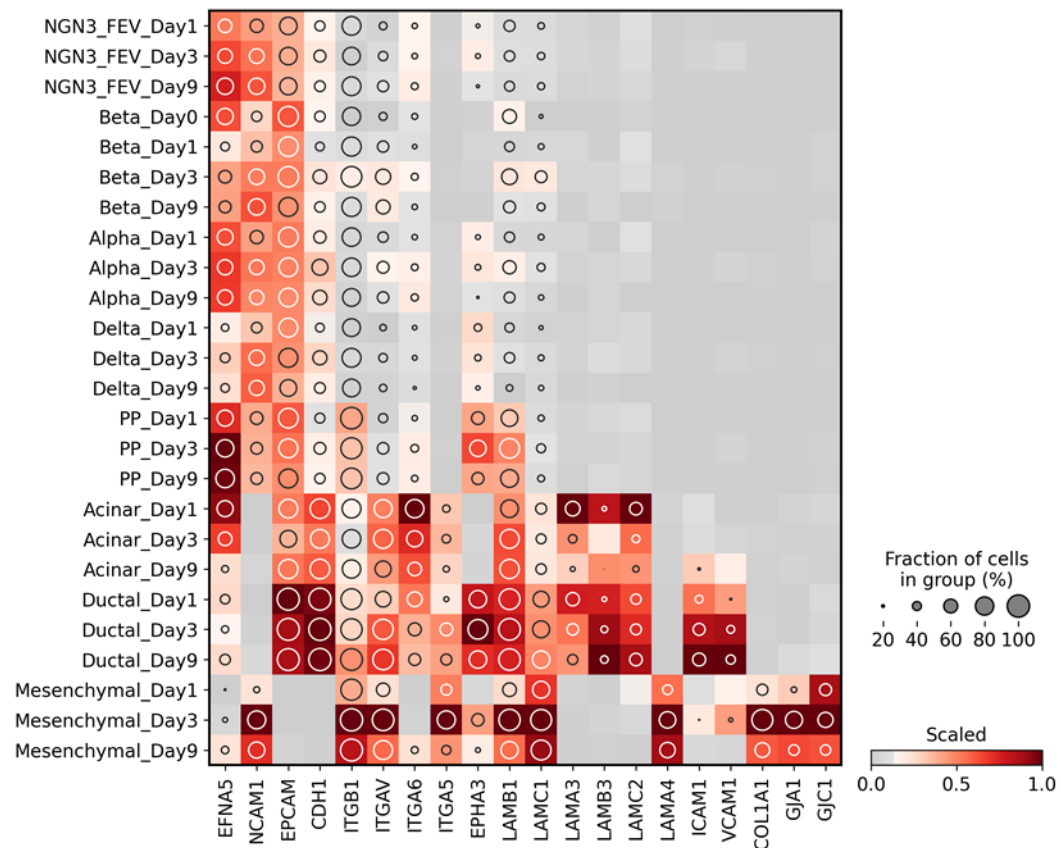


Figure 26: Expression levels of marker genes associated with cell-cell and cell-matrix interaction from scRNA-seq data in pancreatic cell types of pNPCs during culture; the color intensity indicates the expression level and the circle size the fraction of positive cells.

3.5. Endocrine cells show signs of ER-stress in early but also late culture

Due to significant volume losses (**Figure 3**), morphological signs for cell death (**Figure 5**), and signs of stress in endocrine cells (**Figure 15** and **Figure 17**) and the anticipated effects of a non-physiological environment on stress-sensitive pancreatic endocrine cells, markers for different endoplasmic reticulum (ER)-stress cascades were examined using scRNA-seq data. Assessing ER stress presents significant challenges. ER stress is crucial during the maturation of highly specialized β cells, which must evolve into insulin-producing powerhouses equipped with glucose-sensing and vesicle-release mechanisms. However, excessive ER stress can be detrimental, leading to cellular apoptosis.

It was generally observed that many markers, aside from β cells on day 0, showed the highest expression levels in non-endocrine cells (**Figure 27**). This was

particularly evident for the PERK pathway. Considering the significant decrease in non-endocrine cells during culture (**Figure 9**), this could explain the preferential depletion of those cell types. While no clear pattern was observed in ductal cells, acinar cells mainly showed a decreasing trend after day 1, which aligns with the significant depletion of acinar cells in the early days of culture and might be a sign for NGN3 adaptation of residual acinar cells. Interestingly, the NGN3_FEV cluster showed the lowest overall expression levels of ER stress markers. This could be due to the lower protein turnover compared to hormone-producing cells and the high adaptability of precursor cells.

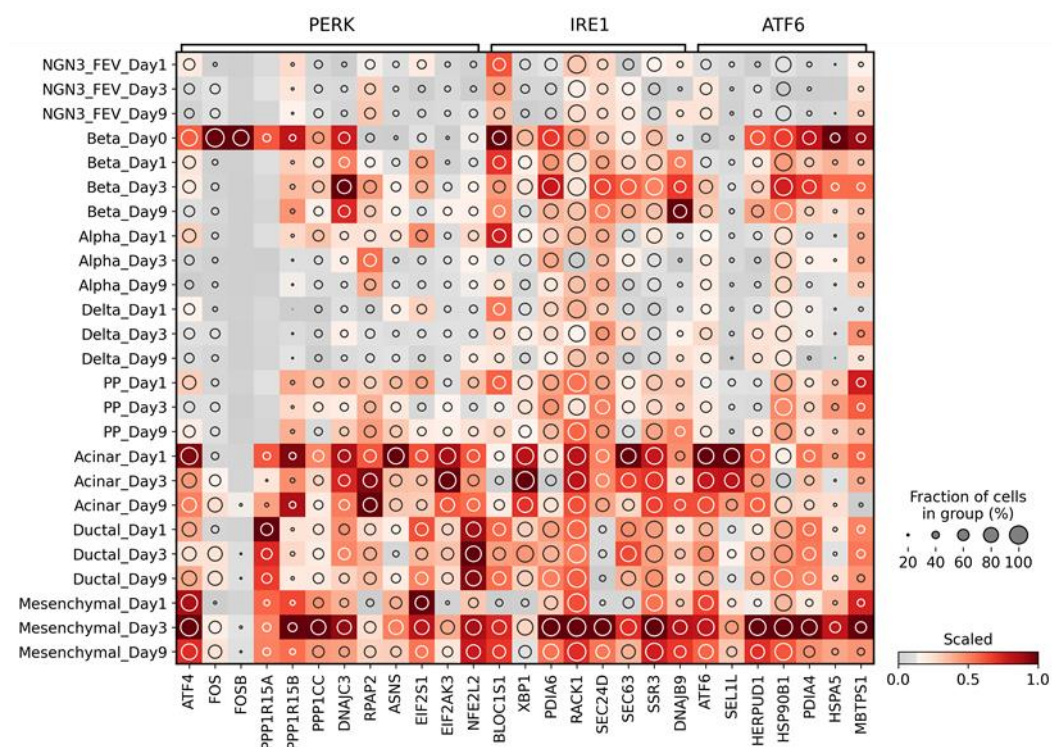


Figure 27: Expression levels of ER-stress-related genes from scRNA-seq data in pancreatic cell types of pNPCs during culture; the color intensity indicates the expression level and the circle size the fraction of positive cells.

Examining β cells individually, it became apparent, that numerous markers exhibited the highest expression levels on culture day 0 (**Figure 28**). This initially high expression levels decreased for all these markers by day 1, potentially indicating a reduction following initially elevated ER stress levels due to cluster isolation and the *in vitro* environment. An example of this stress reduction in β cells with prolonged culture is the decrease in Biogenesis of Lysosomal Organelles Complex 1 Subunit 1 (BLOC1S1) and X-Box Binding Protein 1 (XBP1), both involved

in ER stress via the IRE1 pathway.

Typically, elevated Endoplasmic Reticulum to Nucleus Signaling 1 (ERN1, similarly IRE1) activity, along with increased levels of XBP1 and BLOC1S1, induces apoptosis via DNA Damage Inducible Transcript 3 (DDIT3, similarly CHOP) (BAE et al., 2019) (BRIGHT et al., 2015). This reduction might be associated with the increase of DnaJ Heat Shock Protein Family (Hsp40) Member B9 (DNAJB9), a co-chaperone for Heat Shock Protein Family A (Hsp70) Member 5 (HSPA5, similarly BiP), which also shows a reduction during culture, that acts as a repressor of ERN1-mediated ER stress (FRITZ et al., 2014).

Besides markers with decreasing expression levels throughout culture, some markers show an increase in expression levels after culture day 0, but at low levels compared to other cell types. One example is Eukaryotic Translation Initiation Factor 2 Alpha Kinase 3 (EIF2AK3, similarly PERK) and its downstream target Eukaryotic Translation Initiation Factor 2 Subunit Alpha (EIF2S1, similarly EIF2 α). Signaling of this cascade is essential for the expression of PDX1 and other β -cell maturation markers (BACK et al., 2009). As markers associated with islet development (e.g., PDX1), protein processing, secretory granules, and glucose and calcium-related signaling show similar fluctuations or even an increase at the transcriptome and proteome levels, this might indicate physiological stress and a positive coupling of PERK with the maturation processes.

It is important to emphasize in this context that these results only provide indications, and further investigations are necessary to prove such mechanisms.

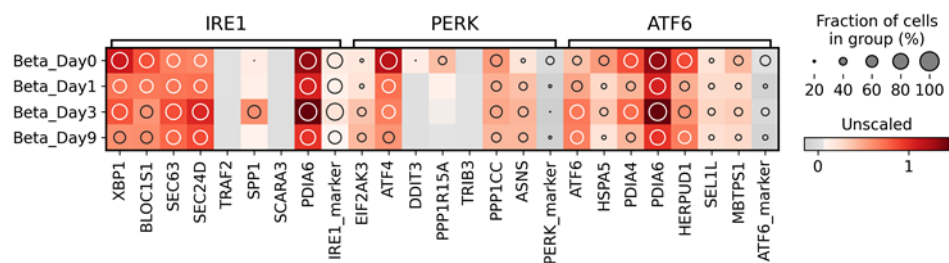


Figure 28: Expression levels of ER-stress-related genes from scRNA-seq data of β cells on culture days 0, 1, 3, and 9; color indicates expression level and circle size the fraction of positive cells.

VI. DISCUSSION

The major bottleneck in islet transplantation is the shortage of human donor pancreata. An alternative source to meet the demands is porcine pancreatic tissue. Although adult porcine islets are fully functional, their isolation is costlier, less predictable and less scalable compared to clusters derived from neonatal pig pancreas (VANDERSCHULDEN et al., 2019). Due to the functional immaturity of the pancreas in neonatal piglets, isolated neonatal pancreatic cell clusters have to undergo an *in vitro* maturation process to develop the capacity for engraftment and to achieve normoglycemia following transplantation into a diabetic recipient. (JIMENEZ-VERA et al., 2015).

However, up to date, there is no consensus on the optimal conditions for this maturation process and the ideal characteristics of the pre-transplant product (KEMTER & WOLF, 2018). Furthermore, the cellular dynamics and molecular changes during *in vitro* culture of pNPCs remain largely unexplored.

In our study, we decided to use the Ham's F10-based medium, initially described by Gregory Korbitt and colleagues, along with their development of the isolation method for clusters from neonatal pig pancreas (KORBUTT et al., 1996). This medium is commonly used today.

Extended culture periods can significantly improve transplant success but are also associated with further loss of transplantable cells mass (JIMENEZ-VERA et al., 2015; MA et al., 2018; ZHANG et al., 2021). Since a sufficient transplant mass is crucial for restoring endogenous blood glucose homeostasis, and considering animal welfare and scalability, we decided to limit the culture period to 9 days.

During these 9 days we demonstrated that pNPCs consist of a diverse mixture of endocrine and non-endocrine cell types. Endocrine cells, particularly β cells, were enriched while non-endocrine cells were depleted. Additionally, β cells exhibited early signs of stress, followed by clear indications of maturation. Evidence of plastic processes, such as β -cell proliferation, the presence of an endocrine progenitor-like pool, and signs of transdifferentiation from non-endocrine to endocrine cells, were observed throughout the culture duration.

1. Endocrine enrichment with preserved heterogeneity

Media compositions for pNPC culture vary among research groups, utilizing different basal media, glucose concentrations, protein sources, along with a variety of additives such as insulin secretagogues. The protocol for the isolation and culture of pNPCs was first described by Dr. Korbitt, who used a serum-free medium based on Ham's F10, with a glucose concentration of 10mmol/L, and supplemented with IBMX, L-Glutamine, and nicotinamide (KORBUTT et al., 1996). Using this media, we achieved an average of 24% β cells, 12% α cells, and 7% δ cells (~60% total endocrine cells) within 9 days. This endocrine cell content in pNPCs is comparable to the findings of other groups using similar media (NIELSEN et al., 2003; ELLIS et al., 2016; AREFANIAN et al., 2022).

Many groups studying pNPCs for its usage for transplantation predominantly focus on later culture time points, often neglecting the compositional and molecular dynamics of the early culture phase. However, the dynamic processes occurring during the initial culture period might significantly influence outcomes in later culture period and after transplantation. Our investigations, for example, revealed an unexpected lack of enrichment in the endocrine cell compartment between day 0 and day 1 of culture, despite a substantial loss in the exocrine cell compartment during the first day post-isolation. This indicates that endocrine cells are also affected by significant mass loss, leading to the demise of many of these cells during early culture.

Additionally, our culture system clearly showed a preferential enrichment of β cells over α cells (increase day 1-9: β cells 5.8-fold, α cells 4.0-fold. Contrary, studies utilizing Ham's F10 and Ham's F12/M199-based media, a greater increase in α cells compared to β cells was observed (NIELSEN et al., 2003; LAU et al., 2020).

A common observation in studies differentiating hiPSCs into β -like cells is the presence of non-functional polyhormonal cells (AIGHA & ABDELALIM, 2020; TIEMANN et al., 2025). This phenomenon might be attributed to suboptimal differentiation methods, which lead to premature endocrine commitment (KARIMOVA et al., 2022). In our study of pNPCs culture, we did not observe an enrichment of polyhormonal cells, as their content consistently remained below

1% of the total cell population. This might be due to the fact that pNPC differentiation and maturation in culture begin with cells already at a later differentiation stage. In contrast, β -like cells are derived from pluripotent cells, and inappropriate differentiation during early stages can lead to improper lineage differentiation in later stages.

Despite the enrichment of primarily β cells, the complexity within the endocrine compartment of pNPCs was preserved, including α , δ , and PP cells. Additionally, the composition within the endocrine compartment underwent significant changes after the day of isolation (day 0) but eventually reverted to the composition observed on day 0, suggesting a return to the original state. This composition mirrors the *in situ*-situation (BRISSOVA et al., 2005; HOANG et al., 2014). In human and pig islets, α cells not only represent the second largest population after β cells but are also significantly more abundant compared to rodent islets, with approximately half the number of β cells in human and pig (CABRERA et al., 2006).

The heterogeneity and composition of endocrine cell types in pNPCs offer a significant advantage over stem cell-derived β -like cells. This diversity is crucial for effective cell-cell communication among endocrine cells and provides the basis for maintaining blood glucose homeostasis, as well as for cell heterogeneity and plasticity (CABRERA et al., 2006; ROSCIONI et al., 2016; ARROJO et al., 2019; HILL & HILL, 2024).

2. Switch from initial dominant molecular stress signature towards a maturation signature in endocrine cells

Endocrine cells are the primary desired cell type for a β -cell replacement therapy product. However, large quantities of endocrine cells alone, without proper function post-transplantation, would be ineffective. Generally, the cultivation of products derived from neonatal pig pancreas is referred to as the "*in vitro* maturation process". Prolongation of the *in vitro* culture period was identified as one factor positively correlating with transplantation success (JIMENEZ-VERA et al., 2015). While the enrichment of endocrine cells in pNPCs is well-documented, it remains unclear whether these endocrine cells undergo functional maturation during the *in vitro* culture period.

Our investigations revealed that, during the early culture period, only a few endocrine cells were present, and these exhibited drastic changes in their molecular profile. For instance, insulin content in β cells dropped by 89% between days 0 and 3, and the abundance of the granular marker synaptophysin (SYP) decreased by more than 60% between culture days 0 and 1. β cells also showed a reduction in β -cell identity markers in the transcriptome, with only low protein levels of PDX1 and NKX6-1. While α and δ cells exhibited similar reductions in SYP protein abundance, the decrease in their hormone levels was less pronounced compared to β cells (days 0-3: β cells 89%, α cells 61%, δ cells 67%). Additionally, many endocrine cells identified by SYP expression lacked clear expression for the hormones INS, GCG, or SST on day 3. One possible explanation for this finding could be the presence of other endocrine cell types, such as ghrelin-secreting ϵ cells or neuronal cells. However, the existence of endocrine cells depleted of hormone storage has been reported (CINTI et al., 2016; MD MOIN et al., 2016). Furthermore, β cells showed high expression levels of ER-stress-associated markers on culture day 0. These observations indicate clear signs of stress in the early culture period and caused by the isolation process itself.

This initial stress experienced by cells can be attributed to various factors, with the loss of tissue integrity being the most significant challenge. Further, cluster size greatly influences cell survival during the culture period. For proper function,

endocrine cells require sufficient oxygen supply, which is physiologically provided *in vivo* by blood flow in the capillaries. Islets, despite constituting only ~2% of the pancreas, require up to 20% of the pancreatic blood supply (JANSSON et al., 2016). However, during the isolation process and in culture, nutrient and oxygen supply are limited to diffusion. Several factors influence sufficient supply, including diffusion length directly associated with cluster size, oxygen content in the media, and dynamic versus static culture conditions (KOMATSU et al., 2018; JUN et al., 2019). The presence of larger clusters (>150 μm) is particularly problematic, as their centers are less well supplied with nutrients and oxygen due to excessive diffusion distances (KOMATSU et al., 2017). β cells, which are highly functional and have high oxygen and nutrient demands, are especially sensitive and likely undernourished. Additionally, the loss of numerous cell-cell and cell-matrix interactions, essential for maintaining these highly specialized cells (WIELAND et al., 2021), might have further negative effects. The release of digestive enzymes from acinar cells could also have detrimental effects on other cells (ROSE et al., 2003).

While the scRNA-seq profiles of pNPCs in the early culture period were enriched with cells exhibiting a stress signature, there was also an enrichment of endocrine cell profiles with a mature hormone-secretion signature. Specifically, β cells showed significant signs of maturation throughout the culture process, encompassing the entire insulin synthesis, glucose sensing, and insulin secretion pathways for glucose-induced insulin release.

The scRNA-seq data revealed that the highest expression levels of most markers related to hormone synthesis and processing, secretory vesicles, and glucose and calcium signaling were observed on culture day 3. Notable markers included proprotein convertases, CHGB, secretogranins, synaptotagmins, and calcium channels. Distinct signs of maturation were also evident at the protein level in endocrine cells. After an initial drop from culture day 0 to day 1, granularity, as assessed by SYP expression, increased in all endocrine cells from day 1 onwards, eventually doubling the SYP levels observed on day 0 by culture day 9. While the β -cell identity and maturation markers PDX1 and NKX6-1 were below the detection limit on culture days 0, 1, and 3 in β cells, their abundance increased

throughout the culture period, with a clear $INS^+PDX1^+NKX6-1^+$ population observed on culture day 9. Like granularity, hormone abundance recovered after an initial drop in α and δ cells, although β cells did not recover by day 9. Another indication that the machinery for glucose sensing and release in β cells is functional is that clusters exhibited biphasic insulin secretion in response to glucose stimulus *in vitro* at day 9.

Together, these findings indicate clear signs of *in vitro* maturation of endocrine cells. However, several questions remain unresolved. While the expression of almost all marker genes for secretory vesicles, such as CHGB, increased in β cells during the culture period, a continuous decline was detected for CHGA, which is described to be found in older insulin granules (NEUKAM et al., 2024). Whether differences in the ratio between old and young granules exist in *in vitro* matured β cells in the pNPCs culture system, and whether these differences might impact the function of the pNPC product, need to be analyzed in a follow-up study. Additionally, the reason why hormone levels in β cells, unlike in α and δ cells, did not recover during the pNPC culture period, should be addressed in future research.

3. pNPCs show cellular and molecular heterogeneity and signs of plastic processes

As described in Chapter VI.1, heterogeneity within the endocrine compartment is vital for β -cells. Another crucial aspect involves interactions with the extracellular matrix (ECM) and to non-endocrine cells. These interactions are necessary for maintaining tissue integrity, but are also essential for β -cell survival and functionality (PINKSE et al., 2006; LLACUA et al., 2016; SIGMUNDSSON et al., 2018; TOWNSEND & GANNON, 2019).

We demonstrated that endocrine cells produce ECM components that are critical for β -cell function, such as integrins and laminins (AROUS & WEHRLE-HALLER, 2017; SIGMUNDSSON et al., 2018). Of note, these components were predominantly expressed by non-endocrine cell types, such as ductal and mesenchymal cells. Mesenchymal cells also expressed collagen IV, which is described to impact β -cell survival and function (KAIDO et al., 2004). These cells are also described as necessary signaling agents for the proliferation and differentiation of the endoderm during development, what might be relevant also in our pNPC culture system due to the ongoing developmental processes in pNPCs (LANDSMAN et al., 2011).

Given the developmental stage of the pancreas from neonatal donor animals and the generally observed cell plasticity, the mesenchymal pool in the neonatal pancreas might hold potential for multipotent mesenchymal stromal cells (MSCs). These cells provide essential regulatory cues for proper β -cell function and have positive effects on revascularization after transplantation (ITO et al., 2010; HAYWARD et al., 2017; MONTANARI et al., 2021).

In addition, we identified cell populations exhibiting dual properties of endocrine and mesenchymal lineages. For example, we found endocrine cells expressing VIM, indicating that these cells were undergoing epithelial to mesenchymal transition (EMT), similar to observations in human islet cultures. In these cultures, endocrine cells co-express VIM and show signs of losing their β -cell phenotype, with reduced levels of INS, NKX6-1, GCK, and PCSK2 (MORENO-AMADOR et al., 2018). To address this issue, EMT inhibitors such as A83-01 could be utilized.

Furthermore, a subpopulation of mesenchymal cells exhibited high expression levels of hormone-processing and vesicle-associated genes such as CPE, PCSK2, secretogranins, and CHGA, suggesting a dynamic process where mesenchymal cells might acquire endocrine-like characteristics. Although this seems unusual, as mesenchymal and endocrine cells are developmentally distinct, such phenomena have been described for the aforementioned MSCs (CHEN et al., 2004; CHAO et al., 2008; CHANDRA et al., 2009).

Furthermore, ductal cells from pNPC exhibit high plasticity, as evidenced by the increase in ductal cells on culture day 3, their cycling properties throughout the culture period, and their positivity for endocrine cell markers. This suggests that these ductal cells might be a source for differentiation towards β cells both *in vitro* and *in vivo* after transplantation, as described in pNPC grafts transplanted in diabetic mice (TRIVEDI et al., 2001). Thus, the preservation of these cells might not only support cellular cohesion and function but also might offer the potential for β -cell neogenesis following transplantation. Whether this leads to the formation of functional endocrine cells and the underlying mechanisms driving this transformation into endocrine-like cells remain to be investigated. One possibility might be that this process involves Notch lateral inhibition, similar to mechanisms observed during embryogenesis (ACKERMANN & GANNON, 2007).

Another indication of high plasticity is the presence of proliferating β cells and endocrine progenitor-like cells in pNPCs throughout the culture period. The presence of proliferating β cells offers an advantage in the islet transplantation setting. Although proliferating β cells are often not fully functional, they provide an opportunity for post-transplantational expansion of β cells (TRIVEDI et al., 2001). A potential benefit of this is that fewer clusters need to be transplanted, distinctly reducing the transplant volume and the number of donor pancreata required to achieve normoglycemia in a diabetic recipient. Over time, however, there would still be enough β cells to restore endogenous glucose homeostasis (AAMODT & POWERS, 2017).

Furthermore, we described populations that showed typical patterns of endocrine progenitors like the expression of NGN3, FEV, and other endocrine lineage markers, but not of hormones. Endocrine progenitors represent an early stage in

the development of the islet of Langerhans but are already committed to the endocrine lineage. These cells serve during development, but also in postnatal life, as multipotent precursor pool with the capacity to give rise to all endocrine cell types of the islets of Langerhans (RAZAVI et al., 2015; GRIBBEN et al., 2021; LICKERT et al., 2024). In the transplantation setting, these cells might be beneficial as they could serve as a source for new endocrine cells without being prone to post-transplant stress (EGUCHI et al., 2022).

The potential multipotency described for mesenchymal and progenitor-like cells, while advantageous, also carries inherent risks. In hiPSC β -like cell products derived from cells capable of forming all three germ layers, the potential for malignant transformation, such as teratoma formation, exists due to the risk of remaining residual undifferentiated cells (HAN et al., 2022). However, since all cells in pNPCs originate from postnatal tissue, which no longer contains cells with such pluripotency (TAKAHASHI & YAMANAKA, 2006), this risk is significantly lower and has not been reported to date.

In general, cell plasticity can offer significant advantages but can also indicate less-functional cells. For xenotransplantation, the goal is to restore endogenous insulin release in response to glucose stimulation by replacing β cells. At first glance, a mature product capable of performing this function immediately after transplantation seems optimal. However, transplanted cell clusters are initially subjected to significant stress, and more mature products often do not perform better after transplantation (LOPEZ-AVALOS et al., 2001). This might be due to oxygen and nutrient deprivation caused by the lack of microvascularization in the early post-transplant period (STERKERS et al., 2013; COHRS et al., 2017). Transplanted islets, irrespective if they were derived from an adult or a neonatal pancreas, must be revascularized and all endothelial cells for this process are known to be derived from the graft recipient. Mature β cells, being highly specialized, are most affected by these stressors, as they have limited adaptability, leading to dedifferentiation and, in the worst case, to cell death. Besides the loss of β -cell mass, this can have negative effects due to immune cell responses, such as immune cell infiltration and inflammation, to remove the cell debris and leading to further cell damage. Therefore, despite the lower degree of maturity described

in neonatal pancreatic clusters, this primarily poses a problem of delayed function after transplantation, but could also offer an advantage for cell survival after transplantation.

In summary, we demonstrated that pNPCs are cell clusters with significant cellular and molecular heterogeneity and plasticity. We identified cell types with the potential for β -cell neogenesis, self-replication, and transdifferentiation. Whether these cells contribute to improved transplant outcomes needs to be investigated in follow-up studies. Overall, our results suggest that pNPCs possess properties that may offer advantages over stem cell-derived and mature β -cell replacement products.

4. Challenges to obtain a pNPC product with constant properties for β -cell replacement therapy

Working with pNPCs presents challenges due to various factors. Literature and experience within our research group indicate significant variability in pNPC isolation and culture outcomes between independent isolation batches, as well as among different isolates from a single batch produced in parallel (HUANG et al., 2021). Factors influencing these outcomes are numerous and include the age of the pancreas donor animal, variations among age-matched donor animals such as body weight and nutritional status, prolonged cold ischemia time of the pancreas, and technical differences in the manually performed isolation and culture process.

Such batch-to-batch heterogeneity can profoundly impact transplant outcomes, potentially leading to misinterpretation of study results. This was demonstrated in a detailed study by Huang and colleagues, which aimed to compare the effects of various genetic modifications in pancreas donor pigs on transplant outcomes (HUANG et al., 2021). However, the study found that transplant outcomes were predominantly affected by the negative effects of prolonged cold ischemia time, rather than the genetic modifications of the donor pigs. Therefore, it is crucial to properly characterize the pNPC product and ensure that it meets certain quality criteria before its use in pre-clinical and, potentially in the future, clinical transplantations. The methods applied for quality control for pNPCs have to result in data interpretation within a short time period prior to the usage in transplantation, prioritizing methods like flow cytometry analysis.

With the panel of targets used in our study, we could detect batch to batch effects, like described previously. For instance, our study revealed differences between isolation batches for various flow cytometry parameters (proportion of α and δ cells, insulin abundance in β cells, granularity in β , α , and δ cells) but no significant differences within single batches with replicates produced in parallel. This indicates variability between, but not within, isolation batches of pNPCs. The minimal differences within isolation batches can be attributed to the fact that donor animals were littermates, sharing the same genetic background and environmental influences. The differences between batches might arise from

variations among donor animals of different isolations and the isolation process itself. Since the animals used for these experiments were all between 3 and 5 days old and came from a farm with consistent breeding genetics and environmental factors, the differences between donor animals across isolation rounds should be minimal (AREFANIAN et al., 2022). Additionally, the isolation is performed by skilled personnel following a stringent protocol.

As a next step, this panel of target proteins used in our study for flow cytometry analysis have to be adapted and enlarged for further target molecules that have a proofed association between pNPC product quality and its efficiency for normalizing blood glucose levels after transplantation in diabetic recipients.

Due to signs of β -cell stress especially in early culture, analyses with non-fixed cells using dyes, such as those for mitochondrial membrane permeability (JC-1), reactive oxygen species (Dihydrorhodamine 123), or early apoptosis (Annexin V) could be helpful. This proved to be challenging during our experiments as these analyses could not be combined with cell type identification. Neither a combination with classical markers like INS or SYP was possible, as cells need to be fixed and permeabilized for this, nor were suitable surface antigens for endocrine or β cells in pigs available.

Furthermore, the markers identified through scRNA-seq data for hormone synthesis and processing, secretory vesicles, and glucose- and calcium-related signaling represent potential new quality indicators. However, these must be validated at the protein level before application.

In summary, quality control of pNPCs is crucial due to significant batch-to-batch variability. However, establishing appropriate quality standards is challenging due to the heterogeneous composition of pNPCs and technical limitations associated with the pig species. Through this work, we have developed several tools and identified potential new markers using scRNA-seq.

5. How to further improve *in vitro* cultivation of pNPCs

With the characterization of the molecular signature and composition of cells in pNPCs during the whole *in vitro* culture period, the present data set will provide the basis for making targeted modifications of the media composition. Various groups have demonstrated that altered culture conditions can significantly enhance both *in vitro* functionality and transplant outcomes (HASSOUNA et al., 2018; MA et al., 2018; ZHANG et al., 2021). Up to date, modifications of culture media were done mainly with additives which were first used for hiPSC-derived β -like cell differentiation protocols. Due to limited knowledge of the human pancreas development, additives for modulating selected signaling pathways were selected on the basis of mouse embryonic pancreas development. However, species differences between mouse and human pancreas development and β -cell differentiation exist (NAIR & HEBROK, 2015) and this might also explain the heterogeneity and difficulties of hiPSC-differentiation protocols to get functional β cells (SIEHLER et al., 2021; BALBOA et al., 2022). In contrast to mice, the molecular signatures of β -cell differentiation from progenitor cells showed greater similarity between humans and pigs than between humans and mice, where there are some clear differences (LICKERT et al., 2024).

Culturing the pNPCs in the Ham's F10 based media adjusted to 10 mM glucose and supplemented with IBMX resulted that certain maturation markers did not further increase after day 3, while specific stress signals peak on day 0 and persist partially in subsequent culture stages. This phenomenon may result from suboptimal culture conditions, which induce cell stress and death. The retention of dead cell material within clusters likely exacerbates the negative impact on surrounding cells by producing damage-associated molecular patterns (ITOH et al., 2012).

Adding protective additives immediately after cluster generation or already during isolation might reduce these negative effects. Radical scavengers, like glutathione ethyl ester or IAC (bis(1-hydroxy-2,2,6,6-tetramethyl-4-piperidinyloxy)decanedioate di-hydrochloride), could be useful to reduce stress caused by reactive oxygen species (DO AMARAL et al., 2013; MANCARELLA et al., 2008). Additionally, apoptosis inhibitors, like Pan-Caspase Inhibitor F573 or JNK inhibitory peptides like 11R-JNKI (NOGUCHI et al., 2005; PEPPER et al., 2017), and protease inhibitors to

block the negative effects of acinar enzymes (LOGANATHAN et al., 2011; ROSE et al., 2003), might also be beneficial.

Additionally, altering the temperature during the early culture phase could reduce stress in endocrine cells. Although reduced culture temperature has adverse effects on the long-term cultivation of adult porcine islets (SAKATA et al., 2023), a reduction at the beginning of the culture might be advantageous (NOGUCHI et al., 2010; SAKAGUCHI et al., 2018; TIRZA et al., 2020). Furthermore, protection from high ER-stress levels, by chemical chaperons like tauroursodeoxycholic acid and sodium phenylbutyrate, could reduce depletion of endocrine cells (BILEKOVA et al., 2021).

Regarding issues in late culture, oversized cell clusters and residual dead-cell material appear to be problematic. A solution could be the dissociation and reaggregation of clusters. This process would remove cellular debris and, with the aid of microwells, allow the formation of smaller cell clusters of uniform size. A technique, based on aggregation within microwells has already been established by cooperation partners in Dresden (HELLER et al., manuscript in revision) and Munich (HONARPISHEH et al., 2022). Due to scalability, cost-effectiveness, and potential functional advantages, reaggregation methods using ultra-low attachment plates on orbital shakers and in spinner bioreactors should also be considered (PAGLIUCA et al., 2014; PETRY & SALZIG, 2022). Considering the loss of mass, signs of cell death in histological sections, and the cellular composition, we propose reaggregation between days 3 and 5. When determining the optimal timepoint, morphology and cellular composition are particularly important. However, a challenge with this method is that, similar to the isolation process, cell-cell and cell-matrix connections, which are crucial for β -cell function, would be lost. Therefore, we suggest that instead of fully dissociating the clusters into single cells, they should be gently fragmented to release dead cells and then reaggregated.

Additionally, incorporating matrix molecules such as laminins and collagens (SINGH et al., 2021), or utilizing decellularized tissues (CITRO et al., 2023) could compensate for the absence of matrix signals. Furthermore, the inclusion of other cell types, such as human endothelial cells or MSCs, may enhance post-

transplantational function (MONTANARI et al., 2021; HONARPISHEH et al., 2025).

In the study by Citro and colleagues, decellularized lung tissue with a preserved three-dimensional ECM structure was used as a scaffold.

After inoculating pNPCs into the air compartment of the decellularized lung and culturing for one week under dynamic media flow conditions through the vessel ECM compartment, the pNPCs were more mature and functional compared to pNPCs from the same isolation batch cultured under static conditions. When endothelial cells were additionally introduced into the vessel compartment of the decellularized lung scaffold, the pNPCs became recapillarized during a one-week culture period. These pNPCs demonstrated an insulin secretion response curve upon dynamic glucose-stimulated insulin secretion similar to that of adult islets. The scaffold containing pNPCs and endothelial cells was then transplanted under the skin of streptozotocin-induced diabetic immunodeficient mice, resulting in immediate normoglycemia in all mice. In contrast, mice receiving grafts of pNPCs from suspension culture did not achieve normoglycemia.

In summary, there is still significant potential for improving *in vitro* culture conditions. Our investigations have already clarified areas where substantial improvements are needed, but further investigations to decipher the underlying mechanisms are essential to identify targets for the modification of *in vitro* culture conditions. This is crucial to enhance pNPCs, ensuring they become an optimal product for β -cell replacement therapy.

6. pNPCs as an *in vitro* model system for islet research

To unravel and dissect molecular mechanisms in both physiological and pathophysiological processes, model systems are indispensable. Human islets as *ex vivo* models closely resemble the *in situ*-situation of β cells within the cellular network of human Langerhans islets, thus serving as a crucial tool (HART & POWERS, 2019). However, the use of human islets is costly and limited due to their scarcity. Additionally, *in vitro* culture conditions influence physiological features, which partially restricts their translatability (HART & POWERS, 2019). Furthermore, regenerative processes in adult human islets occur at a very low level, complicating research (BADER et al., 2016; NIU et al., 2024).

Rodent islets have addressed several questions, but their applicability to humans is limited due to species differences in developmental aspects, islet architecture, and mechanistic features of β cells (CABRERA et al., 2006; HOANG et al., 2014; SKELIN KLEMEN et al., 2017; LICKERT et al., 2024). Besides these *ex vivo* models, several immortal cell lines, such as INS-1, MIN6, and EndoC- β H1 cells, are available as *in vitro* models due to their ease of handling and availability. These cells exhibit general β -cell properties like insulin production and release in response to glucose stimulus (CHENG et al., 2012; TSONKOVA et al., 2018). However, they have some limitations regarding their comparability to β cells *in situ*. For example, MIN6 cells show impaired insulin secretion with higher passage numbers, and EndoC- β H1 cells express the β -cell disallowed genes SLC16A1/MCT1 and LDHA (CHENG et al., 2012; TSONKOVA et al., 2018). Moreover, they lack the physiological environment involving other endocrine and non-endocrine cell types and the matrix that β cells typically interact with. Additionally, INS-1 and MIN6 are rodent cell lines, and like rodent islets, they have limitations regarding translation due to species differences (CABRERA et al., 2006; HOANG et al., 2014; SKELIN KLEMEN et al., 2017; LICKERT et al., 2024). Their immortality and associated higher plasticity must be critically viewed, especially concerning results related to β -cell self-replication, transdifferentiation, and neogenesis (BONNER-WEIR et al., 2010; DOMINGUEZ-BENDALA et al., 2019).

These regenerative processes are promising approaches to reestablish functional β -cell mass and potentially cure insulin-dependent diabetes (SACHS et al., 2020).

Particularly in this context, pNPCs could be beneficial.

In addition to the general developmental and functional similarities between humans and pigs (KIM et al., 2020; TRITSCHLER et al., 2022; LICKERT et al., 2024) pNPCs offer several advantages over previously used model systems. Compared to immortal cell lines, pNPCs exhibit a heterogeneous cell composition that mirrors the pancreas's diversity and resembles the endocrine compartment of human islets (detailed in Chapter VI.1). Additionally, we identified proliferating β cells and endocrine progenitor-like cells. These cells could help elucidate the underlying mechanisms of β -cell self-replication, neogenesis, and transdifferentiation.

Thus, pNPCs might represent an additional model system to investigate β -cell regeneration mechanisms. Furthermore, they could serve as an *in vitro* test system to assess compounds that stimulate such mechanisms *in situ*, thereby endogenously restoring functional β -cell mass in diabetic patients (ZHONG & JIANG, 2019).

VII. SUMMARY

Porcine neonatal pancreatic clusters - characterization of cellular and molecular dynamics during the *in vitro* culture period

Porcine neonatal pancreatic clusters (pNPCs) represent a promising alternative source for β -cell replacement in patients with type 1 diabetes mellitus. Preclinical studies have demonstrated that pNPCs can restore endogenous blood glucose homeostasis in diabetic recipients. However, prior to transplantation, pNPCs must undergo a maturation process *in vitro*. Given the lack of consensus on optimal culture conditions for this *in vitro* maturation and the limited knowledge of the processes involved, we conducted detailed analyses of the cluster composition and molecular dynamics of pNPCs during culture.

Our investigations revealed that pNPCs initially consist of a heterogeneous mixture of endocrine and non-endocrine pancreatic cells but predominantly contain endocrine cells by the end of the *in vitro* culture period. The composition of the endocrine compartment, comprising β , α , δ , and PP cells, changed significantly during culture but reverted to its original composition by the end. This composition mirrors the physiological situation of human and porcine islets, with primarily β cells followed by approximately half as many α -cells.

In addition to changes in cell composition, β cells in particular exhibited maturation into functional cells. This was evidenced by a molecular signature relevant to glucose sensitivity, glucose-induced insulin secretion, hormone synthesis and processing, secretory vesicles, and glucose and calcium signaling pathways. Notably, we observed an initial decline in this molecular signature, followed by an increase to levels higher than the day of isolation by the end of the culture period. This suggests initial stress for the endocrine cells, which diminishes over time, leading to β -cell maturation. Our findings indicate that the *in vitro* maturation of pNPCs involves not only an enrichment of β cells but also their functional maturation.

The heterogeneous composition of Langerhans islets is essential for blood glucose regulation. Unlike β -cell-like products, such as those generated from human stem cells, pNPCs reflect *in situ* conditions more accurately with various endocrine cell types, pancreatic ductal cells, mesenchymal cells, and extracellular matrix production.

Additionally, we described plastic processes during the *in vitro* culture of pNPCs. These include β -cell proliferation, transdifferentiation of non-endocrine cells into endocrine cells, and the presence of endocrine progenitor-like cells, which may have the potential for the formation of new endocrine cells. These processes offer advantages for xenotransplantation, as they may allow for post-transplant expansion of β cells, reducing the transplant quantity and associated complications.

Furthermore, pNPCs could serve not only as an alternative source for β -cell replacement therapy in humans but also hold significant potential for studying β -cell development, plasticity, and maturation due to the similarities between humans and pigs, particularly regarding embryonic development and blood glucose regulation.

In summary, this study provides critical insights into the cellular and molecular processes in pNPCs. The findings offer a foundation for optimizing culture conditions and can be used for quality control of pNPCs in the future. These are crucial steps towards advancing pNPCs for clinical application as an alternative source for β -cell replacement therapy.

VIII. ZUSAMMENFASSUNG

Porzine neonatale pankreatische Cluster - Charakterisierung zellulärer und molekularer Prozesse während der *in vitro* Kultur

Porzine neonatale pankreatische Cluster (pNPCs) stellen eine vielversprechende alternative Quelle für den Ersatz von β -Zellen bei Patienten mit Diabetes mellitus Typ 1 dar. Präklinische Studien haben gezeigt, dass pNPCs die endogene Blutzuckerhomöostase bei diabetischen Empfängern wiederherstellen können. Vor der Transplantation müssen pNPCs jedoch einen Reifungsprozess *in vitro* durchlaufen. Da es keinen Konsens über die optimalen Kulturbedingungen für diese *in vitro*-Reifung gibt und das Wissen über Prozesse in dieser Phase begrenzt ist, haben wir detaillierte Analysen zur Clusterzusammensetzung und molekularen Dynamik der pNPCs im Kulturverlauf durchgeführt.

Unsere Untersuchungen zeigten, dass pNPCs zunächst aus einer heterogenen Mischung endokriner und nicht-endokriner pankreatischer Zellen bestehen, aber am Ende der *in vitro*-Kultur überwiegend endokrine Zellen enthalten. Die Zusammensetzung des endokrinen Kompartiments, bestehend aus β -, α -, δ - und PP-Zellen, veränderte sich während der Kultivierung deutlich, kehrte jedoch am Ende zu seiner ursprünglichen Zusammensetzung zurück. Diese entspricht der physiologischen Zusammensetzung humaner und porziner Inseln, mit hauptsächlich β -Zellen, gefolgt von etwas halb so vielen α -Zellen.

Neben der Veränderung der Zellzusammensetzung wiesen insbesondere β -Zellen eine Reifung hin zu funktionellen Zellen auf. Dies zeigte sich in einer molekularen Signatur, die für die Glukose-Sensitivität, glukoseinduzierte Insulinsekretion sowie für Hormonsynthese und -prozessierung, sekretorische Vesikel und Glukose- und Kalziumsignalwege relevant ist. Als eine Besonderheit in der Dynamik dieser molekularen Signatur haben wir erstmalig nachgewiesen, dass es zunächst einen Abfall dieser Signatur gab, bevor die obig genannten molekularen Profile in den β -Zellen bis zum Ende der Kulturbeobachtungsperiode anstiegen, teilweise auf ein höheres Niveau als am Tag der Clusterisolierung. Dies deutet auf initialen Stress für die endokrinen Zellen hin, der im Verlauf der Kultur abnimmt, gefolgt von einer

Reifung der β -Zellen. Unsere Ergebnisse zeigen somit, dass die *in vitro*-Reifung der pNPCs nicht nur auf einer Anreicherung von β -Zellen, sondern auch auf deren Maturierung beruht.

Die heterogene Zusammensetzung Langerhans'schen Inseln ist essentiell für die Regulation des Blutzuckerspiegels. Im Gegensatz zu reinen β -Zellprodukten, wie sie beispielsweise aus humanen Stammzellen generiert werden, reflektieren pNPCs mit verschiedenen endokrinen Zelltypen, Pankreasgangzellen und mesenchymalen Zellen sowie der Produktion von extrazellulärer Matrix besser die *in situ*-Verhältnisse.

Zusätzlich konnten wir plastische Prozesse in der *in vitro*-Kultur von pNPCs beschreiben. Diese umfassen die Proliferation von β -Zellen, die Transdifferenzierung von nicht-endokrinen Zellen in Richtung endokriner Zellen und das Vorhandensein von endokrinen Vorläuferzellen, welche möglicherweise das Potential für die Neubildung endokriner Zellen besitzen. Diese Prozesse stellen für die Xenotransplantation einen Vorteil dar, da sie das Potential für posttransplantationale Expansion von β -Zellen und somit eine Reduktion der Transplantatmenge und der damit einhergehenden Komplikationen mit sich bringen.

Abschließend sollte betont werden, dass pNPCs in Zukunft nicht nur als alternative β -Zellquelle für den Menschen dienen könnten. Aufgrund der großen Ähnlichkeit zwischen Mensch und Schwein, insbesondere in Bezug auf Embryonalentwicklung und Blutzuckerregulierung, haben sie auch großes Potenzial für die Erforschung der Mechanismen der β -Zellentwicklung, Plastizität und Reifung.

Zusammenfassend liefert diese Studie wichtige Einblicke in die zellulären und molekularen Prozesse in pNPCs. Die im Rahmen dieser Arbeit gewonnen Erkenntnisse stellen eine wichtige Basis für die Optimierung der Kulturbedingungen dar und können in Zukunft für die Qualitätskontrolle von pNPCs genutzt werden. Beides sind wichtige Schritte um pNPCs der klinischen Anwendung als alternative β -Zellquelle näherzubringen

IX. INDEX OF FIGURES

Figure 1: Procedure of cluster generation from neonatal pancreatic tissue. Created with BioRender.com.....	13
Figure 2: Schematic illustration of the relationship between cell plasticity & proliferation and functionality & maturity in the context of physiological development and β -cell sources for replacement therapy. Created with BioRender.com.	15
Figure 3: Distinct loss of cluster volume between culture days 3 and 9. a: absolute volume per isolate in 1,000 AEQs; 3 biological replicates. b: loss of volume compared to previous day per isolate; all values are means, error bars indicate SEM, n=3. GLM: *p<0.05, **p<0.01, ***p<0.001.	42
Figure 4: Dynamic of cluster size categories and corresponding volume between culture days 3 and 9. a: Number of clusters per size category. b: Proportion per cluster size category on total cluster number per day (relCount). c: Proportion per cluster size category on total volume per day (relVolume). Colors represents the size categories as indicated. n=3, error bars indicate SD.	43
Figure 5: Morphology of pNPCs on culture days 0, 1, 3, and 9. a: Stereomicroscopic images of native clusters, scale bar 200 μ m. b and c: H&E staining of cluster section. b: General view, scale bar 100 μ m. c: Detailed view, scale bar 25 μ m. Typical acinus-structures are indicated by #, and ductal by *, and nuclear signs of cell death by +.....	45
Figure 6: Immunostaining for acinar, ductal mesenchymal, and endocrine cells in pNPCs on culture days 0 and 1. a: Immunohistochemistry staining for AMY of pNPCs. b: Immunofluorescence staining for SYP (magenta), VIM (green), and CK7 (yellow) of pancreatic tissue of age-matched animals and cultured pNPCs; nuclei are stained with DAPI (blue); scale bar 50 μ m.	46
Figure 7: Quantification of pancreatic cell types by flow cytometry on culture days 0 and 1. a: Representative gating plots for cells positive for SYP, CK7, and VIM (samples are colored and antibody controls in grey). b: Representative dual-plots for SYP, CK7, and VIM. c: Proportions of endocrine (SYP ⁺), ductal (CK7 ⁺ SYP ⁻), and mesenchymal (VIM ⁺ CK7 ⁻ SYP ⁻) cells on culture days 0 and 1; all values are means; n=9 (3 independent experiments with 3 isolates each); *p<0.05, **p<0.01, ***p<0.001; circles indicate Batch1, squares Batch2, and triangles Batch3. d: Relative distribution of endocrine (SYP ⁺), ductal (CK7 ⁺ SYP ⁻) and mesenchymal/endothelial (VIM ⁺ CK7 ⁻ SYP ⁻) cells, and other cell types (VIM ⁻ CK7 ⁻ SYP ⁻) on culture days 0 and 1. Values are means from c.	47
Figure 8: Quantification of endocrine cell types by flow cytometry on culture days 0 and 1. a: Representative gating plots for cells positive for SYP, INS, GCG and SST. b: Absolute proportions of β (INS ⁺), α (GCG ⁺), δ (SST ⁺), and other endocrine cells (cells positive for SYP, but negative for INS, GCG or SST) on culture days 0 and 1; *p<0.05, **p<0.01; ***p<0.001. Circles indicate Batch1, squares Batch2, and triangles Batch3. c: Relative distribution of cell types within the endocrine compartment on culture day 0. Values are means from b.	48

- Figure 9: Quantification of pancreatic cell types by flow cytometry on culture days 0, 1, 3, and 9. a, b: Proportions of endocrine (SYP⁺), ductal (CK7⁺SYP⁻), and mesenchymal/endothelial (VIM⁺SYP⁻CK7⁻) cells. c-f: Proportions of endocrine cell types detected by the expression of their respective hormone. Other endocrine cells, are SYP⁺INS⁻GCG⁻SST⁻. a, c: Proportions per batch; all values are means; n=9 (3 independent experiments with 3 isolates each). b, d, e: Mean values of a and c of cell types per day. f: Relative proportions of cell types within the endocrine compartment. All values are means; error bars indicate SEM; n=9 (3 independent experiments with 3 isolates each); *p<0.05, **p<0.01, ***p<0.001..... 50
- Figure 10: Immunofluorescence staining for INS (red), GCG (green), SST (white), and PPY (orange) of pNPCs on culture days 0, 1, 3, and 9; nuclei are stained with DAPI (blue); scale bar 50 μ m. 52
- Figure 11: Annotation of pancreatic cell types by Leiden-clustering and expression of marker genes (scRNA-seq). a: Clustree-visualized clustering of different resolutions generated by Leiden-Algorithm. b: Neighborhood graphs showing the expression levels of selected pancreatic cell type markers. c: Expression levels of marker genes in clustered cell types. The color intensity indicates the expression level. The circle size indicates the fraction of positive cells. 53
- Figure 12: Cellular composition and characteristics of pNPCs on transcriptome level (scRNA-seq). a: Neighborhood graph of annotated cell types. b: Proportions of detected cell types for culture days 1, 3, and 9 from 2 experiments (3 biological replicates equally mixed each). c: Neighborhood graph showing the cell distribution on culture days 1, 3, and 9. d: Expression levels of marker genes specific for pancreatic cell types in annotated clusters on culture days 1, 3, and 9; the color intensity indicates the expression level and the circle size the fraction of positive cells. 55
- Figure 13: Expression of endocrine lineage specific markers in endocrine cells of pNPCs during culture. a: Expression levels and distribution of markers for endocrine lineage differentiation and maturation in endocrine cell types on culture days 1, 3, and 9 (scRNA-seq); n=2; the color intensity indicates the expression level; the circle size indicates the fraction of positive cells; violin plots indicate distribution of expression. b, c, and d: Prevalence of PDX1 and NKX6-1 evaluated by flow cytometry. b: Representative dual-plots for PDX1 and NKX6-1 of β cells (INS⁺), endocrine cells (SYP⁺), and INS⁻SYP⁻ cells (other) on culture days 0, 1, ,3, and 9. c: Representative dual-plot for PDX1 and NKX6-1 of β (INS⁺), α (GCG⁺), δ (SST⁺), and other endocrine (SYP⁺INS⁻GCG⁻SST⁻) cells on culture day 9. d: MFI of PDX1 and NKX6-1 in β cells on culture days 0, 1, 3, and 9; All values are means; error bars indicate SEM; n=9 (3 independent experiments with 3 isolates each); *p<0.05, **p<0.01, ***p<0.001..... 58

- Figure 14: Prevalence of polyhormonal cells during the in vitro maturation period in all cells and hormone⁺ cell of pNPCs. a, b: Co-expression of the hormones INS, GCG and SST on culture days 0, 1, 3, and 9, evaluated by flow cytometry; all values are means; error bars indicate SEM; n=9 (3 independent experiments with 3 isolates each); *p<0.05, **p<0.01, ***p<0.001. a: for batches individually. b: means of a. c, d: Expression levels (c', d) and distribution (c'') of INS, GCG, SST, and PPY on culture days 1, 3, and 9 (scRNA-seq); n=2. The color intensity indicates the expression level and the circle size the fraction of positive cells. c: In endocrine cell types. d: in all pancreatic cell types. 60
- Figure 15: Characterization of hormone-associated markers in endocrine cells of pNPCs during culture. a, b: Abundance of INS, GCG, and SST in respective endocrine cell types evaluated by flow cytometry on culture days 0, 1, 3, and 9; all values are means; error bars indicate SEM; n=9 (3 independent experiments with 3 isolates each); *p<0.05, **p<0.01, ***p<0.001. a: Absolute MFI separate per batch. b: Means of relative abundance compared to day 0 (based on a). c: Expression levels of markers associated with hormone synthesis and processing in endocrine cell types on culture days 1, 3, and 9 (scRNA-seq); n=2; the color intensity indicates the expression level; the circle size indicates the fraction of positive cells. 62
- Figure 16: Comparison of different methods to evaluate granularity in vesicle containing cells (SYP⁺) on culture days 0, 1, 3, and 9 by flow cytometry. a: Intensity of SSC-A. b: Intensity of SSC-H. c: MFI of SYP. All values are means; error bars indicate SEM; n=9 (3 independent experiments with 3 isolates each); *p<0.05, **p<0.01, ***p<0.001. 63
- Figure 17: Characterization of vesicle-associated markers in endocrine cells of pNPCs during culture. a - c: Abundance of SYP in β (INS⁺), α (GCG⁺), δ (SST⁺), and other endocrine (SYP⁺INS⁻GCG⁻SST⁻) cells evaluated by flow cytometry; all values are means; n=9 (3 independent experiments with 3 isolates each); *p<0.05, **p<0.01, ***p<0.001. a, b: MFI of SYP on culture days 0, 1, 3, and 9; error bars indicate SEM. c: MFI of SYP on culture day 9; circles indicate Batch1, squares Batch2, and triangles Batch3. d: Expression levels of markers associated with secretory granules in endocrine cell types on culture days 1, 3, and 9 (scRNA-seq); n=2; the color intensity indicates the expression level; the circle size indicates the fraction of positive cells. 65
- Figure 18: Evaluation of markers for glucose stimulated insulin secretion. a, b: Expression levels of markers associated with glucose (a) and calcium (b) in β cell on culture days 1, 3, and 9 (scRNA-seq); n=2; the color intensity indicates the expression level and the circle size the fraction of positive cells. c: dGSIS evaluating β -cell functionality in vitro; insulin release compared to basal secretion (at 3 mM glucose) from pNPCs on stimulus by 16.7 mM glucose, 16.7 mM glucose and forskolin, and 16.7 mM glucose and KCl on culture day 9 in vitro; n=3. 67

- Figure 19: Evaluation of proliferation in pNPCs via MKI67 in pNPCs. a - d: Evaluated by flow cytometry. a: Representative gating plot for the detection of MKI67 positive cells (sample in red and antibody control in grey). b: Proportions of MKI67⁺ cells on culture days 0, 1, 3, and 9; all values are means; error bars indicate SEM; n=9 (3 independent experiments with 3 isolates each); *p<0.05, **p<0.01, ***p<0.001. c: Representative dual-plots for MKI67/SYP and MKI67/INS on culture day 9. d: Proportion of MKI67⁺ cell within endocrine (SYP⁺), non-endocrine (SYP⁻), β (INS⁺), and non- β (INS⁻) cells on culture day 9; n=9 (3 independent experiments with 3 isolates each); *p<0.05, **p<0.01, ***p<0.001; circles indicate Batch1, squares Batch2, and triangles Batch3. e: Immunofluorescence staining for INS (turquoise), GCG (green), and MKI67 (red) of pNPCs on culture day 9; nuclei are stained with DAPI (blue); scale bar 50 μ m. 70
- Figure 20: Prevalence of proliferation in endocrine cells of pNPCs during culture (scRNA-seq); n=2. a, d: Proportions of cells assigned to cell cycle phases G1, S, and G2M in endocrine cell types (a) or β -cell subtypes (d). b, e: Expression levels of cell cycle phase associated genes in endocrine cell types (b) or β -cell subtypes (e); the color intensity indicates the expression level and the circle size the fraction of positive cells. c: Neighborhood graphs of β cells showing the distribution according to culture day, cell cycle phase, and β -cell subtype. 73
- Figure 21: Characterization of endocrine progenitor-like cells in pNPCs. a: Neighborhood graphs showing the expression levels of endocrine progenitor markers FEV, NEUROG3, NEUROD1, NKX6-1, and PDX-1 (scRNA-seq). b: Immunofluorescence staining for NGN3 (green) and SYP (red) of age matched pancreatic tissue and pNPCs on culture day 9, demonstrating NGN3⁺ nuclear staining in few SYP⁻ cells. Nuclei are stained with DAPI (blue); scale bar 20 μ m. 74
- Figure 22: Prevalence of endocrine progenitor-like cells in pNPCs evaluated by flow cytometry. a: Representative gating plots for detection of NGN3 positive cells during culture (sample is colored dark red and antibody controls in light red). b: Proportions of NGN3⁺ cells; all values are means; error bars indicate SEM; n=9 (3 independent experiments with 3 isolates each); *p<0.05, **p<0.01, ***p<0.001. c: Dual-plot for NKX6-1 and PDX1 of hormone negative cells (INS⁻GCG⁻SST⁻) on culture day 9. d: Representative dual-plots for NKX6-1 and PDX1 of β (INS⁺, red), α (GCG⁺, orange), δ (SST⁺, green), and hormone⁻ (INS⁻GCG⁻SST⁻ blue) cells. 76
- Figure 23: Cells with dual properties. a: Representative dual-plots for SYP and CK7/VIM of pNPCs on culture days 0, 1, 3, and 9 evaluated by flow cytometry. b: Immunofluorescence staining for SYP (magenta) and CK7 or VIM (both green) on culture day 9. 78
- Figure 24: Expression levels of marker genes specific for pancreatic cell types from scRNA-seq data in pancreatic cell types of pNPCs during culture; n=2; the color intensity indicates the expression level and the circle size the fraction of positive cells (corresponding to Figure 10d). ... 80
- Figure 25: Neighborhood graphs showing the expression level and distribution of selected endocrine cell markers from scRNA-seq data of pNPCs; n=2; the color intensity indicates the expression level. a: In pancreatic cell types. b: In mesenchymal cells. Population of mesenchymal cells exhibiting endocrine properties marked by circles. 81

Figure 26: Expression levels of marker genes associated with cell-cell and cell-matrix interaction from scRNA-seq data in pancreatic cell types of pNPCs during culture; the color intensity indicates the expression level and the circle size the fraction of positive cells.	83
Figure 27: Expression levels of ER-stress-related genes from scRNA-seq data in pancreatic cell types of pNPCs during culture; the color intensity indicates the expression level and the circle size the fraction of positive cells.	84
Figure 28: Expression levels of ER-stress-related genes from scRNA-seq data of β cells on culture days 0, 1, 3, and 9; color indicates expression level and circle size the fraction of positive cells...	85

X. INDEX OF TABLES

Table 1: Average per capita health-care expenses in € in 2010 of non-diabetic patients and patients with T1DM or T2DM in Germany (VOELTZ et al., 2024).....	7
Table 2: Culture medium.....	29
Table 3: Conversion factors for islet/aggregate equivalents (IEQ/AEQ).	30
Table 4: Staining panels for flow cytometry. * indicates primary fluorophore labeled antibody was used; # indicates fluorophore labeled secondary antibody was used.	31
Table 5: Distinct loss of cluster volume of pNPCs between culture days 3 and 9. Absolute cluster volume is measured in AEQ (corresponds to a cell cluster with a diameter of 150 μm). Relative daily loss is the loss compared to the previous day.	42

XI. REFERENCES

Aamodt KI, Powers AC. Signals in the pancreatic islet microenvironment influence beta-cell proliferation. *Diabetes Obes Metab* 2017; 19 Suppl 1: 124-36.

Abu Aqel Y, Alnesf A, Aigha, II, Islam Z, Kolatkar PR, Teo A, Abdelalim EM. Glucokinase (GCK) in diabetes: from molecular mechanisms to disease pathogenesis. *Cell Mol Biol Lett* 2024; 29: 120.

Ackermann AM, Gannon M. Molecular regulation of pancreatic beta-cell mass development, maintenance, and expansion. *J Mol Endocrinol* 2007; 38: 193-206.

Agerskov RH, Nyeng P. Innervation of the pancreas in development and disease. *Development* 2024; 151

Aigha, II, Abdelalim EM. NKX6.1 transcription factor: a crucial regulator of pancreatic β cell development, identity, and proliferation. *Stem Cell Res Ther* 2020; 11: 459.

Ait-Lounis A, Bonal C, Seguín-Estévez Q, Schmid CD, Bucher P, Herrera PL, Durand B, Meda P, Reith W. The transcription factor Rfx3 regulates beta-cell differentiation, function, and glucokinase expression. *Diabetes* 2010; 59: 1674-85.

Al-Khawaga S, Memon B, Butler AE, Taheri S, Abou-Samra AB, Abdelalim EM. Pathways governing development of stem cell-derived pancreatic β cells: lessons from embryogenesis. *Biol Rev Camb Philos Soc* 2018; 93: 364-89.

Amisten S, Atanes P, Hawkes R, Ruz-Maldonado I, Liu B, Parandeh F, Zhao M, Huang GC, Salehi A, Persaud SJ. A comparative analysis of human and mouse islet G-protein coupled receptor expression. *Sci Rep* 2017; 7: 46600.

Aragón F, Karaca M, Novials A, Maldonado R, Maechler P, Rubí B. Pancreatic polypeptide regulates glucagon release through PPYR1 receptors expressed in mouse and human alpha-cells. *Biochim Biophys Acta* 2015; 1850: 343-51.

Arefanian H, Ramji Q, Gupta N, Spigelman AF, Grynosh D, MacDonald PE, Mueller TF, Gazda LS, Rajotte RV, Rayat GR. Yield, cell composition, and function of islets isolated from different ages of neonatal pigs. *Front Endocrinol (Lausanne)* 2022; 13: 1032906.

Arous C, Wehrle-Haller B. Role and impact of the extracellular matrix on integrin-mediated pancreatic β -cell functions. *Biol Cell* 2017; 109: 223-37.

Arrojo EDR, Jacob S, Garcia-Prieto CF, Zheng X, Fukuda M, Nhu HTT, Stelmashenko O, Pecanha FLM, Rodriguez-Diaz R, Bushong E, Deerinck T, Phan S, Ali Y, Leibiger I, Chua M, Boudier T, Song SH, Graf M, Augustine GJ, Ellisman MH, Berggren PO. Structural basis for delta cell paracrine regulation in pancreatic islets. *Nat Commun* 2019; 10: 3700.

Back SH, Scheuner D, Han J, Song B, Ribick M, Wang J, Gildersleeve RD, Pennathur S, Kaufman RJ. Translation attenuation through eIF2 α phosphorylation prevents oxidative stress and maintains the differentiated state in beta cells. *Cell Metab* 2009; 10: 13-26.

Bader E, Migliorini A, Gegg M, Moruzzi N, Gerdes J, Roscioni SS, Bakhti M, Brandl E, Irmeler M, Beckers J, Aichler M, Feuchtinger A, Leitzinger C, Zischka H, Wang-Sattler R, Jastroch M, Tschop M, Machicao F, Staiger H, Haring HU, Chmelova H, Chouinard JA, Oskolkov N, Korsgren O, Speier S, Lickert H. Identification of proliferative and mature beta-cells in the islets of Langerhans. *Nature* 2016; 535: 430-4.

Bae D, Moore KA, Mella JM, Hayashi SY, Hollien J. Degradation of Blos1 mRNA by IRE1 repositions lysosomes and protects cells from stress. *J Cell Biol* 2019; 218: 1118-27.

Baeyens L, De Breuck S, Lardon J, Mfopou JK, Rooman I, Bouwens L. In vitro generation of insulin-producing beta cells from adult exocrine pancreatic cells. *Diabetologia* 2005; 48: 49-57.

Bais AS, Kostka D. scds: computational annotation of doublets in single-cell RNA sequencing data. *Bioinformatics* 2020; 36: 1150-8.

Balboa D, Barsby T, Lithovius V, Saarimäki-Vire J, Omar-Hmeadi M, Dyachok O, Montaser H, Lund PE, Yang M, Ibrahim H, Näätänen A, Chandra V, Vihinen H, Jokitalo E, Kvist J, Ustinov J, Nieminen AI, Kuuluvainen E, Hietakangas V, Katajisto P, Lau J, Carlsson PO, Barg S, Tengholm A, Otonkoski T. Functional, metabolic and transcriptional maturation of human pancreatic islets derived from stem cells. *Nat Biotechnol* 2022; 40: 1042-55.

Ball CM, Featherstone PJ. The discovery of insulin. *Anaesth Intensive Care* 2023; 51: 165-7.

Barsby T, Otonkoski T. Maturation of beta cells: lessons from in vivo and in vitro models. *Diabetologia* 2022; 65: 917-30.

Bastidas-Ponce A, Tritschler S, Dony L, Scheibner K, Tarquis-Medina M, Salinno C, Schirge S, Burtscher I, Böttcher A, Theis FJ, Lickert H, Bakhti M. Comprehensive single cell mRNA profiling reveals a detailed roadmap for pancreatic endocrinogenesis. *Development* 2019; 146

Bearrows SC, Bauchle CJ, Becker M, Haldeman JM, Swaminathan S, Stephens SB. Chromogranin B regulates early-stage insulin granule trafficking from the Golgi in pancreatic islet β -cells. *J Cell Sci* 2019; 132

Bechard ME, Bankaitis ED, Hipkens SB, Ustione A, Piston DW, Yang YP, Magnuson MA, Wright CV. Precommitment low-level Neurog3 expression defines a long-lived mitotic endocrine-biased progenitor pool that drives production of endocrine-committed cells. *Genes Dev* 2016; 30: 1852-65.

Becht E, McInnes L, Healy J, Dutertre CA, Kwok IWH, Ng LG, Ginhoux F, Newell EW. Dimensionality reduction for visualizing single-cell data using UMAP. *Nat Biotechnol* 2018;

Beiki H, Liu H, Huang J, Manchanda N, Nonneman D, Smith TPL, Reecy JM, Tuggle CK. Improved annotation of the domestic pig genome through integration of Iso-Seq and RNA-seq data. *BMC Genomics* 2019; 20: 344.

Berger C, Zdziebło D. Glucose transporters in pancreatic islets. *Pflugers Arch* 2020; 472: 1249-72.

Bernard-Kargar C, Kassis N, Berthault MF, Pralong W, Ktorza A. Sialylated form of the neural cell adhesion molecule (NCAM): a new tool for the identification and sorting of beta-cell subpopulations with different functional activity. *Diabetes* 2001; 50: S125-S.

Bilekova S, Sachs S, Lickert H. Pharmacological Targeting of Endoplasmic Reticulum Stress in Pancreatic Beta Cells. *Trends Pharmacol Sci* 2021; 42: 85-95.

Bonner-Weir S, Li WC, Ouziel-Yahalom L, Guo L, Weir GC, Sharma A. Beta-cell growth and regeneration: replication is only part of the story. *Diabetes* 2010; 59: 2340-8.

Bosma KJ, Rahim M, Singh K, Goleva SB, Wall ML, Xia J, Syring KE, Oeser JK, Poffenberger G, McGuinness OP, Means AL, Powers AC, Li WH, Davis LK, Young JD, O'Brien RM. Pancreatic islet beta cell-specific deletion of G6pc2 reduces fasting blood glucose. *J Mol Endocrinol* 2020; 64: 235-48.

Bottino R, Wijkstrom M, van der Windt DJ, Hara H, Ezzelarab M, Murase N, Bertera S, He J, Phelps C, Ayares D, Cooper DK, Trucco M. Pig-to-monkey islet xenotransplantation using multi-transgenic pigs. *Am J Transplant* 2014; 14: 2275-87.

Bramswig NC, Everett LJ, Schug J, Dorrell C, Liu C, Luo Y, Streeter PR, Naji A, Grompe M, Kaestner KH. Epigenomic plasticity enables human pancreatic α to β cell reprogramming. *J Clin Invest* 2013; 123: 1275-84.

Braun M, Ramracheya R, Bengtsson M, Zhang Q, Karanauskaite J, Partridge C, Johnson PR, Rorsman P. Voltage-gated ion channels in human pancreatic beta-cells: electrophysiological characterization and role in insulin secretion. *Diabetes* 2008; 57: 1618-28.

Braun M, Ramracheya R, Johnson PR, Rorsman P. Exocytotic properties of human pancreatic beta-cells. *Ann N Y Acad Sci* 2009; 1152: 187-93.

Bright MD, Itzhak DN, Wardell CP, Morgan GJ, Davies FE. Cleavage of BLOC1S1 mRNA by IRE1 Is Sequence Specific, Temporally Separate from XBP1 Splicing, and Dispensable for Cell Viability under Acute Endoplasmic Reticulum Stress. *Mol Cell Biol* 2015; 35: 2186-202.

Brissova M, Fowler MJ, Nicholson WE, Chu A, Hirshberg B, Harlan DM, Powers AC. Assessment of human pancreatic islet architecture and composition by laser scanning confocal microscopy. *J Histochem Cytochem* 2005; 53: 1087-97.

Burganova G, Bridges C, Thorn P, Landsman L. The Role of Vascular Cells in Pancreatic Beta-Cell Function. *Front Endocrinol (Lausanne)* 2021; 12: 667170.

Cabrera O, Berman DM, Kenyon NS, Ricordi C, Berggren PO, Caicedo A. The unique cytoarchitecture of human pancreatic islets has implications for islet cell function. *Proc Natl Acad Sci U S A* 2006; 103: 2334-9.

Calimag APP, Chlebek S, Lerma EV, Chaiban JT. Diabetic ketoacidosis. *Dis Mon* 2023; 69: 101418.

Chance RE, Frank BH. Research, development, production, and safety of biosynthetic human insulin. *Diabetes Care* 1993; 16 Suppl 3: 133-42.

Chandra V, G S, Phadnis S, Nair PD, Bhonde RR. Generation of pancreatic hormone-expressing islet-like cell aggregates from murine adipose tissue-derived stem cells. *Stem Cells* 2009; 27: 1941-53.

Chao KC, Chao KF, Fu YS, Liu SH. Islet-like clusters derived from mesenchymal stem cells in Wharton's Jelly of the human umbilical cord for transplantation to control type 1 diabetes. *PLOS ONE* 2008; 3: e1451.

Chen LB, Jiang XB, Yang L. Differentiation of rat marrow mesenchymal stem cells into pancreatic islet beta-cells. *World J Gastroenterol* 2004; 10: 3016-20.

Cheng K, Delghingaro-Augusto V, Nolan CJ, Turner N, Hallahan N, Andrikopoulos S, Gunton JE. High passage MIN6 cells have impaired insulin secretion with impaired glucose and lipid oxidation. *PLOS ONE* 2012; 7: e40868.

Choi J, Cayabyab F, Perez H, Yoshihara E. Scaling Insulin-Producing Cells by Multiple Strategies. *Endocrinol Metab (Seoul)* 2024; 39: 191-205.

Cinti F, Bouchi R, Kim-Muller JY, Ohmura Y, Sandoval PR, Masini M, Marselli L, Suleiman M, Ratner LE, Marchetti P, Accili D. Evidence of β -Cell Dedifferentiation in Human Type 2 Diabetes. *J Clin Endocrinol Metab* 2016; 101: 1044-54.

Citro A, Neroni A, Pignatelli C, Campo F, Policardi M, Monieri M, Pellegrini S, Dugnani E, Manenti F, Maffia MC, Valla L, Kemter E, Marzinotto I, Olgasi C, Cucci A, Follenzi A, Lampasona V, Wolf E, Piemonti L. Directed self-assembly of a xenogeneic vascularized endocrine pancreas for type 1 diabetes. *Nat Commun* 2023; 14: 878.

Cohrs CM, Chen C, Jahn SR, Stertmann J, Chmelova H, Weitz J, Bähr A, Klymiuk N, Steffen A, Ludwig B, Kamvissi V, Wolf E, Bornstein SR, Solimena M, Speier S. Vessel Network Architecture of Adult Human Islets Promotes Distinct Cell-Cell Interactions In Situ and Is Altered After Transplantation. *Endocrinology* 2017; 158: 1373-85.

Cooper DKC, Mou L, Bottino R. A brief review of the current status of pig islet xenotransplantation. *Front Immunol* 2024; 15: 1366530.

Cowan PJ. Chapter 9 - Transgenic pigs for islet xenotransplantation. In: *Pancreas and Beta Cell Replacement*. Hawthorne WJ, ed.: Academic Press 2022: 153-66.

Crossen S, Xing G, Hoch JS. Changing costs of type 1 diabetes care among US children and adolescents. *Pediatr Diabetes* 2020; 21: 644-8.

Cuesta-Gomez N, Verhoeff K, Jasra IT, Pawlick R, Dadheech N, Shapiro AMJ. Characterization of stem-cell-derived islets during differentiation and after implantation. *Cell Rep* 2022; 40: 111238.

Dağaçan S. Insulin Structure, Function and Diabetes Models in Animals. *Journal of Experimental and Basic Medical Sciences* 2021; 1: 96-101.

De Franco E, Saint-Martin C, Brusgaard K, Knight Johnson AE, Aguilar-Bryan L, Bowman P, Arnoux JB, Larsen AR, Sanyoura M, Greeley SAW, Calzada-León R, Harman B, Houghton JAL, Nishimura-Meguro E, Laver TW, Ellard S, Del Gaudio D, Christesen HT, Bellanné-Chantelot C, Flanagan SE. Update of variants identified in the pancreatic β -cell K(ATP) channel genes *KCNJ11* and *ABCC8* in individuals with congenital hyperinsulinism and diabetes. *Hum Mutat* 2020; 41: 884-905.

do Amaral AS, Pawlick RL, Rodrigues E, Costal F, Pepper A, Galvão FH, Correa-Giannella ML, Shapiro AM. Glutathione ethyl ester supplementation during pancreatic islet isolation improves viability and transplant outcomes in a murine marginal islet mass model. *PLOS ONE* 2013; 8: e55288.

Docherty FM, Riemondy KA, Castro-Gutierrez R, Dwulet JM, Shilleh AH, Hansen MS, Williams SPM, Armitage LH, Santostefano KE, Wallet MA, Mathews CE, Triolo TM, Benninger RKP, Russ HA. ENTPD3 Marks Mature Stem Cell-Derived β -Cells Formed by Self-Aggregation In Vitro. *Diabetes* 2021; 70: 2554-67.

Dominguez-Bendala J, Qadir MMF, Pastori RL. Pancreatic Progenitors: There and Back Again. *Trends Endocrinol Metab* 2019; 30: 4-11.

Dor Y, Brown J, Martinez OI, Melton DA. Adult pancreatic beta-cells are formed by self-duplication rather than stem-cell differentiation. *Nature* 2004; 429: 41-6.

Eguchi N, Damyar K, Alexander M, Dafoe D, Lakey JRT, Ichii H. Anti-Oxidative Therapy in Islet Cell Transplantation. *Antioxidants (Basel)* 2022; 11

Ellis C, Lyon JG, Korbitt GS. Optimization and Scale-up Isolation and Culture of Neonatal Porcine Islets: Potential for Clinical Application. *Cell Transplant* 2016; 25: 539-47.

Esni F, Täljedal IB, Perl AK, Cremer H, Christofori G, Semb H. Neural cell adhesion molecule (N-CAM) is required for cell type segregation and normal ultrastructure in pancreatic islets. *J Cell Biol* 1999; 144: 325-37.

Fritz JM, Dong M, Apsley KS, Martin EP, Na CL, Sitaraman S, Weaver TE. Deficiency of the BiP cochaperone ERdj4 causes constitutive endoplasmic reticulum stress and metabolic defects. *Mol Biol Cell* 2014; 25: 431-40.

Fung TH, Patel B, Wilmot EG, Amoaku WM. Diabetic retinopathy for the non-ophthalmologist. *Clin Med (Lond)* 2022; 22: 112-6.

Gayoso A, Shor J, Carr AJ, Sharma R, Pe'er D. DoubletDetection (v2.4.1). GitHub: 2019: <https://doi.org/10.5281/zenodo.2678042>.

Gayoso A, Lopez R, Xing G, Boyeau P, Valiollah Pour Amiri V, Hong J, Wu K, Jayasuriya M, Mehlman E, Langevin M, Liu Y, Samaran J, Misrachi G, Nazaret A, Clivio O, Xu C, Ashuach T, Gabitto M, Lotfollahi M, Svensson V, da Veiga Beltrame E, Kleshchevnikov V, Talavera-López C, Pachter L, Theis FJ, Streets A, Jordan MI, Regier J, Yosef N. A Python library for probabilistic analysis of single-cell omics data. *Nat Biotechnol* 2022; 40: 163-6.

Germain PL, Lun A, Garcia Meixide C, Macnair W, Robinson MD. Doublet identification in single-cell sequencing data using scDbfFinder. *F1000Res* 2021; 10: 979.

Grapin-Botton A. Ductal cells of the pancreas. *Int J Biochem Cell Biol* 2005; 37: 504-10.

Gregory GA, Robinson TIG, Linklater SE, Wang F, Colagiuri S, de Beaufort C, Donaghue KC, International Diabetes Federation Diabetes Atlas Type 1 Diabetes in Adults Special Interest G, Magliano DJ, Maniam J, Orchard TJ, Rai P, Ogle GD. Global incidence, prevalence, and mortality of type 1 diabetes in 2021 with projection to 2040: a modelling study. *Lancet Diabetes Endocrinol* 2022; 10: 741-60.

Gribben C, Lambert C, Messal HA, Hubber EL, Rackham C, Evans I, Heimberg H, Jones P, Sancho R, Behrens A. Ductal Ngn3-expressing progenitors contribute to adult β cell neogenesis in the pancreas. *Cell Stem Cell* 2021; 28: 2000-8.e4.

Griffith BP, Goerlich CE, Singh AK, Rothblatt M, Lau CL, Shah A, Lorber M, Grazioli A, Saharia KK, Hong SN, Joseph SM, Ayares D, Mohiuddin MM. Genetically Modified Porcine-to-Human Cardiac Xenotransplantation. *N Engl J Med* 2022; 387: 35-44.

Han L, He H, Yang Y, Meng Q, Ye F, Chen G, Zhang J. Distinctive Clinical and Pathologic Features of Immature Teratomas Arising from Induced Pluripotent Stem Cell-Derived Beta Cell Injection in a Diabetes Patient. *Stem Cells Dev* 2022; 31: 97-101.

Hart NJ, Powers AC. Use of human islets to understand islet biology and diabetes: progress, challenges and suggestions. *Diabetologia* 2019; 62: 212-22.

Hassouna T, Seeberger KL, Salama B, Korbitt GS. Functional Maturation and In Vitro Differentiation of Neonatal Porcine Islet Grafts. *Transplantation* 2018; 102: e413-e23.

Hawthorne WJ, Salvaris EJ, Phillips P, Hawkes J, Liuwantara D, Burns H, Barlow H, Stewart AB, Peirce SB, Hu M, Lew AM, Robson SC, Nottle MB, D'Apice AJ, O'Connell PJ, Cowan PJ. Control of IBMIR in neonatal porcine islet xenotransplantation in baboons. *Am J Transplant* 2014; 14: 1300-9.

Hayward JA, Ellis CE, Seeberger K, Lee T, Salama B, Mulet-Sierra A, Kuppan P, Adesida A, Korbitt GS. Cotransplantation of Mesenchymal Stem Cells With Neonatal Porcine Islets Improve Graft Function in Diabetic Mice. *Diabetes* 2017; 66: 1312-21.

Hill TG, Hill DJ. The Importance of Intra-Islet Communication in the Function and Plasticity of the Islets of Langerhans during Health and Diabetes. *Int J Mol Sci* 2024; 25

Hirsch IB, Gaudiani LM. A new look at brittle diabetes. *J Diabetes Complications* 2021; 35: 107646.

Hoang DT, Matsunari H, Nagaya M, Nagashima H, Millis JM, Witkowski P, Periwal V, Hara M, Jo J. A conserved rule for pancreatic islet organization. *PLOS ONE* 2014; 9: e110384.

Holt RIG, DeVries JH, Hess-Fischl A, Hirsch IB, Kirkman MS, Klupa T, Ludwig B, Norgaard K, Pettus J, Renard E, Skyler JS, Snoek FJ, Weinstock RS, Peters AL. The Management of Type 1 Diabetes in Adults. A Consensus Report by the American Diabetes Association (ADA) and the European Association for the Study of Diabetes (EASD). *Diabetes Care* 2021; 44: 2589-625.

Honarpisheh M, Lei Y, Zhang Y, Pehl M, Kemter E, Kraetzl M, Lange A, Wolf E, Wolf-van Buerck L, Seissler J. Formation of Re-Aggregated Neonatal Porcine Islet Clusters Improves In Vitro Function and Transplantation Outcome. *Transplant International* 2022; 35

Honarpisheh M, Lei Y, Follenzi A, Cucci A, Olgasi C, Berishvili E, Lebreton F, Bellofatto K, Piemonti L, Citro A, Campo F, Pignatelli C, Thauinat O, Kemter E, Kraetzl M, Wolf E, Seissler J, Wolf-van Buerck L, Vanguard C. Spheroids Composed of Reaggregated Neonatal Porcine Islets and Human Endothelial Cells Accelerate Development of Normoglycemia in Diabetic Mice. *Cells* 2025; 14

Huang W, Shimizu H, Bianchi J, Matovinovic K, Ayares DL, Gotoh M, Korbitt GS, Rajotte RV, Rayat GR. Impact of donor and prolonged cold ischemia time of neonatal pig pancreas on neonatal pig islet transplant outcome. *Xenotransplantation* 2021; 28: e12663.

Ilonen J, Lempainen J, Veijola R. The heterogeneous pathogenesis of type 1 diabetes mellitus. *Nat Rev Endocrinol* 2019; 15: 635-50.

Ito T, Itakura S, Todorov I, Rawson J, Asari S, Shintaku J, Nair I, Ferreri K, Kandeel F, Mullen Y. Mesenchymal stem cell and islet co-transplantation promotes graft revascularization and function. *Transplantation* 2010; 89: 1438-45.

Itoh T, Takita M, SoRelle JA, Shimoda M, Sugimoto K, Chujo D, Qin H, Naziruddin B, Levy MF, Matsumoto S. Correlation of released HMGB1 levels with the degree of islet damage in mice and humans and with the outcomes of islet transplantation in mice. *Cell Transplant* 2012; 21: 1371-81.

Jacobson AM, Braffett BH, Cleary PA, Gubitosi-Klug RA, Larkin ME, Group DER. The long-term effects of type 1 diabetes treatment and complications on health-related quality of life: a 23-year follow-up of the Diabetes Control and Complications/Epidemiology of Diabetes Interventions and Complications cohort. *Diabetes Care* 2013; 36: 3131-8.

Jacovetti C, Regazzi R. Mechanisms Underlying the Expansion and Functional Maturation of β -Cells in Newborns: Impact of the Nutritional Environment. *International journal of molecular sciences* 2022; 23

Jansson L, Barbu A, Bodin B, Drott CJ, Espes D, Gao X, Grapensparr L, Källskog Ö, Lau J, Liljebäck H, Palm F, Quach M, Sandberg M, Strömberg V, Ullsten S, Carlsson PO. Pancreatic islet blood flow and its measurement. *Ups J Med Sci* 2016; 121: 81-95.

Jennings RE, Berry AA, Kirkwood-Wilson R, Roberts NA, Hearn T, Salisbury RJ, Blaylock J, Piper Hanley K, Hanley NA. Development of the human pancreas from foregut to endocrine commitment. *Diabetes* 2013; 62: 3514-22.

Jiang H, Jiang FX. Human pluripotent stem cell-derived β cells: Truly immature islet β cells for type 1 diabetes therapy? *World J Stem Cells* 2023; 15: 182-95.

Jimenez-Vera E, Davies S, Phillips P, O'Connell PJ, Hawthorne WJ. Long-term cultured neonatal islet cell clusters demonstrate better outcomes for reversal of diabetes: in vivo and molecular profiles. *Xenotransplantation* 2015; 22: 114-23.

Jun Y, Lee J, Choi S, Yang JH, Sander M, Chung S, Lee SH. In vivo-mimicking microfluidic perfusion culture of pancreatic islet spheroids. *Sci Adv* 2019; 5: eaax4520.

Kaestner KH, Campbell-Thompson M, Dor Y, Gill RG, Glaser B, Kim SK, Sander M, Stabler C, Stewart AF, Powers AC. What is a β cell? - Chapter I in the Human Islet Research Network (HIRN) review series. *Mol Metab* 2021; 53: 101323.

Kaido T, Yebra M, Cirulli V, Montgomery AM. Regulation of human beta-cell adhesion, motility, and insulin secretion by collagen IV and its receptor $\alpha 1\beta 1$. *The Journal of biological chemistry* 2004; 279: 53762-9.

Kailey B, van de Bunt M, Cheley S, Johnson PR, MacDonald PE, Gloyn AL, Rorsman P, Braun M. SSTR2 is the functionally dominant somatostatin receptor in human pancreatic β - and α -cells. *Am J Physiol Endocrinol Metab* 2012; 303: E1107-16.

Karimova MV, Gvazava IG, Vorotelyak EA. Overcoming the Limitations of Stem Cell-Derived Beta Cells. *Biomolecules* 2022; 12

Kawai T, Williams WW, Elias N, Fishman JA, Crisalli K, Longchamp A, Rosales IA, Duggan M, Kimura S, Morena L, Borges TJ, Tomosugi T, Karadagi A, Nakamura T, Safa K, Giarraputo A, Avillach CT, Patalas ED, Smith RN, Sachs DH, Cosimi AB, Madsen JC, Cooper DKC, Pierson R, Perrin S, Anand RP, Chhangawala S, Coscarella M, Daigneault A, Li F, Pearce O, Qin W, Serkin WT, Yeung V, Getchell K, Low SC, Curtis M, Colvin RB, Riella LV. Xenotransplantation of a Porcine Kidney for End-Stage Kidney Disease. *N Engl J Med* 2025;

Keenan HA, Sun JK, Levine J, Doria A, Aiello LP, Eisenbarth G, Bonner-Weir S, King GL. Residual insulin production and pancreatic β -cell turnover after 50 years of diabetes: Joslin Medalist Study. *Diabetes* 2010; 59: 2846-53.

Kemter E, Cohrs CM, Schäfer M, Schuster M, Steinmeyer K, Wolf-van Buerck L, Wolf A, Wuensch A, Kurome M, Kessler B, Zakhartchenko V, Loehn M, Ivashchenko Y, Seissler J, Schulte AM, Speier S, Wolf E. INS-eGFP transgenic pigs: a novel reporter system for studying maturation, growth and vascularisation of neonatal islet-like cell clusters. *Diabetologia* 2017; 60: 1152-6.

Kemter E, Wolf E. Recent progress in porcine islet isolation, culture and engraftment strategies for xenotransplantation. *Curr Opin Organ Transplant* 2018; 23: 633-41.

Kemter E, Denner J, Wolf E. Will Genetic Engineering Carry Xenotransplantation of Pig Islets to the Clinic? *Curr Diab Rep* 2018; 18: 103.

Kemter E, Schnieke A, Fischer K, Cowan PJ, Wolf E. Xeno-organ donor pigs with multiple genetic modifications - the more the better? *Curr Opin Genet Dev* 2020; 64: 60-5.

Kim A, Miller K, Jo J, Kilimnik G, Wojcik P, Hara M. Islet architecture: A comparative study. *Islets* 2009; 1: 129-36.

Kim BJ, Shin JS, Min BH, Kim JM, Park CG, Kang HJ, Hwang ES, Lee WW, Kim JS, Kim HJ, Kwon I, Kim JS, Kim GS, Moon J, Shin DY, Cho B, Yang HM, Kim SJ, Kim KW. Clinical Trial Protocol for Porcine Islet Xenotransplantation in South Korea. *Diabetes Metab J* 2024; 48: 1160-8.

Kim S, Whitener RL, Peiris H, Gu X, Chang CA, Lam JY, Camunas-Soler J, Park I, Bevacqua RJ, Tellez K, Quake SR, Lakey JRT, Bottino R, Ross PJ, Kim SK. Molecular and genetic regulation of pig pancreatic islet cell development. *Development* 2020; 147

Kim W, Fiori JL, Shin YK, Okun E, Kim JS, Rapp PR, Egan JM. Pancreatic polypeptide inhibits somatostatin secretion. *FEBS Lett* 2014; 588: 3233-9.

Komatsu H, Cook C, Wang CH, Medrano L, Lin H, Kandeel F, Tai YC, Mullen Y. Oxygen environment and islet size are the primary limiting factors of isolated pancreatic islet survival. *PLOS ONE* 2017; 12: e0183780.

Komatsu H, Kandeel F, Mullen Y. Impact of Oxygen on Pancreatic Islet Survival. *Pancreas* 2018; 47: 533-43.

Konstantinova I, Nikolova G, Ohara-Imaizumi M, Meda P, Kucera T, Zarbalis K, Wurst W, Nagamatsu S, Lammert E. EphA-Ephrin-A-mediated beta cell communication regulates insulin secretion from pancreatic islets. *Cell* 2007; 129: 359-70.

Korbutt GS, Elliott JF, Ao Z, Smith DK, Warnock GL, Rajotte RV. Large scale isolation, growth, and function of porcine neonatal islet cells. *Journal of Clinical Investigation* 1996; 97: 2119-29.

Krickhahn M, Bühler C, Meyer T, Thiede A, Ulrichs K. The morphology of islets within the porcine donor pancreas determines the isolation result: successful isolation of pancreatic islets can now be achieved from young market pigs. *Cell Transplant* 2002; 11: 827-38.

Kulkarni RN, Mizrahi EB, Ocana AG, Stewart AF. Human β -cell proliferation and intracellular signaling: driving in the dark without a road map. *Diabetes* 2012; 61: 2205-13.

Lamb M, Laugenour K, Liang O, Alexander M, Foster CE, Lakey JR. In vitro maturation of viable islets from partially digested young pig pancreas. *Cell Transplant* 2014; 23: 263-72.

Landsman L, Nijagal A, Whitchurch TJ, Vanderlaan RL, Zimmer WE, Mackenzie TC, Hebrok M. Pancreatic mesenchyme regulates epithelial organogenesis throughout development. *PLoS Biol* 2011; 9: e1001143.

Langerhans P (1969) Beiträge zur mikroskopischen Anatomie der Bauchspeicheldrüse. Inaugural-Dissertation, zur Erlangung der Doctorwürde in der Medicin und Chirurgie vorgelegt der Medicinischen Facultät der Friedrich-Wilhelms-Universität zu Berlin

Lau H, Corrales N, Rodriguez S, Luong C, Zaldivar F, Alexander M, Lakey JRT. An islet maturation media to improve the development of young porcine islets during in vitro culture. *Islets* 2020; 12: 41-58.

Lau H, Li S, Corrales N, Rodriguez S, Mohammadi M, Alexander M, de Vos P, Lakey JR. Necrostatin-1 Supplementation to Islet Tissue Culture Enhances the In-Vitro Development and Graft Function of Young Porcine Islets. *Int J Mol Sci* 2021; 22

Li WC, Chen CY, Kao CW, Huang PC, Hsieh YT, Kuo TY, Chen TY, Chia HY, Juang JH. Porcine Neonatal Pancreatic Cell Clusters Maintain Their Multipotency in Culture and After Transplantation. *Sci Rep* 2018; 8: 8212.

Lickert H, Yang K, Spitzer H, Sterr M, Hrovatin K, O S, Zhang X, Setyono E, Ud-Dean M, Walzthoeni T, Flisikowski K, Flisikowska T, Schnieke A, Scheibner K, Wells J, Sneddon J, Kessler B, Wolf E, Kemter E, Theis F (2024) A multimodal cross-species comparison of pancreas development

Lin KY, Hsieh WH, Lin YB, Wen CY, Chang TJ. Update in the epidemiology, risk factors, screening, and treatment of diabetic retinopathy. *J Diabetes Investig* 2021; 12: 1322-5.

Liu Z, Hu W, He T, Dai Y, Hara H, Bottino R, Cooper DKC, Cai Z, Mou L. Pig-to-Primate Islet Xenotransplantation: Past, Present, and Future. *Cell Transplant* 2017; 26: 925-47.

Llacua A, de Haan BJ, Smink SA, de Vos P. Extracellular matrix components supporting human islet function in alginate-based immunoprotective microcapsules for treatment of diabetes. *J Biomed Mater Res A* 2016; 104: 1788-96.

Loganathan G, Dawra RK, Pugazhenthii S, Guo Z, Soltani SM, Wiseman A, Sanders MA, Papas KK, Velayutham K, Saluja AK, Sutherland DE, Hering BJ, Balamurugan AN. Insulin degradation by acinar cell proteases creates a dysfunctional environment for human islets before/after transplantation: benefits of α -1 antitrypsin treatment. *Transplantation* 2011; 92: 1222-30.

Lopez-Avalos MD, Tatarkiewicz K, Sharma A, Bonner-Weir S, Weir GC. Enhanced maturation of porcine neonatal pancreatic cell clusters with growth factors fails to improve transplantation outcome. *Transplantation* 2001; 71: 1154-62.

Lu Y, Wang W, Liu J, Xie M, Liu Q, Li S. Vascular complications of diabetes: A narrative review. *Medicine (Baltimore)* 2023; 102: e35285.

Luca G, Nastruzzi C, Calvitti M, Becchetti E, Baroni T, Neri LM, Capitani S, Basta G, Brunetti P, Calafiore R. Accelerated functional maturation of isolated neonatal porcine cell clusters: in vitro and in vivo results in NOD mice. *Cell Transplant* 2005; 14: 249-61.

Luecken MD, Theis FJ. Current best practices in single-cell RNA-seq analysis: a tutorial. *Mol Syst Biol* 2019; 15: e8746.

Lun AT, Bach K, Marioni JC. Pooling across cells to normalize single-cell RNA sequencing data with many zero counts. *Genome Biol* 2016; 17: 75.

Lun ATL, Riesenfeld S, Andrews T, Dao TP, Gomes T, Marioni JC. EmptyDrops: distinguishing cells from empty droplets in droplet-based single-cell RNA sequencing data. *Genome Biol* 2019; 20: 63.

Ma X, Yang C, Zhang J, Wang J, Li W, Xu C, Rong P, Ye B, Wu M, Jiang J, Yi S, Wang W. Culturing with modified EGM2 medium enhances porcine neonatal islet-like cell clusters resistance to apoptosis in islet xenotransplantation. *Xenotransplantation* 2018; 25

MacDonald MJ, Longacre MJ, Stoker SW, Kendrick M, Thonpho A, Brown LJ, Hasan NM, Jitrapakdee S, Fukao T, Hanson MS, Fernandez LA, Odorico J. Differences between human and rodent pancreatic islets: low pyruvate carboxylase, atp citrate lyase, and pyruvate carboxylation and high glucose-stimulated acetoacetate in human pancreatic islets. *The Journal of biological chemistry* 2011; 286: 18383-96.

Magenheim J, Maestro MA, Sharon N, Herrera PL, Murtaugh LC, Kopp J, Sander M, Gu G, Melton DA, Ferrer J, Dor Y. Matters arising: Insufficient evidence that pancreatic β cells are derived from adult ductal Neurog3-expressing progenitors. *Cell Stem Cell* 2023; 30: 488-97.e3.

Magliano DJ BE (2021) What is diabetes? In: IDF DIABETES ATLAS [Internet], 10th edition edn. International Diabetes Federation, Brussels

Malone JK, Anderson JHJ, Wolpert HA, Ilag LL, Frank BH, De Felippis MR, Paavola CD, Orr AL, Beals JM. Eli Lilly and Company Insulins - A Century of Innovation. *Pediatr Endocrinol Rev* 2020; 17: 138-60.

Mancarella R, Del Guerra S, Masini M, Bugliani M, Valgimigli L, Pedulli GF, Paolini M, Canistro D, Armando A, Soleti A, Filipponi F, Mosca F, Boggi U, Del Prato S, Marchetti P, Lupi R. Beneficial effect of the nonpeptidyl low molecular weight radical scavenger IAC on cultured human islet function. *Cell Transplant* 2008; 17: 1271-6.

Mantovani MDC, Gabanyi I, Pantanali CA, Santos VR, Corrêa-Giannella MLC, Sogayar MC. Islet transplantation: overcoming the organ shortage. *Diabetol Metab Syndr* 2023; 15: 144.

Marfil-Garza BA, Imes S, Verhoeff K, Hefler J, Lam A, Dajani K, Anderson B, O'Gorman D, Kin T, Bigam D, Senior PA, Shapiro AMJ. Pancreatic islet transplantation in type 1 diabetes: 20-year experience from a single-centre cohort in Canada. *Lancet Diabetes Endocrinol* 2022; 10: 519-32.

Marfil-Garza BA, Hefler J, Verhoeff K, Lam A, Dajani K, Anderson B, O'Gorman D, Kin T, Bello-Chavolla OY, Grynock D, Halpin A, Campbell PM, Senior PA, Bigam D, Shapiro AMJ. Pancreas and Islet Transplantation: Comparative Outcome Analysis of a Single-centre Cohort Over 20-years. *Ann Surg* 2023; 277: 672-80.

Matsumoto S, Shimoda M. Current situation of clinical islet transplantation from allogeneic toward xenogeneic. *J Diabetes* 2020; 12: 733-41.

Matsumoto S, Matsumoto K. Clinical Islet Xenotransplantation: Development of Isolation Protocol, Anti-Rejection Strategies, and Clinical Outcomes. *Cells* 2024; 13

Mazur A. Why were "starvation diets" promoted for diabetes in the pre-insulin period? *Nutr J* 2011; 10: 23.

McCulloch LJ, van de Bunt M, Braun M, Frayn KN, Clark A, Gloyn AL. GLUT2 (SLC2A2) is not the principal glucose transporter in human pancreatic beta cells: implications for understanding genetic association signals at this locus. *Mol Genet Metab* 2011; 104: 648-53.

McGinnis CS, Murrow LM, Gartner ZJ. DoubletFinder: Doublet Detection in Single-Cell RNA Sequencing Data Using Artificial Nearest Neighbors. *Cell Syst* 2019; 8: 329-37.e4.

Md Moin AS, Dhawan S, Cory M, Butler PC, Rizza RA, Butler AE. Increased Frequency of Hormone Negative and Polyhormonal Endocrine Cells in Lean Individuals With Type 2 Diabetes. *J Clin Endocrinol Metab* 2016; 101: 3628-36.

Melton D. The promise of stem cell-derived islet replacement therapy. *Diabetologia* 2021;

Meyer T, Czub S, Chodnewska I, Beutner U, Hamelmann W, Klöck G, Zimmermann U, Thiede A, Ulrichs K. Expression pattern of extracellular matrix proteins in the pancreas of various domestic pig breeds, the Goettingen Minipig and the Wild Boar. *Ann Transplant* 1997; 2: 17-26.

Miller I, Min M, Yang C, Tian C, Gookin S, Carter D, Spencer SL. Ki67 is a Graded Rather than a Binary Marker of Proliferation versus Quiescence. *Cell Rep* 2018; 24: 1105-12.e5.

Minami K, Okuno M, Miyawaki K, Okumachi A, Ishizaki K, Oyama K, Kawaguchi M, Ishizuka N, Iwanaga T, Seino S. Lineage tracing and characterization of insulin-secreting cells generated from adult pancreatic acinar cells. *Proc Natl Acad Sci U S A* 2005; 102: 15116-21.

Mobasser M, Shirmohammadi M, Amiri T, Vahed N, Hosseini Fard H, Ghojzadeh M. Prevalence and incidence of type 1 diabetes in the world: a systematic review and meta-analysis. *Health Promot Perspect* 2020; 10: 98-115.

Montanari E, Szabó L, Balaphas A, Meyer J, Perriraz-Mayer N, Pimenta J, Giraud MN, Egger B, Gerber-Lemaire S, Bühler L, Gonelle-Gispert C. Multipotent mesenchymal stromal cells derived from porcine exocrine pancreas improve insulin secretion from juvenile porcine islet cell clusters. *Xenotransplantation* 2021; 28: e12666.

Moreno-Amador JL, Téllez N, Marin S, Aloy-Reverté C, Semino C, Nacher M, Montanya E. Epithelial to mesenchymal transition in human endocrine islet cells. *PLOS ONE* 2018; 13: e0191104.

Nagaraju S, Bottino R, Wijkstrom M, Trucco M, Cooper DK. Islet xenotransplantation: what is the optimal age of the islet-source pig? *Xenotransplantation* 2015; 22: 7-19.

Nagaya M, Hayashi A, Nakano K, Honda M, Hasegawa K, Okamoto K, Itazaki S, Matsunari H, Watanabe M, Umeyama K, Nagashima H. Distributions of endocrine cell clusters during porcine pancreatic development. *PLOS ONE* 2019; 14: e0216254.

Nair G, Hebrok M. Islet formation in mice and men: lessons for the generation of functional insulin-producing beta-cells from human pluripotent stem cells. *Curr Opin Genet Dev* 2015; 32: 171-80.

Nathan DM, Genuth S, Lachin J, Cleary P, Crofford O, Davis M, Rand L, Siebert C. The effect of intensive treatment of diabetes on the development and progression of long-term complications in insulin-dependent diabetes mellitus. *N Engl J Med* 1993; 329: 977-86.

Neukam M, Sala P, Brunner AD, Ganß K, Palladini A, Grzybek M, Topcheva O, Vasiljević J, Broichhagen J, Johnsson K, Kurth T, Mann M, Coskun Ü, Solimena M. Purification of time-resolved insulin granules reveals proteomic and lipidomic changes during granule aging. *Cell Rep* 2024; 43: 113836.

Niclauss N, Meier R, Bédard B, Berishvili E, Berney T. Beta-Cell Replacement: Pancreas and Islet Cell Transplantation. *Endocr Dev* 2016; 31: 146-62.

Nielsen TB, Yderstraede KB, Schröder HD, Holst JJ, Brusgaard K, Beck-Nielsen H. Functional and Immunohistochemical Evaluation of Porcine Neonatal Islet-Like Cell Clusters. *Cell transplantation* 2003; 12: 13-25.

Niu F, Liu W, Ren Y, Tian Y, Shi W, Li M, Li Y, Xiong Y, Qian L. β -cell neogenesis: A rising star to rescue diabetes mellitus. *J Adv Res* 2024; 62: 71-89.

Noguchi H, Nakai Y, Matsumoto S, Kawaguchi M, Ueda M, Okitsu T, Iwanaga Y, Yonekawa Y, Nagata H, Minami K, Masui Y, Futaki S, Tanaka K. Cell permeable peptide of JNK inhibitor prevents islet apoptosis immediately after isolation and improves islet graft function. *Am J Transplant* 2005; 5: 1848-55.

Noguchi H, Naziruddin B, Jackson A, Shimoda M, Ikemoto T, Fujita Y, Chujo D, Takita M, Kobayashi N, Onaca N, Levy MF, Matsumoto S. Low-temperature preservation of isolated islets is superior to conventional islet culture before islet transplantation. *Transplantation* 2010; 89: 47-54.

Norris N, Yau B, Famularo C, Webster H, Loudovaris T, Thomas HE, Larance M, Senior AM, Kebede MA. Optimized Proteomic Analysis of Insulin Granules From MIN6 Cells Identifies Scamp3, a Novel Regulator of Insulin Secretion and Content. *Diabetes* 2024; 73: 2045-54.

Nyeng P, Heilmann S, Löf-Öhlin ZM, Pettersson NF, Hermann FM, Reynolds AB, Semb H. p120ctn-Mediated Organ Patterning Precedes and Determines Pancreatic Progenitor Fate. *Dev Cell* 2019; 49: 31-47.e9.

Ogle GD, Wang F, Gregory GA, Maniam J (2022) Type 1 Diabetes Estimates in Children and Adults. In: *IDF Diabetes Atlas, 10 edn.* International Diabetes Federation, Brussels

Pagliuca FW, Millman JR, Gürtler M, Segel M, Van Dervort A, Ryu JH, Peterson QP, Greiner D, Melton DA. Generation of functional human pancreatic β cells in vitro. *Cell* 2014; 159: 428-39.

Pepper AR, Bruni A, Pawlick R, Wink J, Rafiei Y, Gala-Lopez B, Bral M, Abualhassan N, Kin T, Shapiro AMJ. Engraftment Site and Effectiveness of the Pan-Caspase Inhibitor F573 to Improve Engraftment in Mouse and Human Islet Transplantation in Mice. *Transplantation* 2017; 101: 2321-9.

Perez-Frances M, van Gurp L, Abate MV, Cigliola V, Furuyama K, Bru-Tari E, Oropeza D, Carreaux T, Fujitani Y, Thorel F, Herrera PL. Pancreatic Ppy-expressing γ -cells display mixed phenotypic traits and the adaptive plasticity to engage insulin production. *Nat Commun* 2021; 12: 4458.

Pertea G, Pertea M. GFF Utilities: GffRead and GffCompare. *F1000Res* 2020; 9

Petry F, Salzig D. The cultivation conditions affect the aggregation and functionality of β -cell lines alone and in coculture with mesenchymal stromal/stem cells. *Eng Life Sci* 2022; 22: 769-83.

Pinkse GG, Bouwman WP, Jiawan-Lalai R, Terpstra OT, Bruijn JA, de Heer E. Integrin signaling via RGD peptides and anti-beta1 antibodies confers resistance to apoptosis in islets of Langerhans. *Diabetes* 2006; 55: 312-7.

Puri S, Folias AE, Hebrok M. Plasticity and dedifferentiation within the pancreas: development, homeostasis, and disease. *Cell Stem Cell* 2015; 16: 18-31.

Qiu P. Embracing the dropouts in single-cell RNA-seq analysis. *Nat Commun* 2020; 11: 1169.

Rahier J, Wallon J, Henquin JC. Cell populations in the endocrine pancreas of human neonates and infants. *Diabetologia* 1981; 20: 540-6.

Rao A, McBride EL, Zhang G, Xu H, Cai T, Notkins AL, Aronova MA, Leapman RD. Determination of secretory granule maturation times in pancreatic islet β -cells by serial block-face electron microscopy. *J Struct Biol* 2020; 212: 107584.

Razavi R, Najafabadi HS, Abdullah S, Smukler S, Arntfield M, van der Kooy D. Diabetes enhances the proliferation of adult pancreatic multipotent progenitor cells and biases their differentiation to more β -cell production. *Diabetes* 2015; 64: 1311-23.

Reichert M, Rustgi AK. Pancreatic ductal cells in development, regeneration, and neoplasia. *J Clin Invest* 2011; 121: 4572-8.

Reid L, Baxter F, Forbes S. Effects of islet transplantation on microvascular and macrovascular complications in type 1 diabetes. *Diabet Med* 2021; 38: e14570.

Renner S, Dobenecker B, Blutke A, Zols S, Wanke R, Ritzmann M, Wolf E. Comparative aspects of rodent and nonrodent animal models for mechanistic and translational diabetes research. *Theriogenology* 2016; 86: 406-21.

Rezania A, Bruin JE, Arora P, Rubin A, Batushansky I, Asadi A, O'Dwyer S, Quiskamp N, Mojibian M, Albrecht T, Yang YH, Johnson JD, Kieffer TJ. Reversal of diabetes with insulin-producing cells derived in vitro from human pluripotent stem cells. *Nat Biotechnol* 2014; 32: 1121-33.

Ricordi C, Lacy PE, Scharp DW. Automated islet isolation from human pancreas. *Diabetes* 1989; 38 Suppl 1: 140-2.

Riz M, Braun M, Pedersen MG. Mathematical modeling of heterogeneous electrophysiological responses in human β -cells. *PLoS Comput Biol* 2014; 10: e1003389.

Roscioni SS, Migliorini A, Gegg M, Lickert H. Impact of islet architecture on β -cell heterogeneity, plasticity and function. *Nat Rev Endocrinol* 2016; 12: 695-709.

Rose NL, Palcic MM, Helms LM, Lakey JR. Evaluation of Pefabloc as a serine protease inhibitor during human-islet isolation. *Transplantation* 2003; 75: 462-6.

Rosenfeld L. Insulin: discovery and controversy. *Clin Chem* 2002; 48: 2270-88.

Russ HA, Parent AV, Ringler JJ, Hennings TG, Nair GG, Shveygert M, Guo T, Puri S, Haataja L, Cirulli V, Blelloch R, Szot GL, Arvan P, Hebrok M. Controlled induction of human pancreatic progenitors produces functional beta-like cells in vitro. *Embo j* 2015; 34: 1759-72.

Saberzadeh-Ardestani B, Karamzadeh R, Basiri M, Hajizadeh-Saffar E, Farhadi A, Shapiro AMJ, Tahamtani Y, Baharvand H. Type 1 Diabetes Mellitus: Cellular and Molecular Pathophysiology at A Glance. *Cell J* 2018; 20: 294-301.

Sachs S, Bastidas-Ponce A, Tritschler S, Bakhti M, Böttcher A, Sánchez-Garrido MA, Tarquis-Medina M, Kleinert M, Fischer K, Jall S, Harger A, Bader E, Roscioni S, Ussar S, Feuchtinger A, Yesildag B, Neelakandhan A, Jensen CB, Cornu M, Yang B, Finan B, DiMarchi RD, Tschöp MH, Theis FJ, Hofmann SM, Müller TD, Lickert H. Targeted pharmacological therapy restores β -cell function for diabetes remission. *Nat Metab* 2020; 2: 192-209.

Sakaguchi K, Hinata Y, Kagawa Y, Iwasaki K, Tsuneda S, Shimizu T, Umezu M. Low-temperature culturing improves survival rate of tissue-engineered cardiac cell sheets. *Biochem Biophys Rep* 2018; 14: 89-97.

Sakata N, Yoshimatsu G, Kodama S. Development and Characteristics of Pancreatic Epsilon Cells. *Int J Mol Sci* 2019; 20

Sakata N, Yoshimatsu G, Kawakami R, Aoyagi C, Kodama S. Optimal temperature for the long-term culture of adult porcine islets for xenotransplantation. *Front Immunol* 2023; 14: 1280668.

Sakhneny L, Mueller L, Schonblum A, Azaria S, Burganova G, Epshtein A, Isaacson A, Wilson H, Spagnoli FM, Landsman L. The postnatal pancreatic microenvironment guides β cell maturation through BMP4 production. *Developmental Cell* 2021; 56: 2703-11.e5.

Salama BF, Seeberger KL, Korbitt GS. Fibrin supports subcutaneous neonatal porcine islet transplantation without the need for pre-vascularization. *Xenotransplantation* 2020; 27: e12575.

Satija R, Farrell JA, Gennert D, Schier AF, Regev A. Spatial reconstruction of single-cell gene expression data. *Nat Biotechnol* 2015; 33: 495-502.

Saunders D, Powers AC. Replicative capacity of β -cells and type 1 diabetes. *J Autoimmun* 2016; 71: 59-68.

Saunders DC, Hart N, Pan FC, Reihsmann CV, Hopkirk AL, Izmaylov N, Mei S, Sherrod BA, Davis C, Duryea J, Haliyur R, Aramandla R, Durai H, Poffenberger G, Martin A, Posgai AL, Kusmartseva I, Beery ML, Yang M, Kang H, Greiner DL, Shultz LD, Cartailier JP, Aamodt KI, Bottino R, Atkinson MA, Wright CVE, Powers AC, Brissova M. Mapping histological and functional maturation of human endocrine pancreas across early postnatal periods. *bioRxiv* 2024;

Schaffer AE, Taylor BL, Benthuyzen JR, Liu J, Thorel F, Yuan W, Jiao Y, Kaestner KH, Herrera PL, Magnuson MA, May CL, Sander M. Nkx6.1 controls a gene regulatory network required for establishing and maintaining pancreatic Beta cell identity. *PLoS Genet* 2013; 9: e1003274.

Schook LB, Collares TV, Darfour-Oduro KA, De AK, Rund LA, Schachtschneider KM, Seixas FK. Unraveling the swine genome: implications for human health. *Annu Rev Anim Biosci* 2015; 3: 219-44.

Shapiro AM, Lakey JR, Ryan EA, Korbitt GS, Toth E, Warnock GL, Kneteman NM, Rajotte RV. Islet transplantation in seven patients with type 1 diabetes mellitus using a glucocorticoid-free immunosuppressive regimen. *N Engl J Med* 2000; 343: 230-8.

Shin JS, Kim JM, Kim JS, Min BH, Kim YH, Kim HJ, Jang JY, Yoon IH, Kang HJ, Kim J, Hwang ES, Lim DG, Lee WW, Ha J, Jung KC, Park SH, Kim SJ, Park CG. Long-term control of diabetes in immunosuppressed nonhuman primates (NHP) by the transplantation of adult porcine islets. *Am J Transplant* 2015; 15: 2837-50.

Shin JS, Kim JM, Min BH, Yoon IH, Kim HJ, Kim JS, Kim YH, Kang SJ, Kim J, Kang HJ, Lim DG, Hwang ES, Ha J, Kim SJ, Park WB, Park CG. Pre-clinical results in pig-to-non-human primate islet xenotransplantation using anti-CD40 antibody (2C10R4)-based immunosuppression. *Xenotransplantation* 2018; 25

Siehler J, Blochinger AK, Meier M, Lickert H. Engineering islets from stem cells for advanced therapies of diabetes. *Nat Rev Drug Discov* 2021; 20: 920-40.

Sigmundsson K, Ojala JRM, Öhman MK, Österholm AM, Moreno-Moral A, Domogatskaya A, Chong LY, Sun Y, Chai X, Steele JAM, George B, Patarroyo M, Nilsson AS, Rodin S, Ghosh S, Stevens MM, Petretto E, Tryggvason K. Culturing functional pancreatic islets on α 5-laminins and curative transplantation to diabetic mice. *Matrix Biol* 2018; 70: 5-19.

Singh R, Cottle L, Loudovaris T, Xiao D, Yang P, Thomas HE, Kebede MA, Thorn P. Enhanced structure and function of human pluripotent stem cell-derived beta-cells cultured on extracellular matrix. *Stem Cells Transl Med* 2021; 10: 492-505.

Skelin Klemen M, Dolenšek J, Slak Rupnik M, Stožer A. The triggering pathway to insulin secretion: Functional similarities and differences between the human and the mouse β cells and their translational relevance. *Islets* 2017; 9: 109-39.

Smith KE, Purvis WG, Davis MA, Min CG, Cooksey AM, Weber CS, Jandova J, Price ND, Molano DS, Stanton JB, Kelly AC, Steyn LV, Lynch RM, Limesand SW, Alexander M, Lakey JRT, Seeberger K, Korbitt GS, Mueller KR, Hering BJ, McCarthy FM, Papas KK. In vitro characterization of neonatal, juvenile, and adult porcine islet oxygen demand, β -cell function, and transcriptomes. *Xenotransplantation* 2018; 25: e12432.

Son J, Accili D. Reversing pancreatic β -cell dedifferentiation in the treatment of type 2 diabetes. *Exp Mol Med* 2023; 55: 1652-8.

Steffen A, Kiss T, Schmid J, Schubert U, Heinke S, Lehmann S, Bornstein S, Ludwig B, Ludwig S. Production of high-quality islets from goettingen minipigs: Choice of organ preservation solution, donor pool, and optimal cold ischemia time. *Xenotransplantation* 2017; 24

Sterkers A, Hubert T, Gmyr V, Torres F, Baud G, Delalleau N, Vantghem MC, Kerr-Conte J, Caiazzo R, Pattou F. Islet survival and function following intramuscular autotransplantation in the minipig. *Am J Transplant* 2013; 13: 891-8.

Syed FZ. Type 1 Diabetes Mellitus. *Ann Intern Med* 2022; 175: Itc33-itc48.

Takahashi K, Yamanaka S. Induction of pluripotent stem cells from mouse embryonic and adult fibroblast cultures by defined factors. *Cell* 2006; 126: 663-76.

Taylor BL, Benthuisen J, Sander M. Postnatal β -cell proliferation and mass expansion is dependent on the transcription factor Nkx6.1. *Diabetes* 2015; 64: 897-903.

Taylor GS, Shaw AC, Smith K, Wason J, McDonald TJ, Oram RA, Stevenson E, Shaw JAM, West DJ. Capturing the real-world benefit of residual β -cell function during clinically important time-periods in established Type 1 diabetes. *Diabet Med* 2022; 39: e14814.

Thorel F, Népote V, Avril I, Kohno K, Desgraz R, Chera S, Herrera PL. Conversion of adult pancreatic alpha-cells to beta-cells after extreme beta-cell loss. *Nature* 2010; 464: 1149-54.

Tiemann U, Tian C, Hermann F, Proks M, Skovgaard E, Kulik I, Di Y, Sedzinski J, Semb H. Pancreatic alpha and beta cell fate choice is directed by apical-basal polarity dynamics. *Dev Cell* 2025;

Tirza G, Solodeev I, Sela M, Greenberg I, Pasmanik-Chor M, Gur E, Shani N. Reduced culture temperature attenuates oxidative stress and inflammatory response facilitating expansion and differentiation of adipose-derived stem cells. *Stem Cell Res Ther* 2020; 11: 35.

Townsend SE, Gannon M. Extracellular Matrix-Associated Factors Play Critical Roles in Regulating Pancreatic beta-Cell Proliferation and Survival. *Endocrinology* 2019; 160: 1885-94.

Tritschler S, Thomas M, Bottcher A, Ludwig B, Schmid J, Schubert U, Kemter E, Wolf E, Lickert H, Theis FJ. A transcriptional cross species map of pancreatic islet cells. *Mol Metab* 2022; 66: 101595.

Trivedi N, Hollister-Lock J, Lopez-Avalos MD, O'Neil JJ, Keegan M, Bonner-Weir S, Weir GC. Increase in beta-cell mass in transplanted porcine neonatal pancreatic cell clusters is due to proliferation of beta-cells and differentiation of duct cells. *Endocrinology* 2001; 142: 2115-22.

Tsonkova VG, Sand FW, Wolf XA, Grunnet LG, Kirstine Ringgaard A, Ingvorsen C, Winkel L, Kalisz M, Dalgaard K, Bruun C, Fels JJ, Helgstrand C, Hastrup S, Öberg FK, Vernet E, Sandrini MPB, Shaw AC, Jessen C, Grønborg M, Hald J, Willenbrock H, Madsen D, Wernersson R, Hansson L, Jensen JN, Plesner A, Alanentalo T, Petersen MBK, Grapin-Botton A, Honoré C, Ahnfelt-Rønne J, Hecksher-Sørensen J, Ravassard P, Madsen OD, Rescan C, Frogne T. The EndoC-βH1 cell line is a valid model of human beta cells and applicable for screenings to identify novel drug target candidates. *Mol Metab* 2018; 8: 144-57.

Tsuchitani M, Sato J, Kokoshima H. A comparison of the anatomical structure of the pancreas in experimental animals. *J Toxicol Pathol* 2016; 29: 147-54.

van Gurp L, Fodouliau L, Oropeza D, Furuyama K, Bru-Tari E, Vu AN, Kaddis JS, Rodriguez I, Thorel F, Herrera PL. Generation of human islet cell type-specific identity genesets. *Nat Commun* 2022; 13: 2020.

Vanderniet JA, Jenkins AJ, Donaghue KC. Epidemiology of Type 1 Diabetes. *Curr Cardiol Rep* 2022; 24: 1455-65.

Vanderschelden R, Sathialingam M, Alexander M, Lakey JRT. Cost and Scalability Analysis of Porcine Islet Isolation for Islet Transplantation: Comparison of Juvenile, Neonatal and Adult Pigs. *Cell Transplant* 2019; 28: 967-72.

Veres A, Faust AL, Bushnell HL, Engquist EN, Kenty JH, Harb G, Poh YC, Sintov E, Gürtler M, Pagliuca FW, Peterson QP, Melton DA. Charting cellular identity during human in vitro β -cell differentiation. *Nature* 2019; 569: 368-73.

Vertex (2024) Vertex Announces Positive Results From Ongoing Phase 1/2 Study of VX-880 for the Treatment of Type 1 Diabetes Presented at the American Diabetes Association 84th Scientific Sessions. Ed Incorporated VP

Voeltz D, Vetterer M, Seidel-Jacobs E, Brinks R, Tonnie T, Hoyer A. Projecting the economic burden of type 1 and type 2 diabetes mellitus in Germany from 2010 until 2040. *Popul Health Metr* 2024; 22: 17.

Wieland FC, van Blitterswijk CA, van Apeldoorn A, LaPointe VLS. The functional importance of the cellular and extracellular composition of the islets of Langerhans. *Journal of Immunology and Regenerative Medicine* 2021; 13: 100048.

Wolf FA, Angerer P, Theis FJ. SCANPY: large-scale single-cell gene expression data analysis. *Genome Biol* 2018; 19: 15.

Wolock SL, Lopez R, Klein AM. Scrublet: Computational Identification of Cell Doublets in Single-Cell Transcriptomic Data. *Cell Syst* 2019; 8: 281-91.e9.

Xu SFS, Andersen DB, Izarzugaza JMG, Kuhre RE, Holst JJ. In the rat pancreas, somatostatin tonically inhibits glucagon secretion and is required for glucose-induced inhibition of glucagon secretion. *Acta Physiol (Oxf)* 2020; 229: e13464.

Yang S, Corbett SE, Koga Y, Wang Z, Johnson WE, Yajima M, Campbell JD. Decontamination of ambient RNA in single-cell RNA-seq with DecontX. *Genome Biol* 2020; 21: 57.

Zajec A, Trebusak Podkrajsek K, Tesovnik T, Sket R, Cugalj Kern B, Jenko Bizjan B, Smigoc Schweiger D, Battelino T, Kovac J. Pathogenesis of Type 1 Diabetes: Established Facts and New Insights. *Genes (Basel)* 2022; 13

Zappia L, Oshlack A. Clustering trees: a visualization for evaluating clusterings at multiple resolutions. *GigaScience* 2018; 7

Zhang Y, Lei Y, Honarpisheh M, Kemter E, Wolf E, Seissler J. Butyrate and Class I Histone Deacetylase Inhibitors Promote Differentiation of Neonatal Porcine Islet Cells into Beta Cells. *Cells* 2021; 10

Zhong F, Jiang Y. Endogenous Pancreatic β Cell Regeneration: A Potential Strategy for the Recovery of β Cell Deficiency in Diabetes. *Front Endocrinol (Lausanne)* 2019; 10: 101.

Zhou Q, Law AC, Rajagopal J, Anderson WJ, Gray PA, Melton DA. A multipotent progenitor domain guides pancreatic organogenesis. *Dev Cell* 2007; 13: 103-14.

XII. ACKNOWLEDGEMENTS

First and foremost, I want to express my heartfelt gratitude to my supervisors. Dear Lisbeth and Anika, I have learned so much from you – professionally, from pathology to molecular islet biology, and personally. Thank you for the collaboration and for dedicating so much time to me and this project!

A special thanks to Eckhard Wolf for the warm welcome at the chair, the opportunity to write this dissertation, and the various small assists at all hours of the day and night.

I also want to thank all my colleagues at the Moorversuchsgut. Especially Libera for the support with perfusion, my helpers during the beloved Monday work (Johanna & Nicol, Doro & Magdalena, and Natalie), and the IsoTeam (Christina & Flori). Thank you ALL for the wonderful times together, whether during the week, on holidays, weekends, or late at night.

My gratitude extends to everyone at the Institute of Diabetes and Regeneration Research for your helpfulness and diverse input. I have learned an incredible amount from you and felt very warmly welcomed. A special thanks to Minas for the data processing explosion.

I also appreciate everyone in the Ludwig group at the Paul Langerhans Institute Dresden for the great exchange and collaboration.

Thanks to Tom and the entire band for the mental reset and the incredible energy! This has helped me tremendously through this time!!

Thank you, Lisa, for your support over the past months. Without you, this final sprint would not have been possible!

Finally, I want to especially thank my family and friends from my time in Freising and Vienna. Without you, I wouldn't be where I am now. Thank you all for your support and for always being there for me! That is what family means to me.